KfK 3752
Mai 1985

Accurate Determination of the ^{235}U Isotope Abundance by Gamma Spectrometry

A User's Manual for the Certified Reference Material EC-NRM-171 / NBS-SRM-969

P. Matussek
Institut für Kernphysik

Kernforschungszentrum Karlsruhe

KERNFORSCHUNGSZENTRUM KARLSRUHE

Institut für Kernphysik

KfK 3752

Accurate Determination of the ^{235}U Isotope Abundance by Gamma Spectrometry

A User's Manual for the Certified Reference Material EC-NRM-171 / NBS-SRM-969

P. Matussek

Kernforschungszentrum Karlsruhe GmbH, Karlsruhe

Kernforschungszentrum Karlsruhe GmbH
ISSN 0303-4003

ABSTRACT

The purpose of this manual is to serve as guide in applications of the Certified Reference Material EC-NRM-171/NBS-SRM-969 for accurate ^{235}U isotope abundance measurements on bulk uranium samples by means of gamma spectrometry. The manual provides a thorough description of this non-destructive assay technique. Crucial measurement parameters affecting the accuracy of the gamma-spectrometric ^{235}U isotope abundance determination are discussed in detail and, whereever possible, evaluated quantitatively. The correction terms and tolerance limits given refer both to physical and chemical properties of the samples under assay and to relevant parameters of typical measurement systems such as counting geometry, signal processing, data evaluation and calibration.

Präzisionsmessungen der ^{235}U Anreicherung mit Hilfe der Gammaspektrometrie - Benutzerhandbuch für das nukleare Referenzmaterial EC-NRM-171/NBS-SRM-969

ZUSAMMENFASSUNG

Das vorliegende Handbuch soll als Anleitung dienen für die Verwendung des Referenzmaterials EC-NRM-171/NBS-SRM-969 bei Präzisionsmessungen der ^{235}U Anreicherung mit Hilfe der Gammaspektrometrie. Es enthält eine eingehende Beschreibung dieses zerstörungsfreien Meßverfahrens. Der Einfluß kritischer Parameter der Meßanordnung auf die Genauigkeit der ^{235}U Anreicherungsbestimmung wird diskutiert und, soweit möglich, quantitativ beschrieben. Die angegebenen Korrekturgrößen und Toleranzgrenzen berücksichtigen sowohl die physikalischen und chemischen Eigenschaften der zu untersuchenden Proben als auch wichtige Parameter des verwendeten Meßsystems, wie Meßgeometrie, Signalverarbeitung, Datenauswertung und Kalibrierung.

CONTENTS

APPENDIX A

Derivation of basic formulae for gamma-spectrometric ^{235}U enrichment assays

A.1 Surface gamma radiation of large ^{235}U-bearing samples

A.2 Gamma-ray transmission through a collimator

A.3 Gamma absorbing material between sample and detector

APPENDIX B

Characteristic gamma rays from the decay of uranium isotopes

APPENDIX C

Physical constants used in the calculation of the 186 keV gamma counting rate

APPENDIX D

Tables of test statistics

APPENDIX E

ER2FIT - A BASIC program for the calibration of ^{235}U enrichment assay systems

INTRODUCTION

The non-destructive gamma-spectroscopic determination of the ^{235}U isotope abundance, i.e., the ratio of ^{235}U atoms to total U atoms present in a sample (colloquially called the "^{235}U enrichment" of the sample) has become a mature technique, finding widespread use in nuclear material accountancy and process control applications.

In principle, the ^{235}U enrichment can be determined directly from the absolute number of the characteristic 186 keV gamma rays emitted from the surface of a large uranium sample per unit area and per unit time. However, the accuracy achievable with this direct approach is poor (5 % relative) due to uncertainties of the physical constants involved (^{235}U half-life, emission probability of 186 keV photons per ^{235}U decay, photon attenuation cross sections for 186 keV gamma rays), and also due to errors arising from the difficult determination of the absolute efficiency of the gamma counting set-up. Therefore, in practice, all of the ^{235}U enrichment determinations by gamma spectrometry are made relative to calibration standards consisting of bulk quantities of reference materials with well-known ^{235}U isotope abundance. The availability of accurately characterized reference materials is of major practical importance for the usefulness of the technique. They will permit to achieve relative measurement accuracies of the order of a few tenths of a percent, which otherwise could not be obtained from gamma-spectrometric ^{235}U enrichment analyses.

The European Safeguards Research and Development Association (ESARDA), represented by its Working Group on Techniques and Standards for Non-Destructive Analyses, therefore has taken the initiative to promote the development of highly accurate "Certified Reference Materials" for the gamma-spectrometric determination of the ^{235}U enrichment in low-enriched uranium materials. The Reference Material EC-NRM-171/NBS-SRM-969 now available is the result of a cooperative international project, with the following organizations taking part in its development:

the ESARDA NDA Working Group,
the Commission of the European Communities,
- Joint Research Centre,
  Central Bureau for Nuclear Measurements (CBNM), Geel,
  and
- Joint Research Centre Ispra (JRC Ispra),
the U.S. National Bureau of Standards (NBS), and
the U.S. Department of Energy
- New Brunswick Laboratory (NBL).

In addition, the Safeguards Directorate of Euratom and the International Atomic Energy Agency (IAEA) have participated in the project in such a way that the Reference Material is also acceptable for the purposes of these agencies.

The Reference Material (RM) EC-NRM-171/NBS-SRM-969 consists of a set of 5 Reference Samples with different ^{235}U isotope abundances, which are certified with an accuracy of $\leq \pm$ 0.1 % relative by both authorities, CBNM and NBS. The RM represents the first example of an internationally certified reference material for non-destructive assay, with the parameter of interest traceable to basic SI units.

Beyond the availability of suitable reference materials, highly accurate determinations of the ^{235}U enrichment by gamma spectrometry definitely require some knowledge of the principles of the measurement technique. Relative accuracies of the order of 0.1 % present a challenge for gamma-spectroscopic measurements that necessitates a very careful design of the measurement set-up, and a very careful correction for known systematic errors.

It is therefore the aim of this user's manual:

1. To familiarize the reader with the basic principles of the ^{235}U enrichment assay technique (Chapter 2 and Appendix A).
2. To give a thorough discussion of possible systematic errors specific to gamma-spectrometric ^{235}U enrichment analyses (Chapters 3 and 4), i.e., measurement errors related to physical and chemical properties of the sample material under assay, to properties of the sample container, and to specialities of the measurement geometry.

3. To give some advice concerning general aspects of gamma-ray measurements (such as processing of detector signals and data evaluation), and possible errors arising from this part of the measurement (Chapter 5).

For a rapid guide and survey of the materials presented in this manual the reader might turn to Chapter 6, which gives the relevant informations in a summarized tabular form.

The gamma-spectrometric ^{235}U enrichment assay technique is now being used for more than 20 years, and a lot of experiences have been accumulated during this time at many places around the world. These experiences form the basis for the present manual. It should be noted, however, that the accurately certified RM now available for the first time may help to validate established measurement procedures as well as techniques for data evaluation on a very high level of accuracy, or, possibly, to identify still unknown sources of errors in gamma-spectrometric ^{235}U enrichment assays. It should also be mentioned that most of the correction terms (as, e.g., the normalization factors between different uranium compounds) given in the manual are based on theoretical values for the photon cross sections, which still lack of experimental validation. Some of the data presented in this manual possibly need to be revised as soon as the relevant experimental data become available.

In order to further improve the accuracy and reliability of the gamma-spectrometric ^{235}U assay, the users are kindly asked to contribute their experiences gained from the use of the RM, and to send comments on this and on the manual to the author. These informations will be collected and distributed to the community of users of the RM in a suitable form. With the user's support it will be possible to elaborate, finally, a procedural standard for the gamma-spectrometric determination of the ^{235}U isotope abundance.

1. THE CERTIFIED REFERENCE MATERIAL

This chapter gives a short description of the Reference Samples that form the Certified Reference Material EC-NRM-171/ NBS-SRM-969. More details can be obtained from the Certificate accompanying each RM, and from the Certification Report [1]. A general review of the underlying project, that has resulted in the production of the present RM's, has been published recently [2].

1.1 Physical description of the Reference Samples

The ^{235}U isotope abundance Reference Samples represent "physical standards" in the sense that they provide well-defined bulk quantities of Certified Reference Material in a well-defined, invariable geometry. The Certified Reference Material is U_3O_8 powder with five different ^{235}U enrichments: 0.3 %, 0.7 %, 1.9 %, 2.9 % and 4.5 %. Each sample is made of 200 g U_3O_8 powder sealed in a cylindrical aluminium can of 7 cm inner diameter (Fig. 1.1).

The chemical form of U_3O_8 has been selected for its superior chemical stability compared to other uranium compounds. The amount of 200 g U_3O_8 is choosen to provide for an "infinite-sample" geometry when measuring the 186 keV gamma radiation through the bottom window of the sample container. The window of the cans has a well-specified thickness of 2.00 mm. The U_3O_8 powder is compressed by means of an aluminium plug to a filling height of 2 cm, resulting in a material density of 2.5 $g \cdot cm^{-3}$. The samples containing the 4.5 % enriched material form an exception from this: due to a significantly higher pour density of the initial powder material, as compared to the lower enriched U_3O_8 powders, a higher compression was required in order to assure the physical stability of these samples. Thus, the 4.5 % enriched samples are containing the Reference Material at a filling height of 1.6 cm, corresponding to a material density of 3.3 $g \cdot cm^{-3}$.

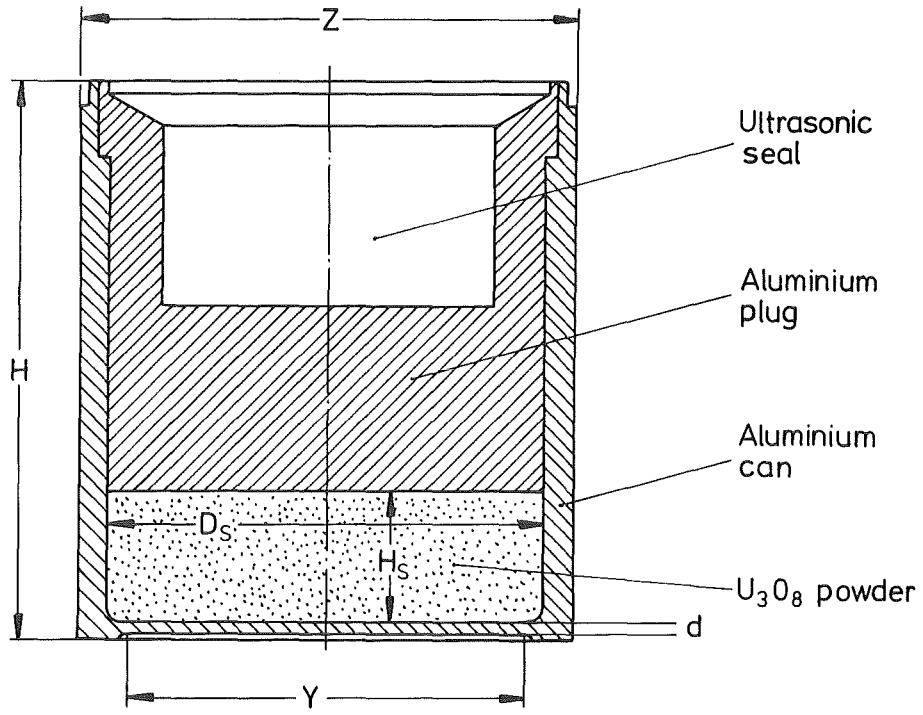

Fig. 1.1 Cross-sectional view of a Reference Sample.

Sample dimensions and tolerances:

Total height	H	$= (90.0 \pm 0.2)$ mm
Outer diameter	Z	$= (80.0 \pm 0, -0.05)$ mm
Inner diameter	D_S	$= (70.0 + 0.02, -0)$ mm
Window diameter	Y	$= (66.0 \pm 0.05)$ mm
Window thickness	d	$= (2.00 \pm 0.02)$ mm
U_3O_8 material height	H_S	$= (20.8 \pm 0.5)$ mm
	or	(15.8 ± 0.5) mm (see below)

The Reference Material is formed of a set of 5 Reference Sample cans containing U_3O_8 powder with 5 different ^{235}U enrichments, and one empty can. The number of 5 different enrichments has been chosen

1. to span the whole range of ^{235}U enrichments as presently common in the low-enriched uranium fuel cycle, and
2. to enable an assessment of calibration errors by testing the theoretically expected linear relationship between enrichment and measured 186 keV gamma counting rate.

The empty can is supplied in order to allow the measurement of materials of unknown ^{235}U enrichment in exactly the same

counting geometry as used for the Reference Samples.

The aluminium plugs on top of the reference cans are equipped with ultrasonic seals [3]. When connected to an appropriate ultrasonic reader (e.g. Sonic MK 1/Euratom modification), the ultrasonic seal provides a unique "finger-print" of the respective can. This feature may be used for a simple and rapid identification of the sample can.

1.2 Certified and specified parameters of the Reference Samples

A Certificate and a Certification Report [1] describing in detail the preparation of the samples and the measurements performed are accompanying each set of samples. Those sample parameters that are of special interest for enrichment measurements are summarized in this section. The ^{235}U isotope abundances (^{235}U enrichments) of the five different Reference Materials are certified with a total uncertainty of less than 0.1 % relative. Chemical and physical properties of the Reference Samples which are of relevance to the enrichment measurements are specified at levels keeping their impact on the enrichment analysis within the error limit of $\pm$ 0.1 % relative.

Certified sample parameters:

	Material No.	$^{235}U/U_{total}$ (atom %)
^{235}U isotope abundance	# 031	(0.3205 $\pm$ 0.0002) %
(^{235}U enrichment)	# 071	(0.7210 $\pm$ 0.0002) %
(uncertainties given at	# 194	(1.9658 $\pm$ 0.0006) %
95 % confidence level)	# 295	(2.9843 $\pm$ 0.0009) %
	# 446	(4.5167 $\pm$ 0.0014) %

Specified sample parameters:

Sample material: Stoichiometric U_3O_8 powder

Cumulative impurities:

with Z <30:	< 5000 $\mu g \cdot g^{-1}$ material
thereof water:	< 3200 $\mu g \cdot g^{-1}$ material
with Z >30:	< 10 $\mu g \cdot g^{-1}$ material

Maximum deviation from ^{235}U isotopic homogeneity per batch (verified by mass spectrometry) ≤ 0.05 % (1 σ, n = 12)

Relative abundances of minor uranium isotopes measured by Gamma Spectrometry (GS) or Mass Spectrometry (MS) (given as atom fraction at the time of certification):

		#031	#071	#194	#295	#446
$^{232}U/^{235}U$	(GS)	$0.8 \cdot 10^{-9}$	$<0.03 \cdot 10^{-9}$	$0.03 \cdot 10^{-9}$	$0.01 \cdot 10^{-9}$	$0.10 \cdot 10^{-9}$
$^{233}U/^{235}U$	(GS)	below detection limit of $5 \cdot 10^{-5}$				
$^{234}U/U$	(MS)	$0.2 \cdot 10^{-4}$	$0.52 \cdot 10^{-4}$	$1.72 \cdot 10^{-4}$	$2.8 \cdot 10^{-4}$	$3.8 \cdot 10^{-4}$
$^{236}U/U$	(MS)	$1.47 \cdot 10^{-4}$	$<0.01 \cdot 10^{-4}$	$<0.01 \cdot 10^{-4}$	$0.33 \cdot 10^{-4}$	$0.72 \cdot 10^{-4}$
$(^{237}U + ^{237}Np)/^{235}U$	(GS)	below detection limit of $3 \cdot 10^{-6}$				

Last chemical separation of uranium daugther products: Sept.1977 for #031, #071, #194 and #204
Sept.1979 for #446

Mass of U_3O_8 powder per can: (200.1 $\pm$ 0.2) g

Filling height: (20.8$\pm$0.5) mm for #031,#071,#194 and #295
(15.8$\pm$0.5) mm for #446

U_3O_8 areal density: (5.2 $\pm$ 0.3) $g \cdot cm^{-2}$

Maximum local variation of areal density within one sample (from transmission experiments): < 5 %

Container material: Aluminium type 6061-T6

Mg: 0.8 % - 1,2 %, Si: 0.2 % - 0.8 %,
Ti: 0.15%, Cr: 0.04 % - 0.35 %,
Mn: 0.15%, Fe: 0.7 %, Cu: 0.6 %,
Zn: 0.25%
other elements: each $\leq$ 0.05 %,
total $\leq$ 0.15 %

Container dimensions: see Fig. 1.1
(a dimensional control sheet is provided for each sample)

Thickness of container bottom window: (2.00 $\pm$ 0.02) mm

specified for each sample to $\pm$ 0.01 mm

Uniformity of bottom window thickness: 0.01 mm

Flatness of bottom window < 0.1 mm

Recession of container bottom: (see Fig. 1.1) 1.0 $\pm$ 0.1 mm

1.3 Handling and storage of the Reference Samples

The Reference Samples should be handled with great care in order to avoid any damage or deformation to the bottom of the cans, since this serves as window for the emitted gamma radiation. Any alteration to the bottom window could therefore affect the gamma-spectroscopic enrichment measurement.

It is recommended to store and handle the samples in such a way that the can window cannot be damaged. For this purpose a transport and storage case for a complete set of Reference Samples is supplied with each RM.

Handling and storage of the ultrasonic transducers integrated into the plug of the Reference Samples deserve special care. Extreme environmental conditions may affect and permanently change the ultrasonic signatures of the samples. The user is therefore strictly advised not to expose the samples to

- strong neutron-radiation fields,
- strong gamma-radiation fields ($> 1\ Gy \cdot s^{-1}$),
- strong magnetic fields,
- temperatures $< -10\,°C$ and $> 40\,°C$,
- rapid strong temperature changes,
- mechanical shocks,
- strong vibrations.

2. PRINCIPLES OF THE ^{235}U ENRICHMENT MEASUREMENT

This chapter gives a short introduction into the physical principles that form the basis for gamma-spectrometric ^{235}U enrichment measurements on bulk samples (for previous general discussions of the technique refer, e.g., to references [4], [5], [6]). Some knowledge of these principles appears necessary for the proper application of the enrichment assay technique in general, and for the use of the ^{235}U isotope abundance Reference Material.

2.1 ^{235}U gamma radiation

The radioactive ^{235}U isotope decays by alpha-particle emission to excited levels of its daughter nucleus ^{231}Th, which in turn emits gamma rays of various energies. Fig. 2.1 shows a part of the gamma spectrum observed from low-enriched uranium taken with a high-resolution germanium detector.

The energies and emission rates of the gamma radiation following the decay of ^{235}U are unique for this isotope, and may thus be used for the qualitative and quantitative non-destructive assay of the ^{235}U content in uranium-bearing materials.

A list of gamma rays from the ^{235}U decay emitted in the energy region of 120 - 300 keV is given in Appendix B. The most prominent gamma line observed in the spectrum has the energy of 185.7 keV. It is emitted with a probability of

$$P_{186} = 0.575 \pm 0.009 \text{ [186 keV photons per } ^{235}U \text{ decay]}$$

(ref. [7]).

The half-life of ^{235}U is

$$T_{1/2} = (7.038 \pm 0.007) \cdot 10^{8} \text{ [a]}$$
$$= (2.229 \pm 0.002) \cdot 10^{16} \text{ [s]}$$

(ref. [8]).

From these two values the number of 186 keV photons emitted per second by a single ^{235}U atom or by one gram of ^{235}U are derived:

$$\dot{n}_{186} = P_{186} \cdot \ln 2 / T_{1/2}$$

$$= (1.80 \pm 0.03) \cdot 10^{-17} [186 \text{ keV photons} \cdot s^{-1} \cdot (^{235}U \text{ atom})^{-1}]$$

or

(2.1)

$$\dot{n}^{M}_{186} = \dot{n}_{186} \cdot A / M_{235}$$

$$= (4.60 \pm 0.07) \cdot 10^{4} [186 \text{ keV photons} \cdot s^{-1} \cdot (g\ ^{235}U)^{-1}], \quad (2.1a)$$

where A is the Avogadro constant and M_{235} is the atomic mass of ^{235}U.

$\dot{n}_{186}$ and $\dot{n}^{M}_{186}$ are nuclear constants, that relate the 186 keV gamma emission rate in a sample directly to the number of ^{235}U atoms, or to the mass of ^{235}U present in the sample.

2.2 The "enrichment meter" principle

In principle, the proportionality between the emission rate of 186 keV gamma rays and the amount of ^{235}U in a sample would allow a very simple direct determination of the ^{235}U content of a sample. Unfortunately, uranium has a very high self-attenuation power for 186 keV gamma radiation, so that this very simple approach for the determination of the ^{235}U content of a sample is only applicable to extremely thin samples, implying inherently low gamma counting rates and therefore impractically long measurement times.

In case of larger samples it becomes necessary to correct for photon attenuation in the sample material. Such corrections, however, are very complicated or even impossible, because they depend critically on sample parameters (as size, density, spatial material distribution) that can be hardly quantified in most real applications. One possibility to avoid the problems associated with self-attenuation corrections is to provide always identical sample geometry as well as identical chemical composition and density of the sample material to be assayed. Since uranium materials in the nuclear fuel cycle exist in va-

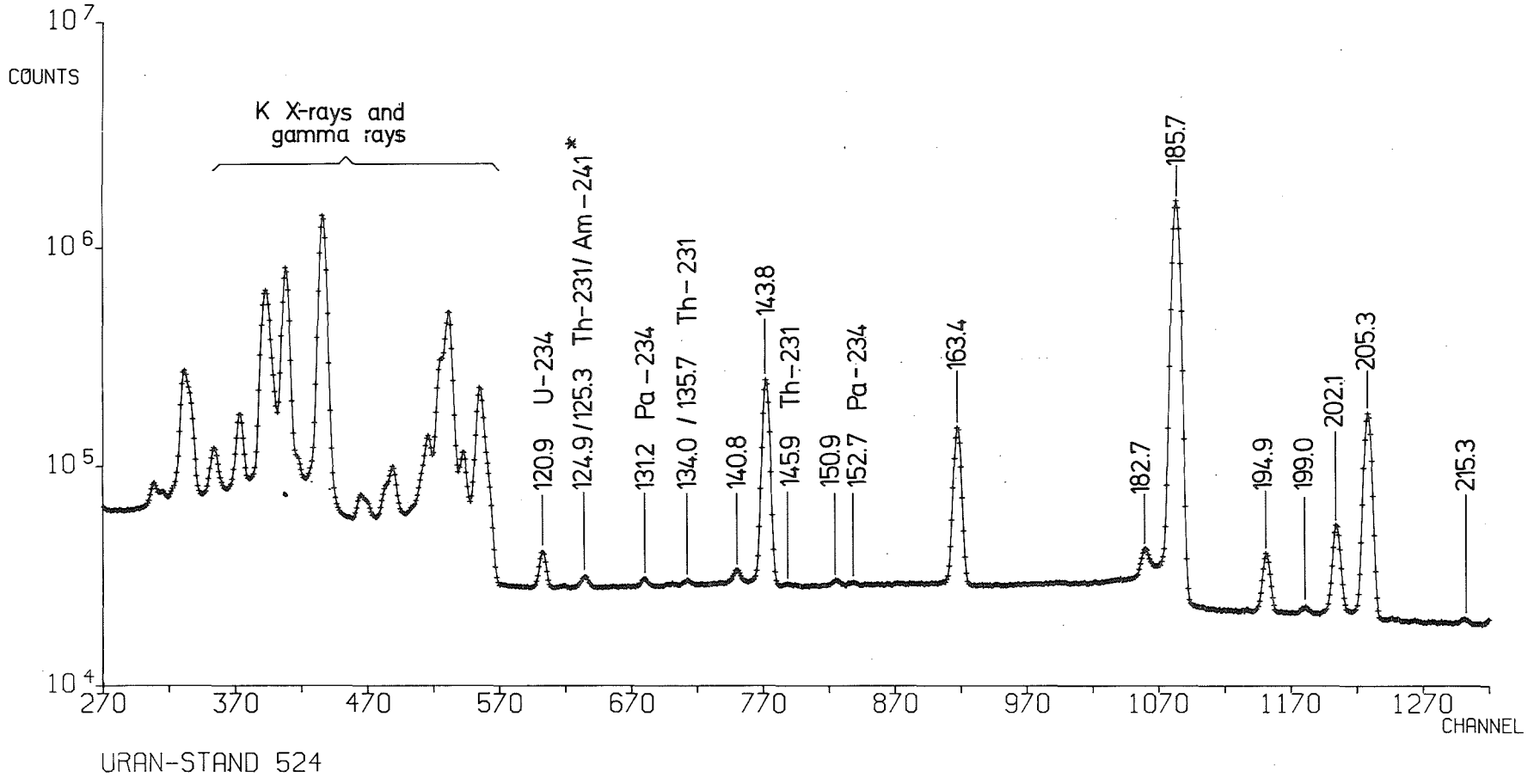

Fig. 2.1 Sectional display of the gamma spectrum from a low-enriched U_3O_8 sample taken with a Ge detector. Gamma-ray energies are given in keV.

* From an external ^{241}Am source used for stabilization.

rious physical and chemical forms, this method generally would imply a careful chemical and physical preparation of the samples.

By contrast, if the uranium sample size is very large, then the gamma radiation originating from ^{235}U atoms deep inside the sample is almost completely absorbed on the way through the material, and will not contribute to the gamma radiation observed at the sample surface. Thus, with increasing sample thickness the 186 keV gamma-ray flux at the surface of bulk uranium samples reaches an equilibrium value which is almost independent of the physical form of the sample material. For pure uranium compounds this value is proportional to the ^{235}U enrichment of the samples, and generally only small corrections for the various chemical compositions of the samples have to be applied.

This is the so called "enrichment meter" principle. It is analytically derived in Appendix A. Its application always requires that the sample under assay is thick enough to be opaque for 186 keV gamma radiation. In this manual we define a sample as "quasi-infinitely thick", if it delivers in a given counting geometry more than 99.9 % of the 186 keV photons that would be observed from a really infinite sample. In Chapter 3 of this manual the conditions for "quasi-infinite" thickness of a sample are discussed for various gamma counting geometries.

2.3 Crucial measurement parameters

The gamma-spectrometric determination of the ^{235}U enrichment of bulk uranium samples is performed by an exact measurement of the number of 186 keV photons emitted from the sample under assay per unit time for a fixed counting geometry. Therefore, all measurement parameters that affect the observed gamma counting rate must be carefully controlled and corrected for. Crucial measurement parameters of the gamma-spectroscopic enrichment assay technique are shown schematically in Fig. 2.2.

The relation between the ^{235}U enrichment and the net peak counting rate $\dot{N}_{186}$ of 186 keV photons observed with a gamma-ray detector in a real counting set-up is influenced by many factors as shown in eq. 2.2 (the ^{235}U enrichment enr is given in %):

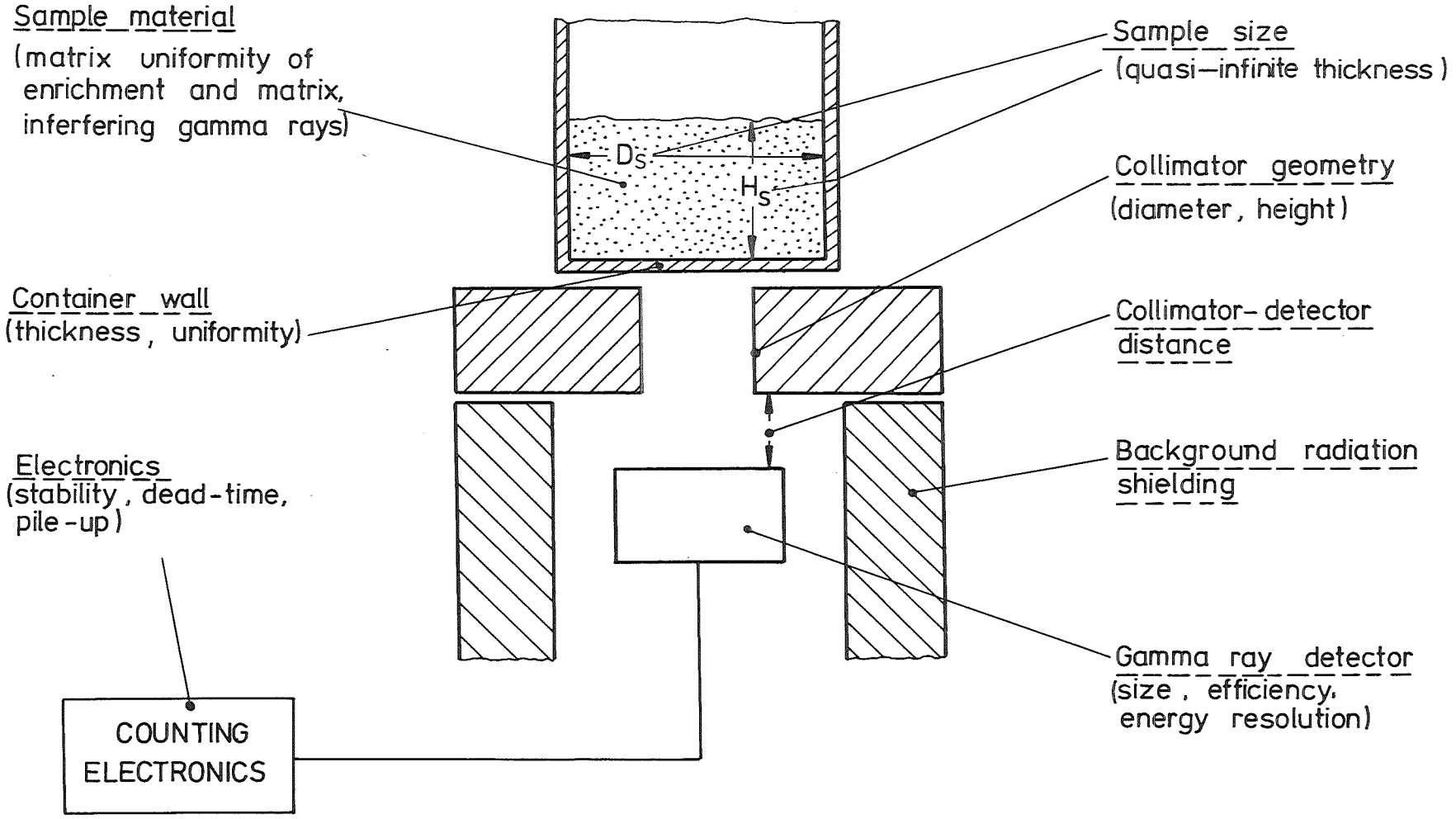

Fig. 2.2 Crucial parameters affecting the accuracy of gamma-spectroscopic ^{235}U enrichment measurements.

$$enr = 100 \cdot \dot{N}_{186} \cdot \frac{4 \cdot \sigma \cdot T_{1/2}}{\ell n\ 2 \cdot P_{186}} \cdot \frac{1}{F \cdot \Omega \cdot \varepsilon} \cdot C_{Ma} \cdot C_{Wa} \cdot C_{El} + C_{Int} \qquad (2.2)$$

$\dot{N}_{186}$ = observed net peak counting rate of 186 keV photons

Nuclear and atomic constants
(σ = photon attenuation cross section at 186 keV for uranium,
$T_{1/2}$ = half-life of ^{235}U,
P_{186} = emission probability of 186 keV photons)

Total efficiency at 186 keV
(F = collimator cross section,
Ω = solid angle formed by collimator and detector,
ε = intrinsic detector efficiency)

C_{Ma} = correction for gamma attenuation in sample matrix materials

C_{Wa} = correction for gamma attenuation in sample container wall

C_{El} = correction for counting rate losses caused by counting electronics

C_{Int} = correction for gamma interference due to photons from uranium isotopes other than ^{235}U

The various terms of eq. 2.2, which are not nuclear constants, are discussed in detail in Chapters 3, 4 and 5 of the manual.

It is evident that for all ^{235}U enrichment measurements three basic prerequisites must be fulfilled in order to arrive at the desired true proportionality between the observed gamma counting rate and the ^{235}U enrichment:

1. "Quasi-infinite" thickness of all samples under assay in a given counting geometry.
2. Uniform ^{235}U enrichment throughout each sample.
3. Constant total efficiency of the counting set-up for 186 keV gamma rays, i.e. invariably fixed detector-collimator geometry.

In most practical applications quantitative corrections will not be possible, if one of these conditions is not met.

Given these basic requirements, the remaining factors influencing the gamma counting rate (and thus the measured ^{235}U enrichment) are:

- gamma attenuation by sample matrix materials,
- gamma attenuation by sample container walls,
- gamma counting rate losses caused by counting electronics, and
- gamma interference.

Corrections for these items are possible, provided additional information is available about the respective parameters such as, e.g., type of the uranium compound, material type and thickness of the container wall, pulse-pair resolving time of the gamma counting system, concentration level of gamma contaminants, etc.

2.4 Need for reference material

Eq. 2.2 shows that the ^{235}U enrichment is almost directly proportional to the 186 keV gamma counting rate observed from a large uniform sample of ^{235}U-bearing material, with the exception of a small offset that accounts for possible interference effects due to gamma contaminants present in the sample. The main proportionality constants can be summarized in two groups:

1. Basic physical constants:
   Half-life of ^{235}U, 186 keV gamma emission probability, and attenuation cross section of uranium for 186 keV photon.
2. Constants depending on the individual gamma counting set-up:
   Collimator-detector geometry, intrinsic efficiency of the gamma detector.

Besides these constants only a few correction factors enter into eq. 2.2, which can be determined with sufficient accuracy in most applications.

Thus, in principle the ^{235}U enrichment could be measured directly without use of any reference materials or calibration standards, provided the physical constants are accurately known,

and the absolute detection efficiency of the gamma counting set-up can be determined precisely. We face, however, at present the following situation:

1. Lack of accurate physical constants

   Both the uncertainty of the nuclear constants (1.5 % relative [7,8]) and the stated error of the photon cross section (2 % to 5 % relative [9]) enter into the determination of the ^{235}U enrichment. These values are far away from the desired accuracy level of 0.1 %.

2. Difficulty of determining the absolute gamma detection efficiency

   A calculation of absolute detection efficiencies will hardly arrive at the desired degree of accuracy. On the other hand, the experimental determination of the absolute detection efficiency of the counting set-up becomes problematic, since gamma-ray standards are presently not commercially available at the desired accuracy level of about 0.1 %. Moreover, point sources commonly used for the efficiency determination of a gamma counting set-up are not suited in this particular case, because the angular characteristic of their radiation is different from that found at the surface of thick radioactive samples (isotropic versus cosine-shaped angular distribution of the radiation).

For the above reasons highly accurate gamma-spectrometric determinations of the ^{235}U enrichment are presently only possible, when the measurements are related to suitable calibration standards.

The Reference Material EC-NRM-171/NBS-SRM-969 now available satisfies the needs for accurate calibration standards for non-destructive ^{235}U enrichment measurements on low-enriched uranium materials. It also provides a valuable means for increasing the harmonization and the compatibility of non-destructive enrichment assays, since the measurements at many places around the world can now be traced to a common reference material.

In this context two alternative methods [10,11] for the gamma-spectrometric ^{235}U enrichment determination should be

mentioned, which utilize the ratio of simultaneously observed gamma responses from ^{235}U and ^{238}U, using different gamma lines from the same spectrum. Both methods, however, suffer from the fact, that they have to employ indirect gamma-ray signatures for ^{235}U and for ^{238}U: high-energy gamma rays from ^{234m}Pa as a measure for ^{238}U in the one method [10], and Th K X-rays and gamma rays from ^{234}Th as a measure for ^{238}U, respectively, in the other method [11]. This leads to specific problems for these measurement techniques, such as

- applicability only for aged uranium > 3 months after separation, or, alternatively, the necessity of significant corrections for non-equilibrium of the ^{238}U descendents ^{234}Th and ^{234m}Pa,
- precise determination of the total relative detection efficiency over a wide energy range [10], and
- evaluation of an unresolved triplett of gamma- and X-rays [11].

However, both methods may be very interesting for many applications because they are less sensitive to sample parameters such as size, geometry, chemical composition and cladding, which are crucial for the "enrichment meter" principle. When used without standards as proposed, one should realize that also these methods rely on physical constants (photon emission probabilities) with the associated uncertainties discussed above. Therefore, the availability of the highly accurate Reference Material may also help to further improve these ^{235}U enrichment assay techniques as a supplement or alternative to the "enrichment meter" principle described in this manual.

2.5 Application of the Reference Material

Ideally, reference materials or physical standards used for the calibration of NDA measurements should be representative of the unknown samples to be measured with respect to all parameters that influence the measurement result. The most

stringent effect observed with gamma-ray measurements is the strong attenuation of the gamma rays in the sample material itself and in the sample cladding. The photon attenuation generally introduces a dependence of the assay result on the sample parameters (such as size, shape, density, matrix composition), and on characteristics of the sample container (such as container material, wall thickness).

In the specific case of ^{235}U enrichment measurements using "quasi-infinitely thick" samples the influence of the sample parameters size, shape and density on the assay result vanishes almost completely. However, effects due to differences in the sample matrix composition and in the container wall still remain. Therefore, in a strict sense, the present Reference Samples are ideally suited only for use with U_3O_8 materials contained in aluminium containers with 2 mm bottom thickness as represented by the empty can delivered along with the RM.

In order to extend the applicability of the Reference Material to the calibration of assay systems used for measurements of other types of uranium samples, correction factors are needed that allow a normalization of the gamma response with respect to differences in the matrix composition and the container wall. Respective correction factors are given in Chapters 3 and 4 of this manual.

It must be emphasized, however, that the correction factors given for gamma attenuation are based on theoretical values for the photon cross sections with stated uncertainties of about 2 % to 5 %. This represents a possible source of systematic errors when the required corrections are large. In those cases it is therefore recommended to validate experimentally the correction terms given, and their range of application, in order to avoid possible systematic errors in the gamma-spectrometric ^{235}U enrichment assays.

The user of the RM should be warned not to expect ultimate measurement accuracy for any type of samples, if crucial sample parameters are not well defined and/or the required corrections are large. To give a practical example: in principle, the Re-

ference Material can be applied for a direct calibration of a counting set-up used for the assay of UF_6 cylinders. But the following specialities of this type of material should be considered with particular care:

- the strong gamma attenuation in the typically 1.5 cm thick container wall requires an experimental determination of the correction factor for absorption (see Sec. 4.2),
- the accurate determination of the wall thickness by means of the ultrasonic thickness gauge may be difficult (rough container wall surface, painting must be removed at the measurement position),
- possible surface deposits at the inner wall of the container and the associated gamma attenuation and gamma interference must be taken into account,
- inhomogeneous distribution of the UF_6 may violate the "quasi-infinite" sample condition (depending on the positioning of the detector),
- the total gamma counting rate and the overall shape of the observed gamma spectrum differs significantly for the two types of samples, thus requiring a careful correction for dead-time and pulse pile-up effects, and a technique for the peak area evaluation that is insensitive to changes in the shape of the background continuum,
- the factor normalizing the gamma response from UF_6 to that of U_3O_8 (see Sec. 3.3.1) is not yet experimentally verified.

In this example it would be therefore recommendable to re-measure, if possible, the UF_6 material after conversion to uranium oxide under well-controlled conditions in order to get an estimate for the uncertainties specific to ^{235}U enrichment measurements of UF_6 cylinders.

For many practical applications it will be desirable to have working standards available that may differ both physically and chemically from the U_3O_8 Reference Samples. In some cases such working standards can be calibrated directly against the

U_3O_8 Reference Samples, provided they can be measured in a counting set-up that assures likewise "quasi-infinite" sample thickness for both types of standards, and appropriate corrections are applied accounting for differing properties of the sample materials and of the sample containers. For other working standards the "quasi-infinite" sample condition may be not fulfilled (as, e.g., for fuel rods). In these cases the ^{235}U enrichment of the raw material used for the production of the working standards can be measured in a "quasi-infinite" thickness geometry against the Reference Material.

Two general conditions limiting the application of the "enrichment meter" principle deserve special attention of the users, and should be carefully examined prior to each gamma-spectrometric ^{235}U enrichment assay:

1. The sample must be "quasi-infinitely" thick for 186 keV gamma rays. This condition inherently restricts the application of the method to relatively thick samples, e.g. for uranium oxides a minimum areal density of about 5.3 $g \cdot cm^{-2}$ is required.

2. The sample material must be very uniform with respect to the ^{235}U enrichment. When mixtures of differently enriched materials are assayed, the sample material must be carefully homogenized prior to the measurement in order to assure that the measured ^{235}U enrichment value is representative for the grand sample mean.

3. PROPERTIES OF THE SAMPLE MATERIAL AFFECTING THE MEASUREMENT ACCURACY

This chapter describes in detail the properties of the sample material that influence the gamma-spectrometric ^{235}U enrichment assay using the "enrichment meter" principle. In particular it comprises effects introduced by the sample size, the sample homogeneity, the type of the uranium compound, the sample matrix material, and the gamma interference due to minor uranium isotopes. Correction terms and figures are given whenever possible. For those parameters which cannot be easily expressed in an analytical form, or which are difficult to quantify (as, e.g., sample inhomogeneity), tolerance limits are defined at the error level of 0.1 % relative.

3.1 The "quasi-infinite" sample size

Unlike other measurement techniques the "enrichment meter" principle requires that the samples to be assayed are sufficiently thick, i.e., that the addition of any amount of uranium material with same enrichment to the sample under assay will not change significantly the flux of the 186 keV gamma radiation observed in a given counting geometry. In this section the conditions for the sample size are discussed that must be fulfilled to keep the relative assay error below a limit of 0.1 %. Special attention is paid to the use of the empty reference can. Recommendations are given for the minimum mass of sample material required, and for the dimensions of the collimator in this case.

3.1.1 "Quasi-infinite" thickness in one direction

Enrichment measurements on the basis of the "enrichment meter" principle will give accurate results only, if the sample under assay is "sufficiently" thick to be opaque for 186 keV gamma rays. As shown in eq. A15 in Appendix A, the 186 keV photon flux at the sample surface seen through a solid angle Ω becomes almost independent of the sample thickness R, if

$$e^{-\int_0^R \lambda(x) \cdot dx} \ll 1, \qquad (3.1)$$

where $\lambda(x)$ is the linear photon attenuation coefficient of the sample material at location x, and R is the linear dimension (thickness) of the sample with respect to the viewing angle Ω.

In order to quantify the term "sufficient thickness", we define a sample as "quasi-infinitely thick" in direction Ω, when the ^{235}U gamma radiation emitted from a fixed sample-surface area reaches 99.9 % of the intensity expected from a really infinitely thick sample within this angle. If a sample meets this condition for any viewing angle Ω and any surface element seen from the gamma detector, then the assay error introduced by its finite size will be definitely less than 0.1 %. Note, that the error limit of 0.1 % used for the definition of "quasi-infinite" thickness is somewhat arbitrary. It has been selected to be comparable to the error limits specified for other parameters of this particular Reference Material.

For a uniform sample material the minimum linear sample dimension r_{min} required for 99.9 % gamma response is obtained from eq. 3.1:

$$e^{-\mu \cdot \rho \cdot r_{min}} = 0.001$$

$$r_{min} = \frac{-\ln 0.001}{\mu \cdot \rho} = \frac{6.91}{\mu \cdot \rho}, \qquad (3.2)$$

where μ is the mass attenuation coefficient, and ρ the density of the sample material.

Linear sample dimensions for 99.9 % response are given in Table 3.1 for some uranium compounds at different density levels. The μ values are taken from Table C2 in Appendix C.

Table 3.1 Linear sample dimensions required for 99.9 % gamma response in one direction.

Uranium compound	Mass attenuation coefficient ($cm^2 \cdot g^{-1}$)	Sample density ($g \cdot cm^{-3}$)	Sample thickness for 99.9 % response (cm)
U metal	1.47	19.0	0.25
UO_2	1.31	1.0	5.27
		2.0	2.64
		11.0	0.48
U_3O_8	1.27	1.0	5.44
		2.0	2.72
		8.3	0.66
UF_6	1.03	1.0	6.71
		4.7	1.43
Uranyl nitrate $UO_2(NO_3) \cdot 6H_2O$	0.77	1.0	8.97
		2.8	3.20

3.1.2 "Quasi-infinite" thickness in all directions seen from a large detector

When we ask for "quasi-infinite" thickness r_{min} of the sample in all directions, in which a large detector sees the sample through a cylindrical collimator (see Fig. 3.1), then the minimum sample height H_s^{all} and the minimum sample diameter D_s^{all} for a cylindrical sample are given by eqs. 3.3a and 3.3b:

$$H_s^{all} = r_{min} \qquad (3.3a)$$

$$D_s^{all} = D_c \cdot \left(1 + \frac{2 \cdot s}{H_c} + \frac{2 \cdot r_{min}}{\sqrt{D_c^2 + H_c^2}}\right), \qquad (3.3b)$$

where H_c is the collimator height, D_c is the collimator diameter, s is the distance between the surface of the sample material and the surface of the collimator including the container wall, and r_{min} is the linear "quasi-infinite" thickness defined in eq.3.2.

The condition for the minimum sample height H_s^{all} in eq. 3.3a can be also expressed in terms of a minimum areal density ρ_{min}^{area} given in $g \cdot cm^{-2}$:

$$\rho_{min}^{area} = \frac{-\ln(0.001)}{\mu} = \frac{6.91}{\mu} \; [g \cdot cm^{-2}], \qquad (3.3c)$$

with the mass attenuation coefficient μ of the sample material given in units of $cm^2 \cdot g^{-1}$.

Note, that eqs. 3.3a, 3.3b and 3.3c are only valid when a uniform sample material is assumed.

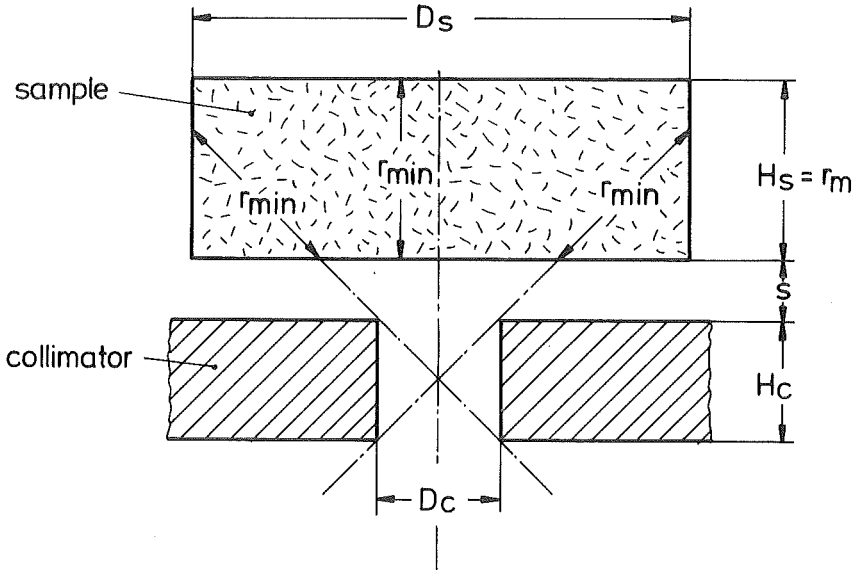

Fig. 3.1 Sample dimensions for "quasi-infinite" sample thickness in all directions visible from a large detector.

In general, the simple relation between counting geometry and "quasi-infinite" sample dimensions given in eqs. 3.3a and 3.3b overestimates significantly the amount of sample material really required for a 99.9 % gamma response, as will be shown in the following section of the manual. On the other hand, when using this approach you will be always "on the safe side". Thus, eqs. 3.a and 3.b may be used as a reliable estimate for the fulfilment of the "infinite-thickness" condition in those cases where enough sample material is available, and the sample container is large enough.

3.1.3 "Quasi-infinite" size for cylindrical samples

When asking for "quasi-infinite" sample thickness in any direction in which the sample is seen by the detector, we normally arrive at sample volumes which are much larger than those required for 99.9 % gamma response, because two factors are not considered in this approach:

1. For a given counting geometry the effective attenuation of 186 keV gamma rays emitted from a sample and viewed through a collimator is better described by their mean path length through the sample material than by the sample thickness. As shown in Fig. 3.2, the mean path length and the associated photon attenuation increase with increasing collimator diameter. Therefore, the sample height required for 99.9 % gamma response is expected to be smaller for wide collimators than for narrow ones. The "quasi-infinite" sample thickness r_{min} defined in eq. 3.2 is required for extremely narrow collimators only.

2. The transmission of 186 keV gamma rays through the collimator is highest for sample material positioned on the symmetry axis of the collimator, it decreases with increasing distance from the symmetry axis because the viewing angle of the collimator exit gets smaller and smaller (see Fig. 3.3). The contribution of sample material far outside the symmetry axis to the observed gamma counting rate is negligibly small. This reduced collimator transmission for "off-axis" material has not been accounted for in Section 3.1.2. We can therefore assume that also the sample diameter D_s^{all} defined in eq. 3.3b is overestimated for 99.9 % gamma response.

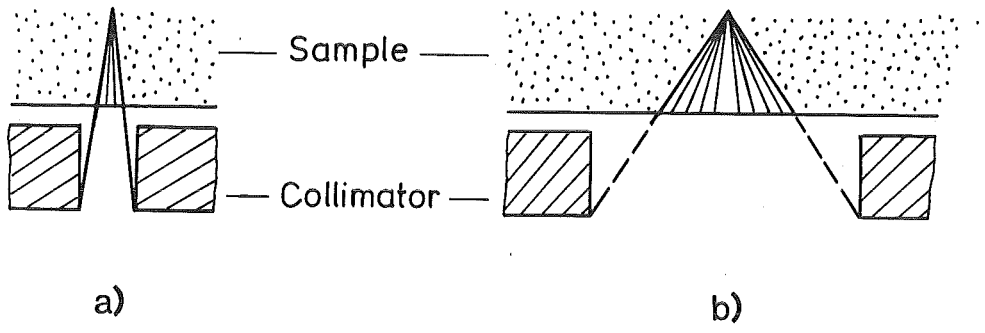

Fig. 3.2 Mean path length of gamma rays through the sample material a) for a narrow collimator, b) for a wide collimator.

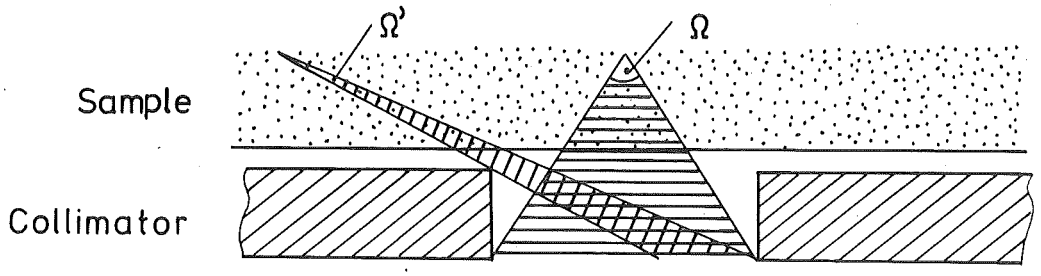

Fig. 3.3 Transmission of gamma rays through a cylindrical collimator.

We therefore expect that the sample dimensions really required for 99.9 % gamma response are generally smaller in size than those dimensions derived from eqs. 3.3a and 3.3b.

Instead of asking for "quasi-infinite" thickness in all visible directions, it is more convenient to define a "quasi-infinite" sample volume that produces 99.9 % of the gamma counting rate expected from an infinite sample.

Considering here only cylindrically shaped samples and collimators with common symmetry axis, we can derive the sample diameter and height, D_s^9 and H_s^9, required for 99.9 % gamma response from the following implicite equation:

$$F(D_s^9, H_s^9) = \frac{I_\gamma(D_s^9, H_s^9, \rho, \mu, D_c, H_c, s, d, \lambda_d)}{I_\gamma(\infty, \infty, \mu, D_c, H_c, d, \lambda_d)} = 99.9\ \%, \qquad (3.4)$$

where the gamma response of the finite sample is compared to that of an infinite sample. D_c is the collimator diameter, H_c is the height of the collimator, s is the distance between the surface of the sample material and the collimator entrance plane, d and λ_d are the thickness and the linear photon attenuation coefficient of the sample container wall, ρ is the density and μ is the photon mass attenuation coefficient of the sample material. More details on the gamma transmission function I_γ are given in Appendix A.

Eq. 3.4 shows that the "quasi-infinite" sample dimensions D_s^9 and H_s^9 are dependent on a large number of parameters that comprise the properties of the sample material (μ, ρ), of the container wall (d, λ_d), and of the counting geometry (s, D_c, H_c).

It should be noted that also the size and the intrinsic efficiency of the gamma detector, and its position relative to the collimator, influences to some extent the "quasi-infinite" sample dimensions, as shown in Sec. 4.2 and Appendix A3. This effect has been neglected here. Thus, in a strict sense, eq.3.4 presents the solution to the problem of "quasi-infinite" sample dimensions with reference to 99.9 % of the gamma rays penetrating the collimator per unit time, rather than to 99.9 % of gamma counting rate observed in the detector. In other words, eq.3.4 is strictly valid only for large-area detectors with uniform efficiency for 186 keV gamma rays, independent of their angle of incidence on the detector.

However, for most collimator-detector arrangements eq. 3.4 yields acceptable estimates of the "quasi-infinite" sample dimensions. Only in a few exceptional and unlikely cases the critical sample dimensions turn out to be different from the solution given in eq. 3.4:

- using a wide collimator and a very thin, large-area detector, or
- using a very small detector (active detector area significantly smaller than the collimator cross section).

The effect of the detector size can be neglected, if the user follows the recommendations for the sample size and the collimator given in the Sections 3.1.4 and 3.1.5 of the manual.

No closed solution has been found for the sample diameters D_s^9 and the sample heights H_s^9 from eq. 3.4. The "quasi-infinite" sample dimensions (D_s^9, H_s^9) giving 99.9 % gamma response have been calculated by numerical integration of eq. 3.4. Because of the relatively high calculational effort necessary, and because of the difficulty to present the multi-parameter relation given in eq. 3.4 in a clearly arranged form, we have restricted all calculations presented in this section to fixed container parameters, using only those of the reference cans, i.e.:

- can bottom of 2 mm aluminum: $\underline{d = 2\ mm}$, $\underline{\lambda_d = 0.329\ cm^{-1}}$,
- an additional distance of 1 mm between collimator and can bottom (due to the recessed bottom form of the reference cans), resulting in a total distance $\underline{s = 3\ mm}$ between collimator and surface of the sample material.

Using these fixed parameters for the sample container, the sample diameters D_s^9 and the sample height H_s^9 giving 99.9 % gamma response have been calculated from eq. 3.4 for several collimator geometries and sample materials. Some of the results are shown in Fig. 3.4 for UO_2, U_3O_8 and UF_6 at various density levels. They are given for a collimator with 4 cm diameter and 2 cm height.

Note, that there is not a single unique sample geometry that gives 99.9 % gamma response for a particular sample material at a particular sample density. Instead, any pair of sample parameters (sample diameter D_s^9, sample height H_s^9) represented by the corresponding curve in Fig. 3.4 satisfies the condition of a "quasi-infinite" sample geometry for the given collimator. This reflects the fact that, starting from a particular sample form giving 99.9 % gamma response, always a second one can be derived by removing a small portion of the sample material from the outer shell of the sample, and by compensating this lack by a larger sample height (see also Table 3.2).

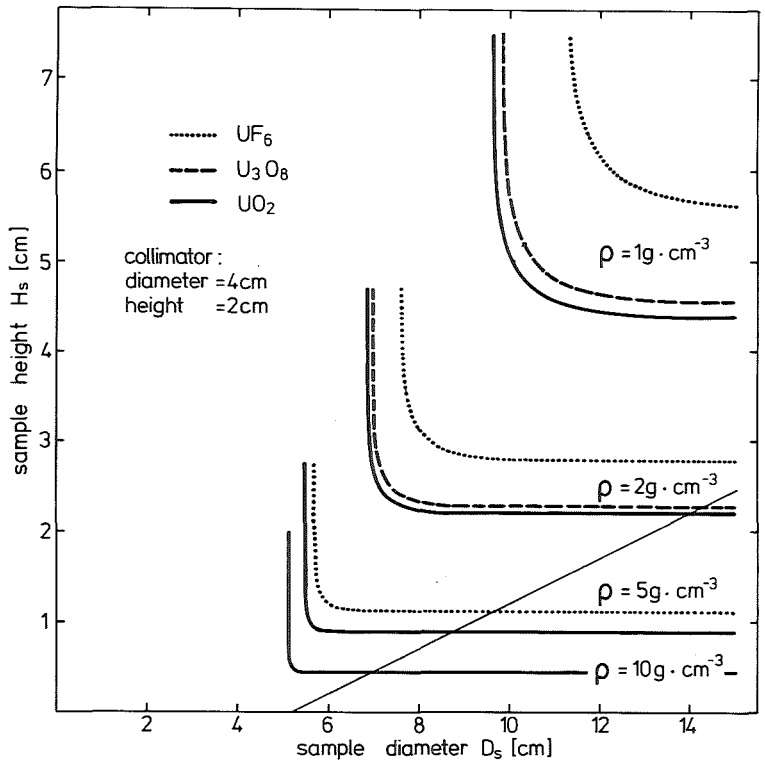

Fig.3.4 Sample dimensions for 99.9 % gamma response given for some uranium compounds at various density levels (from eq. 3.4)

collimator diameter = 4 cm,

collimator height = 2 cm,

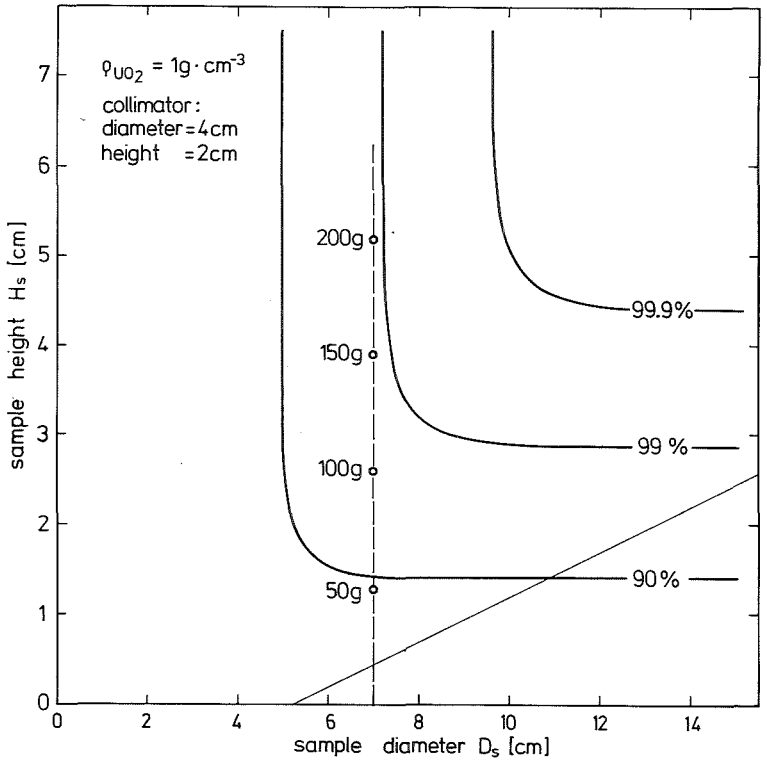

Fig.3.5 Sample dimensions required for 90 %, 99 % and 99.9 % gamma response. (According to eq. 3.4)

UO_2 sample density = 1 g•cm^{-3}

collimator diameter = 4 cm

collimator height = 2 cm

Any ordinate pair (D_s^9, H_s^9) on the curves shown in Fig.3.4 gives exactly 99.9 % gamma response for the respective sample material. Ordinate pairs below the curves give less than 99.9 %, those above the curves give more than 99.9 % gamma response. In order to demonstrate the sensitivity of the gamma response as a function of the sample size, Fig. 3.5 shows the sample dimensions required for 90 %, 99 % and 99.9 % gamma response for UO_2 with a density of 1 $g \cdot cm^{-3}$ and the same collimator as in Fig. 3.4 (collimator diameter 4 cm, collimator height 2 cm). The figure also shows that the amount of sample material must be approximately doubled to reduce the measurement error due to non-infinite thickness by a factor of 10.

Some informations that may be of interest have been added to Figs. 3.4 and 3.5:

- The straight lines starting from the abscissa in the lower right part of Figs. 3.4 and 3.5 indicate the borderline of the "shadow region" of the counting geometry, i.e.: sample volume elements with ordinates below this line are not visible from the detector, and therefore do not contribute to the detected gamma counting rate. Thus, in principle, sample material located in the "shadow region" could be removed without affecting the assay result. This peculiarity may be used to reduce the amount of sample material required for the enrichment assay in cases where the sample mass must be minimized for operational reasons. For this purpose either an insert to the empty reference can having the shape of the "shadow region" may be used, or specially formed empty cans may be supplied by the user, observing the tight specifications for the sample bottom visible from the gamma detector. The sample mass reduction achieved in this way is not included in the minimum sample parameters given in Table 3.2. Note that the form of the "shadow region" is critically dependent on the collimator geometry. It may be deduced from simple geometrical considerations for a particular collimator (see, e.g.,Fig.3.1).
- In Fig. 3.5 the mass and the filling height for UO_2 with a pour density of 1 $g \cdot cm^{-3}$ are given along the dashed line,

Table 3.2 Various sample dimensions and sample masses required for 99.9 % gamma response as function of collimator dimensions calculated from eq. 3.4.

Sample material : U_3O_8 powder,
Sample material density: 2.58 $g \cdot cm^{-3}$
Sample and collimator : Cylindrical shape with common axis,
D_C = collimator diameter,
H_C = collimator height,

Container wall : 2 mm aluminium,
Distance between sample material and collimator entrance plane : 3 mm,
D_s^{min}, D_s, D_s^{RM}, D_s^{all} = sample diameter
H_s^{min}, H_s, H_s^{RM}, H_s^{all} = sample height
W_s^{min}, W_s, W_s^{RM}, W_s^{all} = sample mass

Collimator parameters		True minimum sample parameters			'Approximate-minimum' sample parameters for areal density 5.45 $g \cdot cm^{-3}$			Sample parameters for areal density 5.2 $g \cdot cm^{-2}$			Sample parameters for 99.9 % sample thickness in all directions		
D_C (cm)	H_C (cm)	D_s^{min} (cm)	H_s^{min} (cm)	W_s^{min} (g)	D_s (cm)	H_s (cm)	W_s (g)	D_s^{RM} (cm)	H_s^{RM} (cm)	W_s^{RM} (g)	D_s^{all} (cm)	H_s^{all} (cm)	W_s^{all} (g)
2	1	5.08	2.15	109	5.05	2.18	109	5.19	2.08	110	7.10	2.18	216
2	2	4.21	2.24	78	4.29	2.18	79	4.59	2.08	86	5.68	2.18	138
2	3	3.65	2.28	60	3.78	2.18	61	4.22	2.08	73	4.82	2.18	99
2	4	3.29	2.29	49	3.44	2.18	50	4.14	2.08	70	4.25	2.18	77
3	1	6.34	2.08	165	6.23	2.18	166	6.35	2.08	165	8.93	2.18	342
3	2	5.64	2.16	135	5.63	2.18	135	5.81	2.08	138	7.53	2.18	242
3	3	5.13	2.22	115	5.18	2.18	115	5.50	2.08	123	6.68	2.18	191
3	4	4.75	2.25	99	4.85	2.18	101	5.32	2.08	116	6.06	2.18	157
4	1 *	7.49	2.04	224	7.31	2.18	229	7.42	2.08	225 *	10.63	2.18	483
4	2	6.87	2.11	195	6.78	2.18	197	6.92	2.08	196	9.10	2.18	354
4	3	6.41	2.16	175	6.41	2.18	176	6.61	2.08	178	8.29	2.18	293
4	4	6.08	2.20	159	6.42	2.18	159	6.42	2.08	168	7.68	2.18	252
5	1 *	8.61	2.00	291	8.38	2.18	300	8.48	2.08	293 *	12.27	2.18	644
5	2 *	8.01	2.06	260	7.85	2.18	264	7.98	2.08	260 *	10.55	2.18	476
5	3 *	7.62	2.11	241	7.53	2.18	243	7.70	2.08	242 *	9.74	2.18	406
5	4 *	7.31	2.15	226	7.27	2.18	226	7.49	2.08	229 *	9.15	2.18	358

* These collimators should not be used with Reference Material cans because they deliver less than 99.9 % gamma response
Note: Small inconsistencies of the values given are due to rounding effects of the 3-digit representation.

when the empty reference can with 7 cm inner diameter is used for the assay. It is seen that even 99 % of the gamma response of a really infinite sample is not reached in this counting geometry (collimator diameter 4 cm, collimator height 2 cm), i.e., the relative measurement error is larger than 1 % regardless of the filling height of the 7 cm sample container for this particular density. Thus, either a sample can with a larger diameter or a collimator with a smaller diameter and/or larger height must be used in this case in order to arrive at a "quasi-infinite" sam. ple geometry.

Among all possible cylindrical sample geometries that deliver 99.9 % gamma response for a particular sample material in a given counting set-up, there is one sample form (D_s^{min}, H_s^{min}) that requires the minimum amount of sample material. Such minimum "quasi-infinite" sample dimensions along with the corresponding sample masses are given in Table 3.2 for U_3O_8 powders with a density of 2.5 $g \cdot cm^{-3}$ for various collimator geometries. For comparison, "approximate-minimum" sample dimensions are also shown for fixed areal densities of 5.45 $g \cdot cm^{-2}$ (as recommended in the following section for unknown U_3O_8 samples), and of 5.2 $g \cdot cm^{-2}$ (as specified for the Reference Material samples). The last three columns in Table 3.2 give the sample size and mass for the case that "quasi-infinite" thickness is assumed in all directions visible through the collimator, as discussed in Section 3.1.2 (note that the latter sample geometry delivers more than 99.9 % gamma response). All sample configurations given in Table 3.2 refer to U_3O_8 powder material and to a sample density of 2.5 $g \cdot cm^{-3}$.

When talking about sample dimensions that deliver exactly 99.9 % gamma response, and their associated minimum mass values, one should keep in mind that these "quasi-infinite" sample dimensions can be only defined exactly, if all of the following parameters are well known:

- Type of uranium compound (and sample matrix material).
- Sample density.
- Material type and thickness of container wall.

- Distance between sample material and collimator entrance plane.
- Diameter and height of the collimator.
- Position, size and intrinsic efficiency of the gamma detector.

It should be noted that the evaluation of minimum "quasi-infinite" sample sizes given in this section is restricted to the special case, that the characteristics of the container wall are identical to those of the Reference Samples, i.e., 2 mm aluminium wall thickness and 3 mm distance between sample material and collimator entrance plane. Furthermore, a uniform sample material is assumed.

If one of these masurement conditions changes, then also the minimum sample dimensions required for 99.9 % gamma response will change, e.g.:

- If the distance between sample and collimator is increased, obviously also the minimum sample diameter must be increased to maintain the 99.9 % gamma response.
- If the gamma attenuation in the container wall increases by using, e.g., a 2 mm steel can instead of the 2 mm aluminium reference can, then the minimum sample dimensions turn out to be slightly larger in height and somewhat reduced in diameter due to the higher relative attenuation of 186 keV gamma rays in the container wall originating from "off-axis sample material (see also Appendix A3). However, this effect can be neglected when the user follows the recommendations for the "approximate-minimum" sample height given in the following section, instead of using the true minimum sample dimensions derived from eq. 3.4.

Therefore, the recommendations given in the following sections regarding minimum sample mass and maximum collimator geometry should be applied only to the use of the empty reference can, or to sample geometries that provide the same distance between sample material and collimator surface as the Reference Samples (3 mm). If the sample under assay deviates strongly from the form of the Reference Samples, then either the approach

described in Section 3.1.2 may be used, or eq. 3.4 may be solved for this particular counting geometry in order to arrive at proper estimates for the required minimum sample mass and maximum collimator geometry. Note that the selected collimator geometry must provide the "quasi-infinite" sample condition for both the Reference Samples and the unknown samples to allow a correct calibration of the counting set-up.

3.1.4 Recommendations for minimum sample mass

An examination of the minimum sample heights (see, e.g., Table 3.2), that are required to produce 99.9 % of the gamma radiation obtained from an infinite sample, shows that these values are only slightly different (up to a few percent) from the "quasi-infinite" sample thickness r_{min} defined in Sec.3.1.1. In order to simplify the estimate of minimum sample dimensions, we substitute in further calculations the real minimum sample height H_s^{min} by the linear "quasi-infinite" sample dimension r_{min} given in eq. 3.2. The corresponding sample diameter D_s for 99.9 % gamma response is then obtained from eq. 3.4 by setting $H_s^9 = r_{min}$. This approach has the advantage that the sample height required for 99.9 % gamma response is no longer dependent on the properties of the collimator and of the detector. One can verify that the sample mass in this case is only slightly larger than the true minimum mass (see Table 3.2).

With the new "approximate-minimum" sample height

$$H_s = r_{min} = \frac{-\ln(0.001)}{\mu \cdot \rho} = \frac{6.91}{\mu \cdot \rho} \qquad (3.5)$$

from eq. 3.2 and the - still unknown - sample diameter D_s, we can derive an expression for the mass M_s of the sample material required for 99.9 % gamma response:

$$M_s = \pi \cdot \frac{D_s^2}{4} \cdot H_s \cdot \rho = \frac{\pi \cdot 6.91}{4 \cdot \mu} \cdot D_s^2 = \frac{5.43}{\mu} \cdot D_s^2, \qquad (3.6)$$

where μ is the mass attenuation coefficient of the sample material for 186 keV gamma rays, and ρ is the sample density.

Eq. 3.6 shows that the "approximate-minimum" sample mass defined in this way does not depend on the sample density. It is only a function of the sample diameter D_s and the mass attenuation coefficient μ of the sample material. Thus the question of the sample size necessary for 99.9 % gamma response is reduced to the problem of finding the adequate sample diameter for a given collimator geometry and a given sample material. A general solution of this problem is not given in the manual since the critical sample diameter D_s still depends on too much parameters of the counting geometry and of the sample under assay, as discussed in Section 3.1.3. Instead of this, in the following section the inverse problem is solved for a special case that will be of particular interest for the user: finding the adequate collimator for a given sample material when the empty reference can with 7 cm inner diameter is used for the ^{235}U enrichment assay of unknown samples.

"Approximate-minimum" sample masses for uniform U_3O_8 samples as a function of the sample diameter have been calculated from eq. 3.6. They are displayed in Fig. 3.6. The dashed line represents the diameter of the Reference Sample containers. If uranium compounds U_x other than U_3O_8 are measured, then the "approximate-minimum" sample mass obtained from Fig. 3.6 must be multiplied with a correction term

$$M_s\ (U_x) = \frac{\mu\ (U_3O_8)}{\mu\ (U_x)} \cdot M_s\ (U_3O_8). \qquad (3.7)$$

The mass attenuation coefficients μ for some uranium compounds are given in Table C2 in Appendix C.

Note: The determination of the "approximate-minimum" sample mass is based on the assumption that the density of the sample material is uniform. This restricts the applicability of eq. 3.6 to fairly homogeneous sample materials. When using minimum-dimensioned samples it is recommended to control visually the homogeneous filling of the empty can prior to the measurement. Moreover, it is a good practice to apply a safety margin to the "approximate-minimum" sample mass values given in this section in order to account for remaining inhomogeneities of the sample density. For most uranium powder materials a

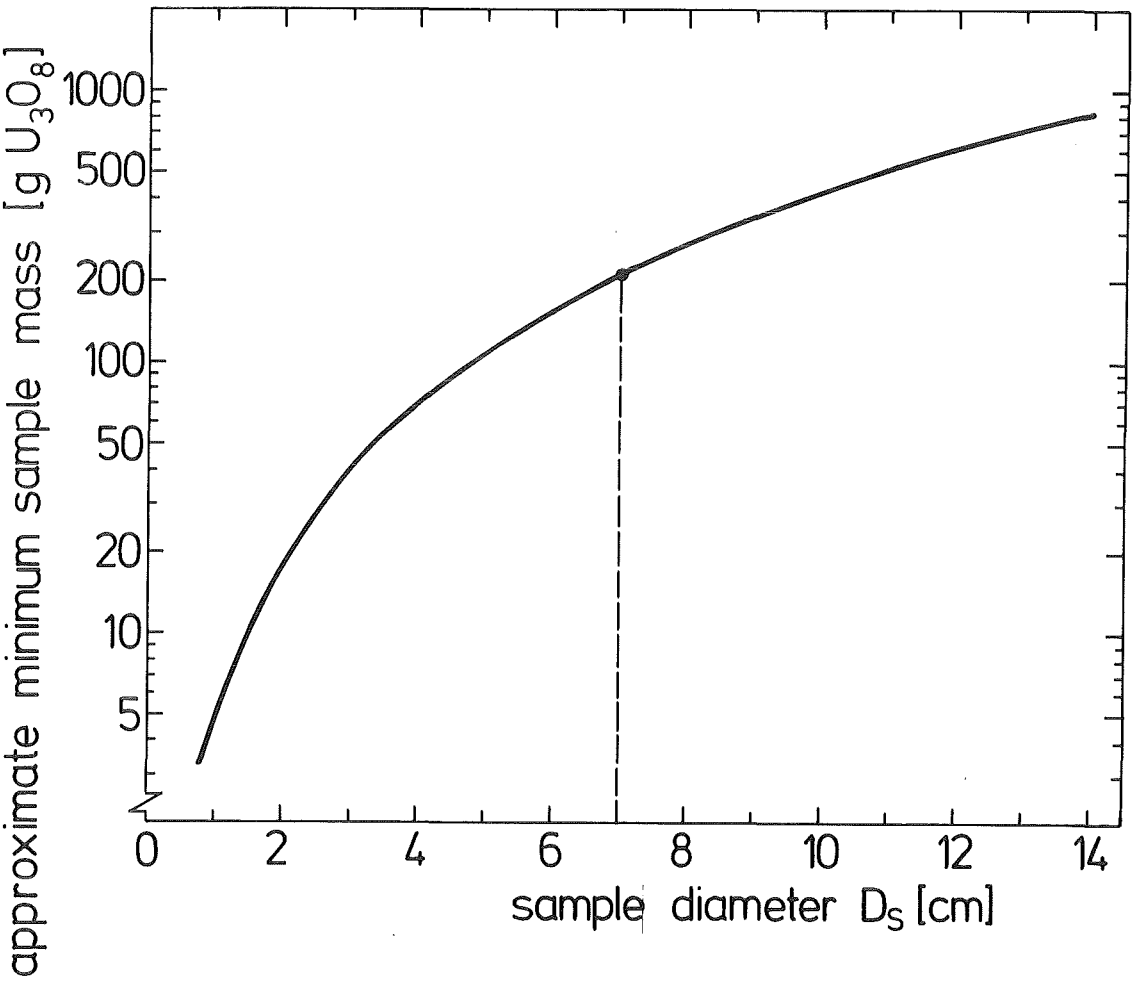

Fig. 3.6 "Approximate-minimum" U_3O_8 sample mass required for 99.9 % gamma response as a function of the sample diameter.

safety margin of about +5 % to +10 % seems to be sufficient.

In case of highly non-uniform samples, such as an assembly of pellets, eq. 3.6 is not applicable. The minimum amount of material required for accurate ^{235}U enrichment assays must then be determined experimentally by adding successively more and more material to the sample under assay until the observed 186 keV gamma counting rate will no longer increase. Further information about requirements for sample homogeneity is given in the following Section 3.2 of the manual.

When using the empty reference can with 7 cm inner diameter for the ^{235}U enrichment assay of an uniform sample material, the

"approximate-minimum" sample mass (in gram) from eq. 3.6 evaluates to the simple form:

$$W_S\ (D_s = 7\ cm) = \frac{\pi \cdot 6.91}{4 \cdot \mu} \cdot 7^2 = \frac{266}{\mu}\ [g], \qquad (3.8)$$

with the mass attenuation coefficient μ of the sample material given in units of $cm^2 \cdot g^{-1}$.

From eq. 3.8 we obtain the "approximate-minimum" values of the sample mass for UO_2 and U_3O_8 powders, if the empty reference can is used for the assay:

$M_s\ (D_s = 7\ cm) = 202.5\ g$ for UO_2 powder, and
$M_s\ (D_s = 7\ cm) = 209.7\ g$ for U_3O_8 powder.

Applying a safety margin of + 10 % we finally arrive at the recommended minimum sample mass M_s^{recom} for the reference can:

$M_s^{recom}\ (D_s = 7\ cm) = 220\ g$ for UO_2 powder, and
$M_s^{recom}\ (D_s = 7\ cm) = 230\ g$ for U_3O_8 powder.

These recommended minimum sample mass values are not dependent on the sample density, i.e., any amount of U_3O_8 powder greater than 230 gram, regardless of its density, is suited for enrichment measurements using the empty reference can, provided a fairly uniform distribution of the material in the reference can is assured. However, the adequate collimator geometry must be selected according to the sample density as shown in the next Section 3.1.5.

It must be noted that there seems to be a discrepancy between the recommended minimum sample mass of 230 g U_3O_8 and the amount of only 200 g U_3O_8 powder contained in the Reference Samples. This discrepancy can be solved considering two facts:

1. The Reference Samples have been prepared very carefully in order to assure a uniform density of the sample material. Even local non-uniformities of the areal density do not exceed $\pm$ 5 % as verified by gamma transmission experiments [1]. Therefore, no safety margin is required.

2. It is shown in Section 3.1.3 that within certain limits many sample dimensions (H_s^9, D_s^9) deliver 99.9 % gamma response. The dimensions of the Reference Samples are well within these limits. The only consequence of the lower mass contained in the Reference Samples is, that the maximum tolerable collimator dimensions for the Reference Samples will be slightly different from those of the samples with "approximate-minimum" dimensions. This effect has been taken into account in the recommendations given for the collimator dimensions in Section 3.1.5 and in Fig. 3.7.

Therefore, we can assume that for nearly all commonly used collimator geometries the Reference Samples fulfill the conditions required for 99.9 % gamma response. This has been also proven by measurements [1]. Limitations and recommendations for the selection of suitable collimator dimensions are given in Section 3.1.5. Only in the very unlikely case of extreme narrow and high collimators the "quasi-infinite" sample condition is not strictly fulfilled for the Reference Samples. But even in this case the gamma response of the Reference Samples still reaches 99.86 % of an infinite sample. Taking also the limit specified for local density inhomogeneities of the Reference Samples (- 5 %) into account, we arrive at a worst-case estimate of 99.81 % gamma response for a "needle-form" collimator. However, in practical applications such narrow collimators are not used because of their extremely low gamma transmission and, accordingly, the very long counting times required.

Note, that in many practical applications of the "enrichment meter" principle there generally exists a small systematic error, which is caused by the finite size of the samples, including the Reference Samples. Fulfilment of the "quasi-infinite" sample condition as defined in this manual means that the sample size is equal to or exceeds the dimensions required to achieve 99.9 % of the gamma response obtained from an infinite sample. Thus, if we compare the gamma counting rates from two differently sized samples both fulfilling the "quasi-infinite" sample condition - as we do in most applications using the Reference Material and an unknown sample - we must be aware that small deviations

below the error level of 0.1 % may still remain that are introduced by differing sample dimensions and/or differing sample densities. The recommendations regarding the sample size and the collimator geometry given in this section will only ensure that this error is less than 0.1 % relative. However, the exact value of the error within the 0.1 % limit, and the sign of the deviation, cannot be easily predicted.

If it happens in practice that samples are measured which are almost infinitely thick (e.g., large powder cans, UF_6 cylinders), then a correction factor of around 1.0005 to 1.001 should be applied to the measured enrichment value that accounts for the finite size of the Reference Samples used for the calibration of the assay system.

3.1.5 Recommended collimator dimensions for sample cans with 7 cm inner diameter

When using sample cans with a fixed inner diameter of 7 cm for the gamma-spectrometric ^{235}U enrichment assay, then also the "approximate-minimum" amount of sample material M_s is fixed, regardless of the material density, as shown in eq. 3.6. As derived in the preceding section, the "appropriate-minimum" sample mass is, e.g., 203 g UO_2 powder or 210 g U_3O_8 powder for all powder densities. Evidently, any sample mass exceeding these minimum values will also fulfill the condition of the "quasi-infinite" sample size, i.e., it will deliver more than 99.9 % of the 186 keV gamma rays that are expected from a really infinite sample.

Once the sample diameter (here 7 cm) and the density of the sample material is given, then only the collimator dimensions must be selected according to the density of the sample under assay in order to satisfy the "quasi-infinite" sample condition. When selecting the collimator, one should also consider that the collimator geometry determines the expected 186

keV gamma counting rate: Smaller collimator diameters and larger collimator heights result in lower gamma counting rates, i.e. longer measurement times. Therefore, the optimum choice will be a collimator that satisfies the condition of "quasi-infinite" sample geometry at the highest possible gamma transmission for a given sample density.

Both informations can be taken from Fig. 3.7. It displays the number of 186 keV photons observed at the collimator exit in units of photons per second and per % ^{235}U enrichment as a function of the collimator diameter for 4 different collimator heights (1 cm, 2 cm, 3 cm and 4 cm). Upper limits of the collimator dimensions that provide "quasi-infinite" sample geometry are represented by dashed lines in Fig. 3.7 for several U_3O_8 sample densities: all collimator dimensions below a dashed line given for a particular sample density do meet the "quasi-infinite" sample condition for this density and all higher sample densities. Collimator dimensions above this line may give rise to systematic errors > 0.1 % for this and any lower sample density, and should not be used. Note: though the upper limits are given for "approximate-minimum" sample geometries defined in section 3.1.4, they obviously hold also for larger samples as, e.g., for the recommended minimum-mass samples.

Collimator geometries in the shaded region in Fig. 3.7 should not be used because they do not provide "quasi-infinite" sample geometry for the Reference Samples. Note, that the border line of this region is slightly lower than the upper-limit curve given for "approximate-minimum"-mass samples having the same density of 2.5 $g \cdot cm^{-3}$ as the Reference Samples. This is due to small sample mass differences for both types of samples (200 g U_3O_8 for the Reference Samples versus 210 g U_3O_8 for the "approximate-minimum" mass samples). The Reference Samples do fulfill the "quasi-infinite" sample condition for all collimator geometries outside the shaded region in Fig. 3.7.

The values given in Fig. 3.7 for the number of 186 keV photons transmitted per second through the collimator include

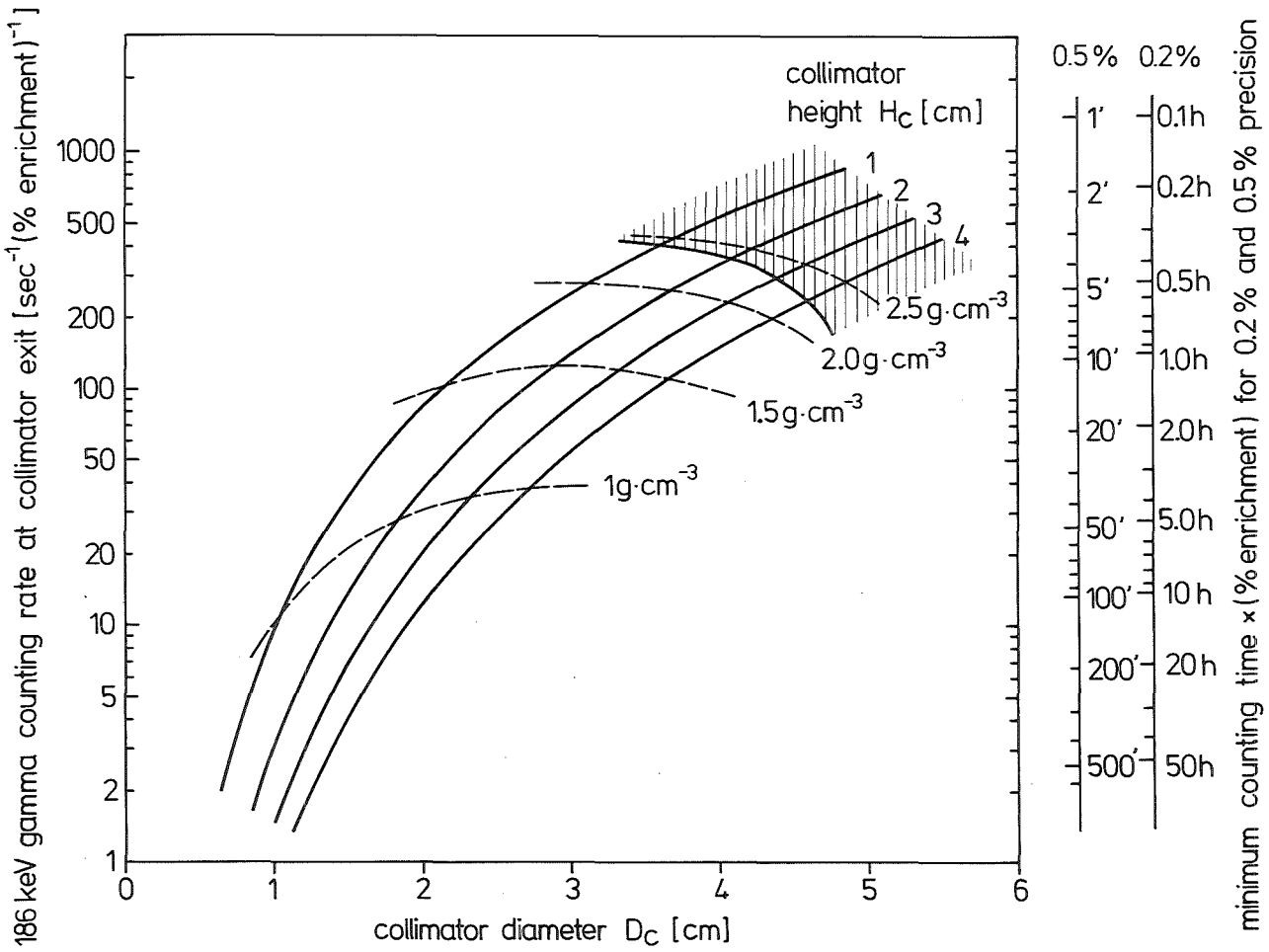

Fig. 3.7 Recommended collimator dimensions, expected counting rates and approximate counting times.
Upper limits for collimator dimensions given by dashed lines refer to the indicated U_3O_8 material density, and to standard sample containers with 7 cm inner diameter. Collimator geometries in the shaded region do not fulfill the "quasi-infinite" sample condition for the Reference Samples EC-NRM-171/NBS-SRM-969.

the correction for the gamma absorption in the 2 mm thick aluminium bottom of the reference cans. The figures given account also for the distance of 1 mm between collimator entrance plane and the can bottom due to the recessed bottom form of the reference cans, which results in a total distance of 3 mm between sample material and collimator.

Note, that the number of 186 keV gamma rays observable at the collimator exit is not identical to the number of photons really registered by the gamma detector in the 186 keV photopeak. In order to allow a rough estimate of the counting time required for counting precisions of 0.5 % and 0.2 %, we have made the somewhat arbitrary assumption that the total peak efficiency of the gamma detector at 186 keV is 50 %. This value is a reasonable approximation for commonly used germanium detectors with an active area comparable to the cross section of the collimator. It may be significantly lower for smaller germanium detectors (see, e.g., Fig. 4.3), and may be slightly higher for large-area NaI detectors. The approximate measurement times required for counting precisions of 0.5 % and 0.2 % per percent ^{235}U enrichment are shown on the right-hand scales in Fig. 3.7. Note, that the counting time is given for 1 % enriched U_3O_8 powder. Thus, for 2 % enriched uranium the values must be devided by a factor of 2, for 3 % enriched uranium by a factor of 3 etc. For compounds having a lower uranium mass fraction than U_3O_8, e.g. UF_6, the gamma emission rate will be slightly lower, and the corresponding counting time will be slightly longer.

It must be stressed that the figures given for the counting time are only rough estimates. In particular, it should be noted that the compton background below the 186 keV peak contributes to the statistical error of the net-peak counting rate. This effect is neglected here. It may present a significant part of the total counting error in case of aged natural and depleted uranium materials.

As seen in Fig. 3.7, the collimator dimensions required for 99.9 % gamma response depend strongly on the density of the uranium material under assay. In practice it will often happen

that the ^{235}U enrichment assay system to be calibrated with the Reference Samples is used for enrichment measurements of samples with varying material density. In this case the selected collimator dimensions must guarantee "quasi-infinite" sample geometry for the full range of expected sample material densities, including the density of the Reference Samples.

As an example, in Tab. 3.3 the relevant collimator parameters are extracted from Fig. 3.7 for a minimum sample density of 1 $g \cdot cm^{-3}$. The maximum observable 186 keV photon counting rate and the rough estimates for the measurement time required for counting precisions of 0.5 % and 0.2 % per percent ^{235}U enrichment are also given in the Table.

Table 3.3 Collimator dimensions, maximum 186 keV gamma counting rates and approximate measurement times for a U_3O_8 sample with a ^{235}U enrichment of 1 % and a density of 1 $g \cdot cm^{-3}$, measured using the empty reference can.

Collimator height (cm)	Maximum collimator diameter (cm)	Maximum 186 keV gamma counting rate (counts$\cdot s^{-1} \cdot$(%enr)$^{-1}$	Counting time per % enr for rel.counting errors 0.5 %	0.2 %
1	1.04	11	121′	12.6 h
2	1.83	28	48′	5.0 h
3	2.31	35	38′	4.0 h
4	2.73	38	35′	3.7 h

All collimator geometries given in Tab. 3.3 fulfill the "quasi-infinite" sample condition for sample densities > 1 $g \cdot cm^{-3}$. As seen from the Table, a collimator with 4 cm height and 2.73 cm diameter provides the best choice for optimum counting rate in this case. At higher sample densities, other collimator dimensions may show better counting rate performance (see Fig. 3.7). We deduce from the data given in Tab. 3.3 that, e.g., for uranium material with 3 % ^{235}U enrichment approximate counting times of 10 minutes and of about 1 hour will be necessary to arrive at counting precisions of 0.5 % and 0.2 %, respectively.

If the counting time turns out to be too long for practical assay purposes, then a collimator with a larger diameter and/or a smaller height must be used. This, in turn, necessiates

- either an increase of the density of the sample material, e.g., by compressing the sample material under assay to a higher density level (a warning must be given here not to deform the carefully prepared bottom window of the empty can!),
- or the use of sample containers with a larger diameter.

In the latter case more than the amount of 230 gram U_3O_8 powder recommended for use with the empty reference can is necessary to maintain the "quasi-infinite" sample geometry (see Section 3.1.4 for more details).

In general, a higher material density allows the use of a larger collimator diameter, which, in turn, increases the observable 186 keV gamma counting rate, thus reducing the counting time required for a particular counting precision. To give a practical example: we assume again that the empty reference can (7 cm inner diameter) is used, but that the minimum density of all sample materials under assay is now $\geq$ 2.5 g·cm^{-3}. Then the optimum collimator dimensions deduced from Fig. 3.7 are

1 cm (2 cm) collimator height and
3.6 cm (4.1 cm) collimator diameter.

Approximate assay times necessary for counting errors of 0.5 % and 0.2 % are now

3.3 minutes (3.8 minutes) for 0.5 % error and
21 minutes (24 minutes) for 0.2 % error,

respectively, for 1 % enriched material. (The values given in brackets correspond to a collimator with 2 cm height. The enlarged collimator thickness provides a better shielding against the high-energy gamma rays from ^{238}U at the cost of a slightly reduced 186 keV gamma counting rate.) A comparison of the counting times with those given in Table 3.3 for a minimum sample

density of 1 $g \cdot cm^{-3}$ shows that the counting time can be reduced by about a factor of 10 by increasing the minimum sample density from 1 $g \cdot cm^{-3}$ to 2.5 $g \cdot cm^{-3}$, and by selecting the appropriate collimator dimensions.

Fig. 3.7 can be utilized also to determine the suitable collimator geometries if uranium compounds other than U_3O_8 are measured in the empty reference can. In this case, instead of using the true sample density ρ_x of the uranium compound x under assay, an effective sample density ρ_{eff} must be applied in Fig. 3.7:

$$\rho_{eff} = \frac{\mu(x)}{\mu(U_3O_8)} \cdot \rho_x, \qquad (3.9)$$

where $\mu(x)$ and $\mu(U_3O_8)$ denote the mass attenuation coefficients of the uranium compound x and U_3O_8, respectively. For UO_2, e.g., the μ ratio in eq. 3.9 evaluates to a value of 1.035, which is very close to 1. Therefore, Fig. 3.7 may be directly used for both types of uranium oxides, UO_2 and U_3O_8, as well.

It should be finally noted that the use of minimum sample dimensions or maximum collimator geometries in a counting set-up requires a careful positioning of the sample in order to maintain the "quasi-infinite" sample geometry.

3.2 Sample inhomogeneities

All of the considerations in the previous section of this chapter were based on the assumption, that the sample material is uniform with respect to the parameters enrichment and matrix composition, or, more precisely, that the ratios

$$^{235}U \text{ atoms}/U_{total} \text{ atoms, and}$$
$$\text{matrix atoms}/U_{total} \text{ atoms}$$

are constant for any sub-sample taken from the grand sample under assay. However, particles or domains with different ^{235}U enrichment and/or different matrix composition within the sample can introduce significant errors to the gamma-spectrometric enrichment assay.

Note, that in contrast to this, sample density inhomogeneities can be neglected for enrichment assays based on "infinite thickness" geometry. Even cavities in the sample material do not affect the assay result as long as the "quasi-infinite" thickness geometry is maintained by sufficient material "behind" the cavity.

For samples with non-uniform enrichment or matrix the gamma-spectrometric assay result depends in a complex manner on the form, the size, the degree and the position of the inhomogeneities in the sample. Thus, we will discuss here only some general aspects of the problem. Let us first define the conditions with respect to homogeneity, which a bulk uranium sample has to satisfy for assuring a representative enrichment measurement.

3.2.1 Homogeneity requirements for representative enrichment measurements

Due to the high photon self-attenuation of uranium materials most of the observed 186 keV gamma rays emerge from a thin layer near the sample surface facing the detector. This fact leads to rather stringent requirements for the sample homogeneity with respect to ^{235}U enrichment and matrix composition, if representativeness of the measured enrichment value for the whole sample is to be assured.

Assume that F is the sample area viewed by the gamma-ray detector. Then the sample volume that produces about 50 % of the registered 186 keV gamma radiation is approximately given by

$$V_{50} = F \cdot \Lambda \quad , \tag{3.10}$$

where $\Lambda = \frac{1}{\mu \cdot \rho}$ is the mean free path length of the gamma rays in the sample, μ is the mass attenuation coefficient for 186 keV photons, and ρ is the density of the material under assay. Values for Λ vary, e.g., from 0.03 cm for uranium metal to 1 cm for UO_2 powder with a density of 0.7 $g \cdot cm^{-3}$.

If the enrichment value determined by gamma spectrometry shall be representative for the grand sample within the error limits of 0.1 % relative, then the enrichment of the surface layer V_{50} must be representative for the whole sample within these error limits, or, in other words, the mean enrichment value of any sub-sample with volume V_{50} or its mass equivalent, taken from the grand sample, should not deviate by more than 0.1 % relative from the mean enrichment of the grand sample.

A similar condition can be derived for the degree of matrix inhomogeneities, taking into account the impact of matrix material on the enrichment assay result as described below in section 3.3 of this chapter. The ratio of matrix mass / uranium mass in any sub-sample of volume V_{50} should not vary by more than 1 % for low Z matrix material, or not more than 0.1 % for heavy elements to keep the relative assay errors < 0.1 %.

Note: These general conditions for the sample homogeneity only assure that the measured enrichment is representative for the whole sample. They do not give, however, tolerance limits for local inhomogeneities.

In order to illustrate consequences of the above conditions for maximum permissable local inhomogeneities, we shall briefly discuss two different types of inhomogeneities, which may be of some practical relevance.

3.2.2 Inhomogeneity in form of a layer at the sample surface

This presents the worst case for gamma-spectrometric enrichment assays. We consider a thin layer of sample material at the sample surface with enrichment enr_ℓ differing from the mean enrichment enr of the rest of the sample. Then the following estimate holds for the maximum thickness ℓ_{max} of the layer for relative assay errors $\leq$ 0.1 %:

$$\left|\frac{enr_\ell - enr}{enr}\right| \cdot \ell_{max} <= 0.001 \cdot \Lambda \,, \qquad (3.11)$$

where Λ is the mean free path length for 186 keV gamma rays in the layer.

To give an extreme example: if the ^{235}U enrichment of the surface layer is 50 % lower or higher than the mean enrichment of the rest of the sample (e.g., 1.5 % or 4.5 % ^{235}U enrichment of the surface layer, 3 % ^{235}U enrichment of the rest of the sample) then the following values for the thickness ℓ_{max} of such a layer should not be exceeded for assay errors < 0.1 % relative:

ℓ_{max} = 0.7 µm !! for U metal, and

ℓ_{max} = 22 µm for UO_2 with a density of 0.7 $g \cdot cm^{-3}$.

In case of a surface layer with <u>different matrix</u> we get a similar relation for the maximum tolerable layer thickness ℓ_{max}:

$$\left| \frac{\frac{1}{\beta_\ell} - \frac{1}{\beta}}{\frac{1}{\beta}} \right| \cdot \ell_{max} <= 0.001 \cdot \Lambda, \qquad (3.12)$$

where β_ℓ and β are the matrix attenuation factors for the layer and the rest of the sample, respectively. The matrix attenuation factors will be defined in eqs. 3.16 and 3.16a in section 3.3. They are tabulated for some typical uranium compounds in Table 3.4.

For example, assume that the surface layer is pure U_3O_8 and the rest of the sample is pure UO_2 of same enrichment. Then the tolerance values ℓ_{max} for the thickness of the U_3O_8 layer are:

ℓ_{max} = 2.0 mm for a U_3O_8 density of 1 $g \cdot cm^{-3}$, and
ℓ_{max} = 0.8 mm for a U_3O_8 density of 2.5 $g \cdot cm^{-3}$.

The numerical examples given demonstrate that surface layers formed of sample material with an ^{235}U enrichment or with a matrix differing from the grand sample mean may give rise to significant errors in gamma-spectrometric ^{235}U enrichment assays.

In practical applications the effect of the formation of a surface layer with an enrichment or matrix differing from the grand sample mean may occur, when the sample material is a mixture of two powders with different enrichment or matrix composition, and when the two powders differ significantly with respect to particle size and/or particle density. In this case the powder material with smaller particle size and/or higher particle density will accumulate at the bottom of the sample container (powder segregation), especially, when the sample is exposed to vibrations. In particular, extreme care has to be taken if blended powders with different ^{235}U enrichments are measured. The material must be carefully homogenized prior to the measurement in order to assure a uniform distribution of the different materials throughout the sample.

3.2.3 Maximum tolerable particle size in well homogenized powders with non-uniform enrichment or matrix

A rough estimate of the maximum tolerable particle size can be derived from statistics following the binominal distribution. We neglect here gamma-absorption effects and make the following simplifying assumptions:

- The sample is composed of particles with equal size, density and matrix composition.
- Two types of particles are present in the sample: type 1 with enrichment enr_1 and type 2 with enrichment enr_2.
- The mean enrichment of the grand sample is enr.
- The number of particles in the sample is very large.
- The two types of particles are randomly distributed in the sample.

Similar to the sampling problem when drawing black and white spheres out of a box, we get an estimate for the minimum number of particles required for a sub-sample whose mean enrichment does not differ from the grand sample mean enr by more than 0.1 % relative:

$$N_{min} = 10^6 \cdot \left| \frac{enr_1 - enr}{enr} \right| \cdot \left| \frac{enr_2 - enr}{enr} \right| . \qquad (3.13)$$

From this we can estimate the maximum diameter of the particles, remembering that the sample volume V_{50} defined in subsection 3.2.1 contributes about 50 % to the observed 186 keV gamma-ray counting rate. Thus, V_{50} should contain at least N_{min} particles. Dividing V_{50} into N_{min} equal cubes we arrive at a rough estimate for the maximum particle diameter D_{max}:

$$D_{max}^3 = \frac{V_{50}}{N_{min}} = \frac{F}{\mu \cdot \rho \cdot N_{min}} ,$$

$$D_{max} = \sqrt[3]{\frac{F}{\mu \cdot \rho \cdot N_{min}}} . \qquad (3.14)$$

For example, if the visible sample area F is 10 cm^2, and the sample material is a homogeneous mixture of 50 % UO_2 powder with 0.7 % ^{235}U enrichment and 50 % UO_2 powder with 4 % ^{235}U enrichment resulting in a mean enrichment of 2.35 %, then the minimum number of particles N_{min} in the volume V_{50} is given by eq. 3.13:

$$N_{min} = 493\ 000,$$

and the particle size D_{max} should not exceed

$D_{max} = 375\ \mu m$ for a UO_2 density of 0.7 $g \cdot cm^{-3}$, and

$D_{max} = 275\ \mu m$ for a UO_2 density of 2.5 $g \cdot cm^{-3}$

in order to keep the assay error below 0.1 % relative.

In a similar way we get an estimate of the minimum number of particles in case of a non-uniform sample matrix composition:

$$N_{min} = 10^6 \cdot \left| \frac{\frac{1}{\beta_1} - \frac{1}{\beta}}{\frac{1}{\beta}} \right| \cdot \left| \frac{\frac{1}{\beta_2} - \frac{1}{\beta}}{\frac{1}{\beta}} \right| , \qquad (3.15)$$

where β_1, β_2 and β are the matrix attenuation factors of the two types of sample matrix materials and of their grand sample mean value, respectively. The maximum tolerable particle diameter is then given in eq. 3.14.

For example, in a mixture of 50 % U_3O_8 powder and 50 % UO_2 powder with equal enrichment and equal density the particle diameter should be less than D_{max}:

D_{max} = 1.8 cm for a sample density of 1 $g \cdot cm^{-3}$, and

D_{max} = 1.3 cm for a sample density of 2.5 $g \cdot cm^{-3}$,

assuming again a visible sample area of 10 cm^2.

This example demonstrates that the particle size in uniform UO_2/U_3O_8 mixtures is not a critical parameter for ^{235}U enrichment measurements. However, care must be taken for possible powder segregation as discussed in the previous section.

Summarizing the content of this section we can state that even a carefully homogenized sample material will not guarantee an accurate assay result, if the sample material is a mixture of coarse-grained particles with <u>different ^{235}U enrichment.</u> This excludes, in particular, the application of gamma-spectrometric ^{235}U enrichment assays to samples composed of large particles (e.g. pellets) with significantly different ^{235}U enrichments, except when a very large number of particles (large compared to N_{min}) is viewed by the gamma detector in a "far-distance geometry".

By contrast, an assembly of pellets with <u>equal enrichment</u> and matrix composition can be considered as uniform with respect to gamma-spectrometric ^{235}U enrichment assays, if the pellets are properly arranged to provide "quasi-infinite" sample thickness. This may be achieved by using a large number of pellets randomly filled into a sample container, or by arranging the pellets as a layer of densely packed items. Note, that two or more of such layers must be stacked to guarantee infinite thickness for any viewing angle, and to avoid open channels between the pellets. Then the enrichment assay result for the pellet assembly is expected to be identical to that obtained from powder material having same enrichment and matrix composition.

When the uniformity requirements are met for a sample under assay, then the measured enrichment value is considered as representative for the whole sample volume. Any corrections that have to be applied to the assay result, as, e.g., the matrix attenuation correction, then refer to the grand sample mean values of the respective sample parameters.

3.3 Sample matrix composition

All elements other than uranium present in the sample material are considered here as matrix material. Obviously, the attenuation of photons in the matrix material reduces the observed 186 keV gamma-ray flux at the sample surface, and thus influences the measured ^{235}U enrichment value. This influence is described by the matrix attenuation factor ß derived in Appendix A:

$$ß = \frac{1}{1 + \sum_{i \neq U} \frac{N_i \cdot \sigma_i}{N_U \cdot \sigma_U}} \qquad (3.16)$$

for the case that the matrix is given in terms of atom fraction N_i/N_U, or, equivalently,

$$ß = \frac{1}{1 + \sum_{i \neq U} \frac{\rho_i \cdot \mu_i}{\rho_U \cdot \mu_U}} \qquad (3.16a)$$

if the matrix is given as mass fraction ρ_i/ρ_U of uranium. ρ_i/ρ_U are the mass ratios, N_i/N_U are the atom ratios, μ_i and μ_U are the mass attenuation coefficients, and σ_i and σ_U are the photon attenuation cross sections for matrix material i and uranium, respectively. The summation extends over all matrix elements i.

If the U_3O_8 Reference Samples are used for the calibration of the enrichment assay system, then the ^{235}U enrichment values measured from unknown samples with different matrix com-

position need to be normalized relative to U_3O_8:

$$enr = enr_{measured} \cdot C_{Ma} \quad , \tag{3.17}$$

where C_{Ma} denotes the normalization factor. This implies, of course, that the matrix of the samples under assay must be known in order to permit the necessary corrections.

The matrix correction factor C_{Ma} has been separated into three terms that account for the three major contributions to matrix attenuation, namely

1. different uranium compounds and stoichiometry variations,
2. sample impurities, and
3. moisture content:

$$C_{Ma} = C_{compound} \cdot C_{impurity} \cdot C_{moisture}. \tag{3.18}$$

Examples of the various types of gamma-ray attenuation by matrix material are described in the following three sections in more detail.

3.3.1 Uranium compounds and stoichiometry

The matrix attenuation factor ß has been calculated for some typical uranium compounds. The ß values are listed in Table 3.4 together with the expected change of the 186 keV gamma-ray counting rate relative to U_3O_8. The corresponding uranium-compound correction factors

$$C_{compound} = \frac{ß(x)}{ß\ (U_3O_8)} = \frac{1 + \dfrac{8 \cdot \sigma_O}{3 \cdot \sigma_U}}{1 + \sum\limits_{i \neq U} \dfrac{N_i(X) \cdot \sigma_i}{N_U(X) \cdot \sigma_U}} \quad , \tag{3.19}$$

which normalize the gamma response of the sample material X to that of U_3O_8, are also given in the Table (notations in eq.3.19 are the same as for eq. 3.16). The attenuation cross sections σ are are taken from Tab. C1 in Appendix C.

Note: Since the values of the correction factors given in Tab. 3.4 are based on atomic cross sections with stated errors in the order of 5 %, it is recommended to verify experimentally the correction terms, particularly, if materials other than uranium oxides are measured.

Table 3.4 Matrix attenuation factors, matrix correction factors, and relative change of the 186 keV gamma-ray counting rate for some uranium compounds (U_3O_8 used as reference)

Uranium compound	Matrix attenuation factor ß	Relative change of 186 keV gamma counting rate	Matrix correction factor $C_{compound}$
U metal	1.0000	+ 1.51 %	0.9849
UO_2	0.9886	+ 0.38 %	0.9962
U_3O_8	0.9849	0 (reference)	1
UF_4	0.9750	- 1.00 %	1.0101
UF_6	0.9630	- 2.22 %	1.0228
Uranyl nitrate $UO_2(NO_3)_2 \cdot 6H_2O$	0.9098	- 7.62 %	1.0825

As can be seen from the Table, different chemical sample composition as well as different stoichiometry of the uranium compound change the observed 186 keV gamma-ray counting rate, and thus the ^{235}U enrichment value derived from it. Hence, both the type of compound and the stoichiometry must be specified for samples under assay in order to arrive at valid enrichment values.

For example, the gamma response of the two uranium oxides given in the Table differs by 0.38 %, their oxygen-to-metal atom ratio differs by 33 %. Thus, the stoichiometry of uranium oxydes is to be known with an accuracy of 10 % if the systematic error of the ^{235}U enrichment measurement due to varying oxygen-to-metal ratios is to be kept below 0.1 %.

For uranium oxydes with given oxygen-to-metal atom ratios $r_{OM} = N_O/N_U$, normalization relative to the U_3O_8 Reference Material is achieved using the following correction:

$$C_{compound}\ (r_{OM}) = 0.985 + 0.0056 \cdot r_{OM} \ . \qquad (3.20)$$

The corresponding correction for uranium fluorides reads

$$C_{compound}\ (r_{FM}) = 0.985 + 0.0063 \cdot r_{FM} \ , \qquad (3.21)$$

where $r_{FM} = N_F/N_U$ is the fluorine-to-metal atom ratio.

3.3.2 Sample impurities

Minor element concentrations in the sample material will not affect the enrichment measurement, if the relation

$$\sum_{i \neq U} \mu_i \cdot \frac{\rho_i}{\rho_{comp}} \ll \mu_{comp} \qquad (3.22)$$

holds, where ρ_i/ρ_{comp} denotes the concentration of the minor element i given as mass fraction of the uranium compound, and μ are the associated mass attenuation coefficients. μ values for typical impurities are given in Tab. C1 in Appendix C. The corresponding values for some uranium compounds are listed in Tab. C2 in Appendix C.

μ values vary from 0.15 $cm^2 \cdot g^{-1}$ for light matrix material (atomic number Z < 30) to 1.5 $cm^2 \cdot g^{-1}$ for heavy elements. When comparing this with the mass absorption coefficient of about 1.5 $cm^2 \cdot g^{-1}$ for uranium, we get a rough estimate for those cumulative impurity concentrations that should be not exceeded for assay errors < 0,1 %:

1 mass % of the U compound	for low Z matrix material
0.1 mass % of the U compound	for heavy elements.

The present U_3O_8 RM fulfills these requirements [1]. If the mass fraction of impurities in a sample under assay is greater than the critical limits given, then their contribution has to be included in the matrix correction factor for highly accurate ^{235}U enrichment assays. The following correction factor has to be applied to the measured ^{235}U enrichment value when the assay system was calibrated with the U_3O_8 Reference Samples:

$$C_{impurity} = 1 + \sum_{i \neq U} \frac{\rho_i \cdot \mu_i}{\rho_{comp} \cdot \mu_{comp}}, \qquad (3.23)$$

with same notations as in eq. 3.22.

For example, if the reactor fuel UO_2 is poisoned with 5 % Gd, with the Gd concentration given as mass fraction of the uranium oxide, then the impurity correction factor from eq. 3.23 is

$$C_{impurity}\ (5\ \%\ Gd) = 1.024.$$

To arrive at measurement accuracies of 0.1 % relative for the ^{235}U enrichment assay, the Gd content of the fuel material must be known with an accuracy of 4 % relative, i.e., the Gd content in this case should be kept within the limits (5.0 $\pm$ 0.2) %.

Sample impurities do have a negligible influence on the measured 186 keV gamma-ray counting rate, when they occur within the limits specified for minor elements in LWR fuel. An example of specifications for upper concentration limits of different chemical elements in a LWR fuel are given in Tab. 3.5 together with the mass attenuation coefficients at 186 keV and the value $(\rho_i/\rho_U) \cdot \mu_i$.

In the case that all elements given in the Table are present in the sample with concentrations corresponding to the given upper-level limits, the impurity correction factor equals only to

$$C_{impurity}\ (LWR\ upper\ limit) = 1.0004\ .$$

Thus we find that all impurities together at the upper limit concentration will change the ^{235}U enrichment analysis result by only -0.04 % (relative) as compared to chemically pure fuel material.

Table 3.5 Example of specifications for upper concentration limits of impurities in LWR fuel, and mass attenuation coefficients for 185.7 keV gamma rays (see Appendix C).

Element i	Upper concentration level ρ_i/ρ_U [ppm]	μ_i at 185.7 keV [$cm^2 \cdot g^{-1}$]	$(\rho_i/\rho_U) \cdot \mu_i$ [$cm^2 \cdot g^{-1}$]
B	1.5	0.116	$1.74\ 10^{-7}$
C	100.	0.125	$1.25\ 10^{-5}$
N	75.	0.125	$9.38\ 10^{-6}$
F	25.	0.119	$2.98\ 10^{-6}$
Mg	50.	0.124	$5.95\ 10^{-6}$
Al	300.	0.122	$3.66\ 10^{-5}$
Si	500.	0.127	$6.35\ 10^{-5}$
Cl	20.	0.125	$2.50\ 10^{-6}$
Ca	100.	0.136	$1.36\ 10^{-5}$
Ti	40.	0.129	$5.16\ 10^{-6}$
V	1.	0.130	$1.30\ 10^{-7}$
Cr	500.	0.135	$6.75\ 10^{-5}$
Mn	10.	0.137	$1.37\ 10^{-6}$
Fe	500.	0.144	$7.20\ 10^{-5}$
Co	6.	0.147	$8.82\ 10^{-7}$
Ni	300.	0.157	$4.71\ 10^{-5}$
Cu	50.	0.155	$7.75\ 10^{-6}$
Zn	20.	0.161	$3.22\ 10^{-6}$
Cd	1.	0.321	$3.21\ 10^{-7}$
In	3.	0.336	$1.01\ 10^{-6}$
Sn	5.	0.348	$1.74\ 10^{-6}$
Sm,Eu,Gd,Dy	0.6	0.6	$3.6\ 10^{-7}$
W	50.	0.892	$4.41\ 10^{-5}$
Pb	20.	1.13	$2.26\ 10^{-5}$
Bi	2.	1.17	$2.34\ 10^{-6}$
		$\Sigma\ (\rho_i/\rho_U) \cdot \mu_i =$	$4.63\ 10^{-4}$

3.3.3 Moisture content

A high moisture content in a sample may contribute to systematic errors, especially in cases of hygroscopic sample material like UO_2. When the assay system was calibrated with the U_3O_8 reference samples having a very low moisture content, then the correction factor for unknown samples with higher water content is given by the following equation

$$C_{moisture} = 1 + \frac{\rho_{water}}{\rho_{comp}} \cdot \frac{\mu_{water}}{\mu_{comp}} , \qquad (3.24)$$

where $(\rho_{water}/\rho_{comp})$ is the water content of the sample given as mass fraction of the dry sample material, and the μ's are the mass attenuation coefficients of water and sample material for 186 keV photons.

Using the values of the mass attenuation coefficients for water and UO_2 given in Appendix C

$$\mu_{water} = 0.139 \text{ cm}^2 \cdot \text{g}^{-1}, \text{ and}$$
$$\mu_{UO_2} = 1.313 \text{ cm}^2 \cdot \text{g}^{-1},$$

we get the moisture correction factor for UO_2 which is representative for most uranium compounds:

$$C_{moisture}\ (UO_2) = 1 + 0.105 \cdot \frac{\rho_{water}}{\rho_{comp}} . \qquad (3.25)$$

Eq. 3.25 shows that the moisture content can reach values as high as 1 % of the sample material mass before affecting the measured ^{235}U enrichment by more than 0.1 % relative. If the water content of a sample is higher than 1 %, a correction must be applied to the assay result, as given in eq. 3.25.

3.4 Interfering gamma rays

Gamma radiation from radioactive nuclei other than ^{235}U present in a sample is defined as interfering with the 186 keV radiation when its energy is so close to 186 keV, that it cannot be resolved by the gamma-ray detector. Thus, the impact of

interfering gamma lines becomes dependent on the energy resolution of the detector used.

When using a high-resolution Ge detector, we have to examine an energy window of approximately ± 1.5 keV around the 185.7 keV peak for interfering gamma radiation. Note, that also the background windows required for the determination of the Compton continuum below the peak are possibly subjected to interference effects.

The situation is much worse, if a NaI detector is used. Typical energy windows are then from 160 keV to 210 keV for the peak region, and 220 keV to 280 keV for the background region. Both large windows are affected by interfering gamma rays.

The gamma interference simulates an additional ^{235}U enrichment (see eq. 2.2). The magnitude and the sign of this bias depend on the radiation properties of the interfering isotope, on its concentration in the sample, and on the selection of the counting windows. In order to get an estimate of the gamma interference term, we assume that the detector efficiency and the photon attenuation in the sample material and in the sample cladding are not depending on the gamma-ray energy within the regions of interest. Then we get the following expression for the gamma interference C_{Int} introduced by the radioactive isotope x:

$$C_{Int} = 100 \cdot \frac{N_x\,(t)}{N_U} \cdot \frac{P_x - b \cdot B_x}{P_{235} - b \cdot B_{235}} , \qquad (3.26)$$

where C_{Int} is given in units of simulated ^{235}U enrichment (in atom %), N_x/N_U is the content of the interfering isotope x in the sample material given as atom fraction of total uranium (all uranium isotopes), P_x and B_x denote the cumulative emission rates (per atom) of those interfering photons whose energies fit into the peak window and into the background window, respectively. P_{235} and B_{235} are the corresponding emission rates for photons from ^{235}U, and b is the ratio of the integrated background continuum in both windows. Instead of referring to the units of atom fraction and emission rates per atom, one may

equivalently use the units of mass fraction and specific emission rates (photons emitted per gram isotope) in eq. 3.26. Note that the content of the interfering isotope x present in the sample may decrease or increase as a function of the time t after chemical purification of the sample material, depending on the half-life of the particular isotope, and on the half-lives of its predecessors in the decay chain.

We restrict the discussion of gamma interference effects in this section to highly purified uranium materials. Then only gamma rays originating from the decay of uranium isotopes and their descendants in the decay chain must be considered. The photon energies and the specific emission rates of all relevant uranium isotopes within the energy region of interest are summarized in Appendix B of the manual. Note that in recycled uranium materials spurious amounts of other actinides and of fission products may also contribute to the gamma interference.

A) Interference from the decay of ^{238}U

In low enriched uranium materials ^{238}U is always present in large quantities. Thus, interference with gamma rays originating from the decay chain of ^{238}U must be carefully examined. Especially the decay product protactinium emits many gamma rays with energies up to 2 MeV. Protactinium grows in from the ^{238}U decay after chemical purification of the uranium, and reaches secular equilibrium with ^{238}U about 3 months after separation. In the equilibrium, the Pa activity is proportional to the ^{238}U content and thus appears constant for low enriched uranium.

Fortunately, within the 186 keV peak region used with Ge detectors, only two weak gamma lines with energies of 185.95 keV and 184.7 keV have been identified. These photons are emitted from the decay of ^{234}Pa and ^{234m}Pa, respectively. The protactinium content in the sample grows in after separation according to

$$\frac{N_{Pa}}{N_U} = \left(1 - \frac{enr}{100}\right) \cdot \left(1 - \exp(-0.029 \cdot t)\right), \qquad (3.27)$$

where enr is the ^{235}U enrichment in atom %, and t is the time after separation given in days. Assuming that the background window is free of interfering gamma rays, and using the values for the specific photon activities given in Appendix B, we arrive at the following estimate for the interference term C_{Int}, if the measurement is performed with a high-resolution Ge detector.

$$C_{Int}(Pa) = (100 - enr) \cdot (1-\exp(-0.029 \cdot t) \cdot 1 \cdot 10^{-5}, \quad (3.28)$$

which for low-enriched uranium can be approximated to

$$C_{Int}(Pa) = 0.001 \cdot (1-\exp(-0.029 \cdot t) \quad . \quad (3.28a)$$

C_{Int} is given in units of simulated ^{235}U enrichment (in atom %), and t denotes the time after separation in days.

Due to interfering Pa gamma rays, "aged" sample material exhibits a somewhat higher gamma counting rate in the energy window around the 185.7 keV peak as compared to freshly separated sample material. This results in a small positive bias C_{Int} for "aged" sample material. On the other hand, if the assay system has been calibrated using the "aged" Reference Material, then the enrichment value of freshly separated material is measured slightly too low. In this case the ^{235}U enrichment assay result must be corrected according to

$$enr_{true} = enr_{calib} + 0.001 \cdot \exp(-0.029 \cdot t) \quad . \quad (3.29)$$

(enrichment given in atom %, time t in days after separation).

Note, that the protactinium correction given in eq. 3.29 is small and approaches zero for "aged" uranium sample material, i.e., about three months after chemical separation. The correction can be neglected (error < 0.1 % relative), if the ^{235}U enrichment of the sample material exceeds 1 %. However, the assay result for freshly separated, depleted uranium material (^{235}U enrichment 0.2 % to 0.3 %) may be biased by about -0.4 % relative without the correction given in eq. 3.29.

When a NaI detector is used for enrichment measurements, a larger energy range has to be scanned for interfering gamma radiation because of the lower energy resolution of this type

of detector. Since many gamma lines with different energies and different emission rates are observed from the ^{238}U decay in the energy window of interest, the value of the interference correction term becomes critically dependent on the selection of the counting windows (width and position in the gamma spectrum), and it cannot be easily predicted.

The most intense gamma line from the ^{238}U decay in the energy range considered is observed at 258.7 keV. It originates from the decay of the ^{238}U descendant ^{234m}Pa. If this line is included in the background window, and the widths of the peak window and the background window are approximately equal (b=1 in eq. 3.26), then we expect a negative value for the interference correction term C_{Int} simulating a ^{235}U enrichment of about -0.003 % to -0.005 % for "aged" sample material. Thus, a negative correction corresponding to eq. 3.29 must be applied to freshly separated sample material if the assay system has been calibrated with the "aged" reference material.

Note, that the gamma interference effect will vanish, if the numerator in eq. 3.26 becomes zero. Under certain conditions that depend on the gamma spectrum of the respective interfering isotope, this can be achieved by a proper selection of the counting windows (width and position). Details of such a procedure are not given here. A first approach to this type of window setting may be obtained from eq. 3.26 using the gamma ray energies and the specific gamma activities of uranium isotopes and their descendants tabulated in Appendix B of the manual. Some further aspects relevant to the selection of the counting windows will be discussed in Section 5.3.

B) Interference from the decay of ^{237}U

The by far most intense gamma line observed from the ^{237}U decay has the energy of 208 keV, which is relatively close to 186 keV for low resolution detectors. Due to the short half-life of ^{237}U (6.75 d), its gamma activity per gram isotope is very high, about 10^{10} times higher than that of ^{235}U. Therefore even spurious amounts of ^{237}U (that is always present in

freshly separated recycled uranium material) will falsify the ^{235}U enrichment assay result obtained with a NaI detector.

In contrast to this, interference effects from ^{237}U are not expected when a Ge detector is used, and the background windows are properly selected.

^{237}U decays rapidly. A few weeks after separation its activity has fallen below a measurable level, provided its predecessor ^{241}Pu has been removed properly during the separation process. The remaining gamma activity from the ^{237}U descendants ^{237}Np and ^{233}Pa can be neglected for measurements with both types of gamma detectors, NaI as well as Ge detectors.

C) Interference from the decay of ^{236}U and ^{234}U

No gamma interference is expected form these isotopes for both types of gamma detectors.

D) Interference from the decay of ^{233}U

A multi-line gamma-spectrum is emitted from ^{233}U and its descendants. Four photons with energies around 186 keV are reported [12] originating from the decay of ^{233}U and its descendant ^{225}Ac. Due to the long half-life ($1.6\ 10^5$ y) of ^{233}U the total gamma activity is relatively low. Therefore, gamma interference effects can be neglected (assay errors < 0.1 % relative) at concentration levels of

$$\frac{^{233}U}{^{235}U} < 0.005 \quad \text{for Ge detectors, and}$$

$$\frac{^{233}U}{^{235}U} < 0.0005 \quad \text{for NaI detectors.}$$

The concentration limits have been derived from eq. 3.26 using the specific gamma activities of ^{235}U and its descendants given in Appendix B. The ^{233}U content of the Reference Samples has been determined [1] to be below the detection limit of $5 \cdot 10^{-5}$.

E) Interference from the decay of ^{232}U

The total gamma activity from the decay of ^{232}U and its descendants grows in after separation and reaches a flat maximum about ten years after separation.

No gamma interference is expected for high-resolution Ge detectors, if the ^{232}U content is below a concentration limit of about

$$\frac{^{232}U}{^{235}U} < 0.001,$$

and if the background windows are properly selected.

Extreme care must be taken when a NaI detector is used for the ^{235}U enrichment assay, because several strong gamma lines are emitted from ^{232}U descendants with energies falling into the background window normally used with NaI detectors. The most intense of these lines originates from the ^{232}U descendant ^{212}Pb and has the energy 238.6 keV. If this gamma line is included in the background window, and if assay errors comparable to the interference due to the ^{238}U decay are to be avoided, then the ^{232}U concentration must be kept below a very low limit:

$$\frac{^{232}U}{^{235}U} < 1.5 \cdot 10^{-10} \qquad !!!$$

It has been demonstrated (see Certification Report [1]) that this condition is not fulfilled for the depleted Reference Sample and, possibly, for the 4.5 % enriched Reference Sample. Thus, a bias effect due to the interference from the ^{232}U decay is expected which is of the order of about 0.5 % and 0.1 % relative for the respective samples, when the measurements are performed with a NaI detector. It is therefore recommended in this case to use a background window that does not contain the 238 keV peak. However, the problem remains if unknown samples are measured having a higher ^{232}U content than the Reference Samples.

Summing up the content of this section it may be said that interfering gamma radiations from uranium isotopes other

than ^{235}U may affect significantly the gamma-spectroscopic ^{235}U enrichment determination. The interference will not only disturb the gamma counting rate in the selected 186 keV energy window, but will also make it difficult to find a suitable energy region for the determination of the background continuum below the peak, in particular when NaI detectors are used.

Considering the target accuracy of a few tenths of a percent in ^{235}U enrichment assays, one should keep in mind that then the peak ratios of interfering gamma rays relative to the 186 keV peak must also not exceed a value of about 0.001 within the selected counting windows. In routine measurements using relatively short counting times, such small gamma peaks are often hidden within the counting statistics, and are not recognized by the user. Therefore, when setting up a ^{235}U enrichment assay system, a careful selection of the counting windows is necessary to keep the impact of interfering gamma radiation on the assay result as small as possible. This applies to both types of gamma detectors, NaI as well as Ge.

Reliable assay results cannot be obtained with NaI detectors, if the sample material contains ^{237}U or ^{232}U. Therefore, it is strongly recommended to use NaI detectors only if it can be assured that the uranium material is really virgin, otherwise the presence of recycled uranium in the sample material can lead to severe measurement errors.

4. INFLUENCE OF COUNTING GEOMETRY AND SAMPLE CONTAINER

In the previous chapter we have discussed the properties of the sample material (sample size, sample composition) which will affect the gamma-spectrometric ^{235}U enrichment assay. This chapter provides information on the influence of those measurement parameters that are not related to the sample material itself. It comprises effects introduced by the geometrical arrangement of the counting set-up, and by the gamma attenuation within the sample container wall.

4.1 Collimator-detector geometry

The maximum 186 keV gamma counting rate which can be observed in a measurement set-up is determined by the geometrical elements, that define the solid viewing angle for the gamma radiation. These elements are the collimator-entrance area, the collimator-exit area, and, in some cases, the active area of the gamma detector. Fig. 4.1 shows some typical collimator-detector arrangements with varying detector diameters. A cylindrical form and a common axis are assumed here for both the detector and the collimator. The respective viewing angles are indicated in Fig. 4.1 by dashed areas.

It can be seen from the figure that variations of the collimator-detector distance in cases a), b) and c) do influence the solid viewing angle and, thus, the measured gamma counting rate, whereas in case d) the gamma response of the counting system is unaffected by small variations of the distance collimator-to-detector.

In previous discussions of the "quasi-infinite" sample size and of the expected 186 keV gamma counting rates we have always assumed that the active area of the gamma detector is significantly larger than the cross section of the collimator, as illustrated in case d) of Fig. 4.1. The use of smaller detectors raises some questions that are of particular interest for ^{235}U enrichment assays:

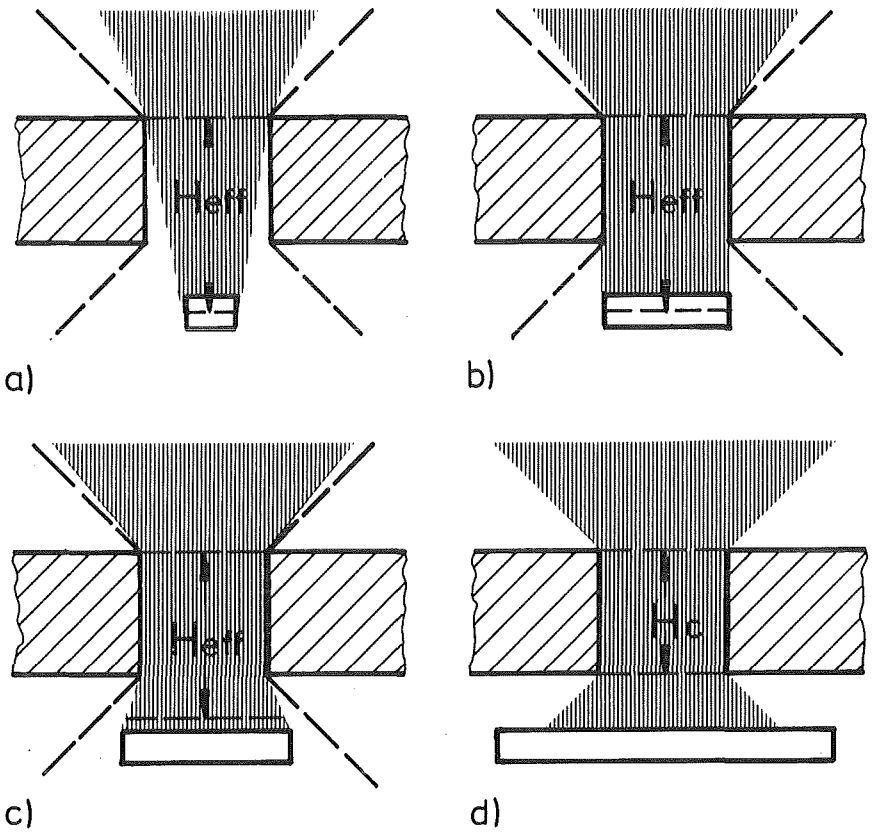

Fig. 4.1 Collimator-detector geometries.

1. Are the "quasi-infinite" sample sizes recommended in Section 3.1.5 valid for all types of collimator-detector geometries considered here?

2. What is the expected 186 keV gamma counting rate in the various cases?

3. To what extent are the assay results affected by small variations of the distance between collimator and detector?

The first question can be easily answered from simple geometrical considerations. It can be deduced from Fig. 4.1 that the solid angle, through which the sample material is seen from the detector, decreases with decreasing detector size and with increasing distance between collimator and detector. Along with

the viewing angle also the sample diameter will decrease that is required to provide the "quasi-infinite" sample condition. Therefore, if this condition is fulfilled for a particular sample and a particular collimator using a large-area detector (as referred to in Section 3.1 of the manual), then it is also satisfied for any smaller detector and any distance between the detector and the collimator exit plane.

Estimates of the expected 186 keV gamma counting rate and of the associated counting time required for a particular counting precision will be useful for the design of a new counting set-up. Note that the approximate counting times given in Fig. 3.7 refer to large-area detectors only. The counting rates obtainable from smaller detectors can be estimated form an "effective" counting geometry as indicated in Fig. 4.1. The four typical collimator-detector geometries depicted in the figure are characterized by the following relative sizes of the collimator diameter D_C and the detector diameter D_{Det}:

a) $D_{Det} < D_C$. In this case the viewing angle is determined by the collimator entrance area and by the cross section of the active volume of the detector. This geometry corresponds approximately to a conical collimator with diameters D_C and D_{Det} for the collimator entrance area and the collimator exit area, respectively. The effective collimator height H_{eff} is approximated by the distance between collimator entrance plane and the half-thickness plane of the detector. Estimates of the maximum observable 186 keV gamma counting rate may be obtained from eq. A23 in Appendix A for conical collimators.

b) $D_{Det} = D_C$. This counting arrangement forms a counting geometry which is approximately equivalent to a cylindrical collimator with a diameter D_C and with an effective collimator height H_{eff}, corresponding to the distance between collimator entrance plane and the half-thickness plane of the detector. Eq. A22 in Appendix A describes the geometrical efficiency in this case.

c) $D_{Det} > D_C$. In this case an estimate of the maximum observable 186 keV gamma counting rate is obtained from eq. A22 in Appendix A for a cylindrical collimator using the colli-

mator diameter D_C and an effective collimator height H_{eff} that extends from the collimator entrance plane to a level in between the collimator exit plane and the half-thickness plane of the detector as indicated in Fig. 4.1c.

d) $D_{Det} >> D_C$. In this case the geometrical efficiency is solely determined by the collimator dimensions D_C and H_C. It is exactly described by eq. A22 in Appendix A.

Note that the values of the maximum observable 186 keV gamma counting rate obtained from eqs. A22 and A23 do not account for the intrinsic efficiency of the gamma detector. Calculations of the detector efficiency are quite laborious and not very accurate. In order to get a rough estimate of the really observable 186 keV peak counting rate, one may use values of about 40 % to 60 % for the intrinsic peak efficiency of the detector at 186 keV, which represent an acceptable approximation for the most commonly used Ge detectors having an active layer of about 2 cm thickness.

Effects of the collimator-detector geometry on the 186 keV gamma counting rate are illustrated in Fig. 4.2 for two typical collimators assuming cylinder geometry with a common symmetry axis for both the collimator and the detector. The graphs are given as a function of the ratio detector diameter/collimator diameter. The upper part of the figure shows the fraction of gamma rays reaching the detector as compared to the total number of photons penetrating the collimator. The "geometrical counting efficiency" defined in this way increases from about 0 % for extremely small detectors to 100 % for large-area detectors. The curves are displayed for 0 cm, 0.5 cm and 1 cm distance between collimator exit plane and detector surface.

Considerable systematic errors can be introduced to the enrichment assays by variations of the collimator-detector distance between measurements due to an unstable mounting of the collimator. The lower part of Fig. 4.2 shows those variations of the collimator-detector distance which cause a change of 0.1 % in the gamma counting rate. It demonstrates a very high sensitivity of the counting set-up to variations of the detector-collimator distance, if the detector area is smaller than the

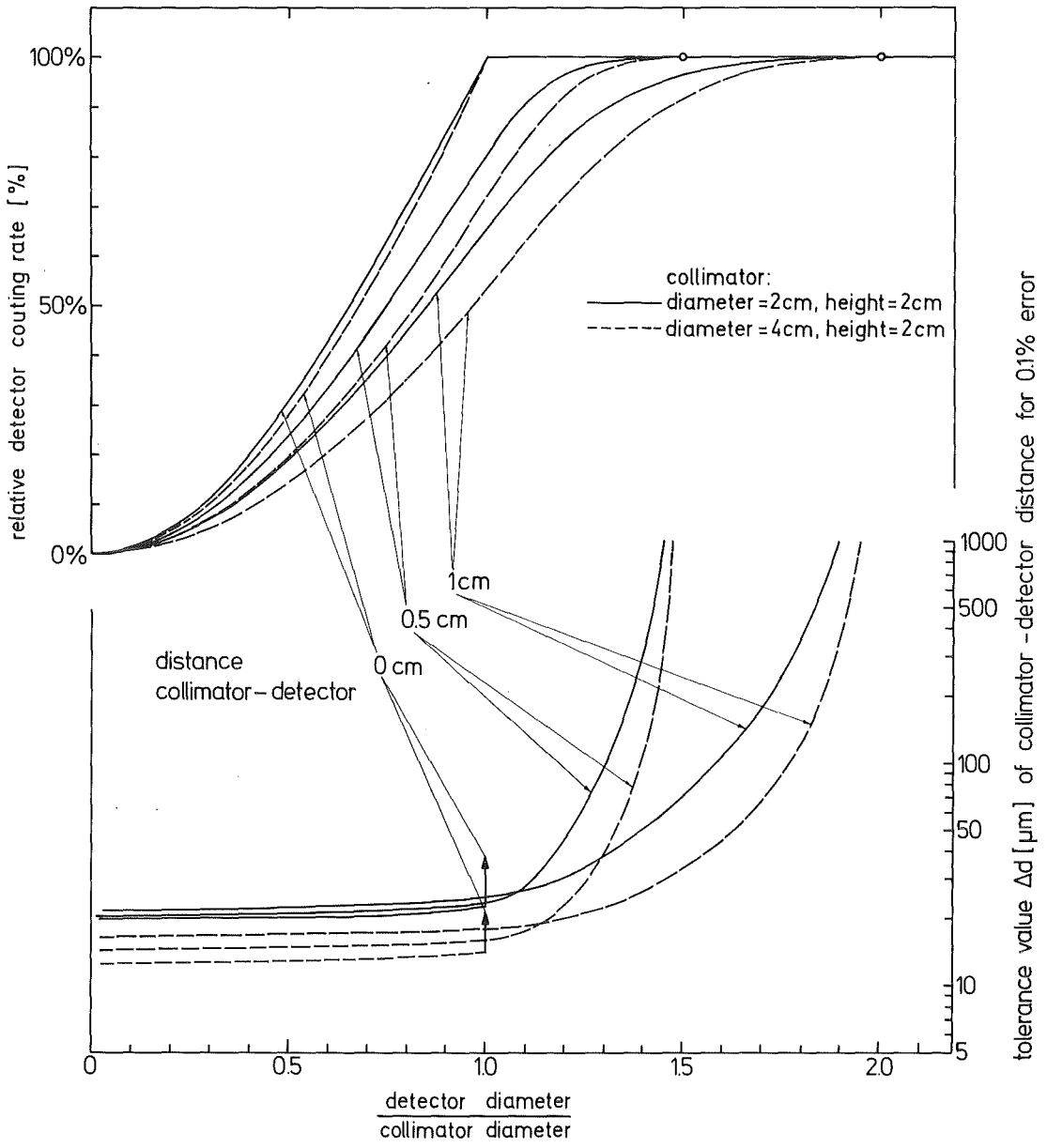

Fig. 4.2 Relative geometrical detector efficiency as a function of the detector size, and tolerance limits for variations of the detector-to-collimator distance at the 0.1 % error level.

collimator area. A change by only 20 µm will affect the assay result by 0.1 %. This extreme sensitivity decreases only slowly with increasing detector diameter for realistic collimator-detector distances (see Fig. 4.2). Therefore, precautions must be taken to keep the distance between detector and collimator rigidly fixed during the measurements.

In order to reduce the influence of distance variations between detector and collimator upon the assay result, it is recommended

1. either to use only collimators with diameters being significantly smaller than the diameter of the active area of the gamma detector as shown in case d) of Fig. 4.1, or
2. to fix the collimator rigidly to the detector cap. (Caution! Do not damage the detector cap or the vacuum flange of the detector!).

4.2 Photon attenuation in the sample container wall

Gamma-spectrometric ^{235}U enrichment assays have the inherent advantage that the enrichment can be measured non-destructively through the wall of a sample container. However, the gamma-ray attenuation within the container wall has to be corrected for. This requires strict specifications and control of the container wall thickness and of the container material as well. This section gives tolerance values for the variation of the container wall thickness, and describes the necessary attenuation corrections.

The attenuation of photons in an absorbing layer with a thickness d is usually expressed by the relation

$$A_{abs} = e^{-\lambda \cdot d} \quad , \qquad (4.1)$$

where λ denotes the linear attenuation coefficient of the layer material. However, eq. 4.1 describes in a strict sense only the attenuation of gamma rays penetrating the layer perpendicular to

its surface, so that this approach is valid only in case of extremely narrow collimators.

For realistic collimators one has to consider that the effective pass length of the photons through the container wall (and thus the attenuation) increases with increasing inclination angle between the direction of the photon and the axis perpendicular to the wall surface (see Fig. 4.3).

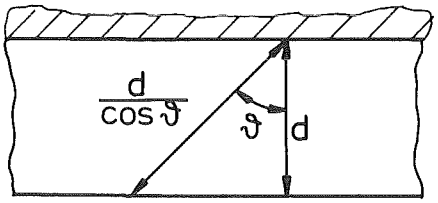

Fig. 4.3
Path length of gamma rays through an absorbing layer

This effect causes the effective photon attenuation to become dependent on the angular distribution of the gamma source (here a cosine distribution) and on the angular acceptance of the collimator-detector geometry. Moreover, also the intrinsic peak efficiency of the gamma detector depends in most cases on the incidence angle and on the incidence position of the incoming gamma ray at the detector surface.

Therefore, for highly accurate attenuation corrections one has to take into account the type and thickness of the container wall, the collimator geometry, and the type and the geometry of the gamma detector as well. It is expected that the effective photon attenuation is higher for wide collimators than for narrow ones, that it is higher for large-area detectors than for small detectors, and that it is higher for thin detectors than for thick ones. Some more details are given in Appendix A. In this section we first discuss the particular case, in which the photon attenuation in the container wall is comparable to that of the Reference Samples, and in which a cylindrical collimator and a large-area detector is used. Then, an example of an experimental procedure is given which is generally applicable to attenuation corrections.

Fig. 4.4 shows the calculated tolerance limits for variations of the bottom thickness of a standard aluminium container that correspond to a change of the gamma response by 0.1 %. The tolerance limits are displayed as a function of the collimator geometry given by the ratio collimator diameter/collimator height assuming a thick large-area detector.

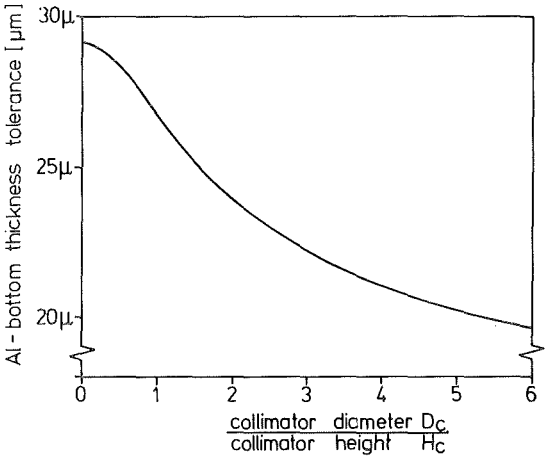

Fig. 4.4
Tolerance values for the aluminium container wall thickness as a function of the collimator geometry for errors $\leq$ 0.1 %.

It can be seen from Fig. 4.4 that for most collimators the wall thickness of aluminium containers must be known with an accuracy of about 0.02 mm in order to keep the assay error below 0.1 %.

Table 4.1 shows approximate tolerance values for variations of the container wall thickness and linear attenuation coefficients for some typical sample container materials, assuming a maximum effect of 0.1 % on the measured 186 keV gamma response.

Table 4.1 Linear attenuation coefficients and tolerances of the wall thickness for typical sample container materials.

Container material	Linear attenuation coefficient at 186 keV	Tolerance for container wall thickness
Polyethylene	0.14 cm^{-1}	0.05 mm
Aluminium	0.34 cm^{-1}	0.02 mm
Steel	1.28 cm^{-1}	0.005 mm

These very tight tolerance limits necessitate a careful determination of the container wall thickness of unknown samples. The bottom thickness of the set of Reference Samples and of the empty reference can is specified within the given tolerance limits.

The wall thickness of an unknown container can be measured with the required degree of accuracy using a high-precision ultrasonic thickness gauge. Thickness measurements should be performed at several positions on the container surface, which is seen by the gamma-ray detector. If the wall thickness is found to be uniform within a few units of the tolerance limits given in Tab. 4.1, its mean value should be used for the gamma attenuation correction. Non-uniformities of the wall thickness far outside these limits will imply complicated correction calculations. Small scratches on the container surface, however, will not affect the accuracy of an enrichment measurement, if their cumulative volume can be considered as very small compared to the total volume of the container wall viewed by the gamma detector.

When only aluminium containers are used for the enrichment assays, and when the difference between the wall thickness d_{ref} of the Reference Samples and the mean wall thickness d of the unknown sample exceeds the tolerance limits defined above, then an attenuation correction is required. Eq. 4.2 gives the correction factor C_{WA} that has to be applied to the ^{235}U enrichment value obtained from a measurement in a counting set-up calibrated with the Reference Samples:

$$C_{Wa} = \left(e^{\lambda_{Al} \cdot DK_{abs} \cdot (d-d_{ref})} \right) \qquad (4.2)$$

λ_{Al} is the linear attenuation coefficient of aluminium at 186 keV (see Table 4.1), d and d_{ref} are the wall thicknesses of the unknown sample and of the Reference Samples, respectively, and DK_{abs} is a correction function that accounts for the effective difference of the photon path lengths in the two sample container walls. DK_{abs} is given in Fig. 4.5 for two types of large-area detectors as a function of the collimator geometry. Note that

the correction function C_{Wa} is normalized to the reference containers, i.e., $C_{Wa} = 1$ for the Reference Samples.

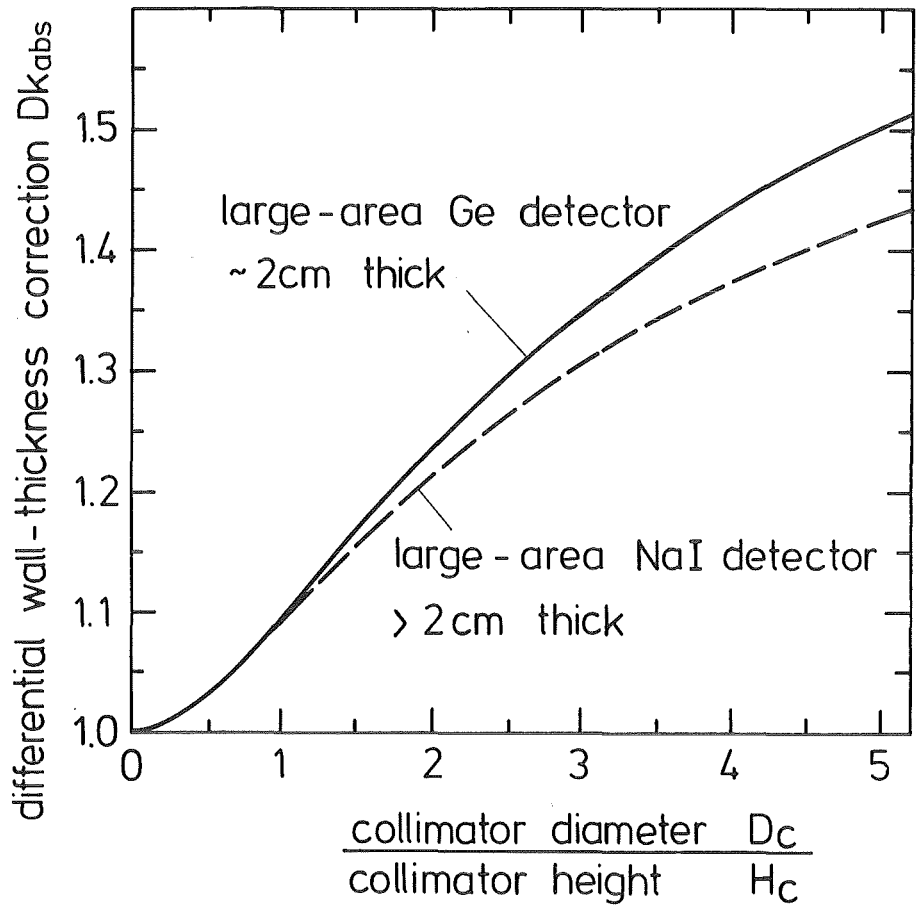

Fig. 4.5 Differential correction function DK_{abs} versus collimator geometry for two types of large-area detectors.

The relative error of the attenuation correction C_{Wa} is derived from the relative errors $\Delta DK_{abs}/DK_{abs}$ and $\Delta\lambda_{Al}/\lambda_{Al}$, and from the error Δd of the wall thickness determination of the unknown sample

$$\frac{\Delta C_{Wa}}{C_{Wa}} = Dk_{abs} \cdot \lambda_{Al} \sqrt{(d-d_{ref})^2 \cdot [(\frac{\Delta Dk_{abs}}{Dk_{abs}})^2 + (\frac{\Delta\lambda_{Al}}{\lambda_{Al}})^2] + (\Delta d)^2} \quad . \qquad (4.3)$$

The uncertainty in the wall thickness of the Reference Samples is neglected here. Note that for large corrections the error term given in eq. 4.3 is dominated by the stated uncertainty [9] of $\pm$ 2 % to $\pm$ 5 % for the linear attenuation coefficient λ_{Al}.

Therefore, it is recommended to restrict the application of Eq. 4.2 to small variations of the container wall thickness, e.g., 1.5 mm to 2.5 mm for aluminium cans, in order to avoid systematic errors greater than 0.1 %. In this case the error of the attenuation correction is approximately given by

$$\frac{\Delta C_{Wa}}{C_{Wa}} = \lambda_{Al} \cdot DK_{abs} \cdot \Delta d \quad . \qquad (4.3a)$$

If the gamma attenuation in the container wall is significantly different from the value found for the 2 mm aluminium bottom of the Reference Samples, then the attenuation correction should be determined experimentally by transmission measurements using appropriate layers of material which is representative for the material of the sample containers to be assayed. Care must be taken to provide the "infinite-sample" geometry in any case. If this condition cannot be met for the Reference Samples (e.g., when using thick absorbers), one may utilize a suitable bulk quantity of ^{235}U bearing material in a thin-walled container (e.g., in a plastic bag) as a gamma source, that provides the "infinite-sample" condition. The use of conventional point gamma sources may lead to erroneous results due to their different angular radiation characteristics (isotope radiation versus cosine radiation!).

To give an example for an experimental determination of the attenuation correction in case of a thick container wall: we assume a counting set-up for which the "infinite-sample" condition for the Reference Samples is violated when a thick absorber is inserted between collimator and Reference Sample. In this case the "bulk gamma source" mentioned above may serve as a suitable radiation source. The transmission measurements are performed by placing appropriate layers of container material between this gamma source and the collimator, and by determining the corresponding 186 keV net peak counting rates $\dot{N}$ from the measured spectra (see Section 5.3). If the thickness of the container wall for the samples to be assayed is expected to range from d_l to d_u, then the measurements should be performed using three different layers:

1. A 2.00 mm thick aluminium layer. This measurement is required to normalize for the gamma attenuation within the bottom of the reference cans. $\dot{N}1$ denotes the 186 keV gamma counting rate observed from this measurement.

2. A layer of container material whose thickness d_l represents the lower limit of the expected wall thickness of the samples under assay. The observed 186 keV counting rate is $\dot{N}2$.

3. A layer of container material whose thickness d_u corresponds to the upper limit of the expected wall thickness of the samples under assay, or a layer in addition to d_l whose thickness corresponds to the range of expected wall thickness variations. The observed 186 keV gamma counting rate is now $\dot{N}3$.

When the assay system has been calibrated using the Reference Samples, then eq. 4.5 gives the attenuation correction required for a sample container made of material X with a wall thickness d, varying within the range $d_l \leqq d \leqq d_u$:

$$C_{Wa}(d) = \frac{\dot{N}1}{\dot{N}2} \cdot e^{\overline{D\lambda} \cdot (d-d_l)} \quad , \qquad (4.5)$$

where $\overline{D\lambda}$ is obtained from measurements 2 and 3:

$$\overline{D\lambda} = \frac{\ln \dot{N}2 - \ln \dot{N}3}{d_u - d_l} \quad . \qquad (4.6)$$

The experimentally determined value $\overline{D\lambda}$ is only valid for this particular counting geometry, for this particular container material, and for this particular range of the wall thickness. $\overline{D\lambda}$ corresponds to

$$\overline{D\lambda} = \lambda \cdot DK_{abs}$$

given for the standard aluminium cans in eq. 4.2.

It is recommended to devote great care on these measurements, because the errors propagate to all following enrichment assays. The uncertainty of the attenuation correction is derived from

the relative errors $\dot{\Delta N}/\dot{N}$ of the measured counting rates, and from the uncertainty Δd of the wall thickness measurements:

$$\frac{\Delta C_{Wa}}{C_{Wa}} = \sqrt{\left(\frac{\dot{\Delta N}1}{\dot{N}1}\right)^2 + \left(\frac{d-d_u}{d_u-d_l}\right)^2 \cdot \left[\left(\frac{\dot{\Delta N}2}{\dot{N}2}\right)^2 + \overline{D\lambda}^2 \cdot (\Delta d_l)^2\right] + \left(\frac{d-d_l}{d_u-d_l}\right)^2 \cdot \left[\left(\frac{\dot{\Delta N}3}{\dot{N}3}\right)^2 + \overline{D\lambda}^2 \cdot (\Delta d_u)^2\right] + \overline{D\lambda}^2 \cdot (\Delta d)^2} \qquad (4.7)$$

4.3 Container wall deformation and sample positioning

The considerations given in this Section 4.3 are not intended to serve as a basis for quantitative corrections. They only describe the order of magnitude to which variations in the positioning of the samples, and deformations of the container wall can be tolerated without introducing a significant loss of assay accuracy. Note that for "quasi-infinite" samples the spatial distribution of the sample material will not affect the assay result, so that the effects considered here are exclusively caused by the different gamma attenuation within the container wall.

The tolerance values for variations the container wall thickness given in Tab. 4.1 can be used to arrive at a rough estimate of the maximum tolerable inclination angle between container wall and collimator surface with reference to a systematic error < 0.1 %.

If the container wall is inclined by an angle relative to the collimator surface, then the effective wall thickness to be penetrated by the 186 keV gamma rays in forward direction increases from d to d + Δd (see Fig. 4.6).

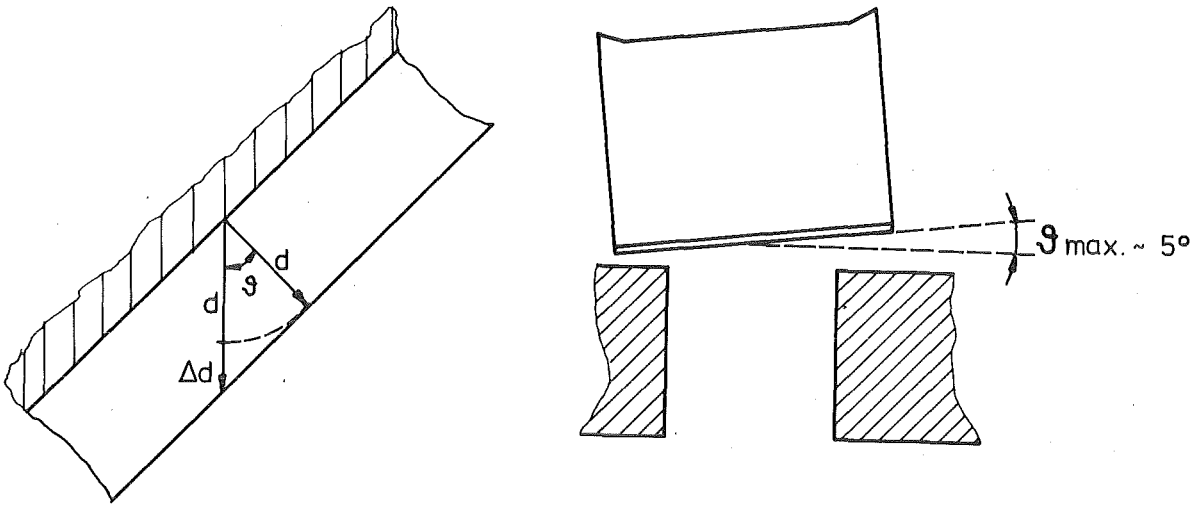

a) b)

Fig. 4.6 Container inclination relative to the collimator surface.

Thus, using the tolerance value Δd_{max} of the wall thickness variations described in the previous section, the following estimate holds:

$$\theta_{max} = \arccos\left(\frac{d}{d+\Delta d_{max}}\right) \quad . \qquad (4.8)$$

From this relation we get the approximate inclination angle that can be tolerated for a container with a 2 mm thick aluminium wall (at the level of 0.1 % relative error):

$$\theta_{max} \approx 5^\circ \ ,$$

provided the "infinite-sample" geometry of the counting set-up is not violated by inclining the container.

From the tolerance value for the container inclination we get, in turn, a simple estimate of the maximum tolerable deformation of the container bottom, as shown in Fig. 4.6 for a container of 7 cm diameter and a container wall of 2 mm aluminium. The tolerable bottom deformation f_{max} at the 0.1 % error level becomes in this case:

$$f_{max} \approx 3 \text{ mm.}$$

This estimate holds for both convex and concave deformations.

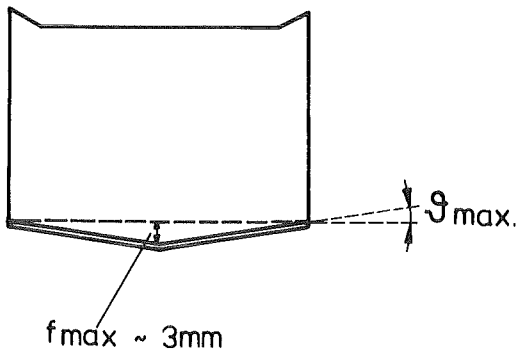

Fig. 4.7
Maximum tolerable deformation of a 2 mm thick aluminium container bottom.

A variation of the distance between container and collimator (sample lifting), as well as a shift of the container parallel to the collimator surface will not influence the observed 186 keV counting rate provided the "infinite-sample" geometry of the counting arrangement is preserved in any case, and the thickness of the container wall is uniform in the regions viewed by the gamma detector.

Although careful sample positioning is not required for very large samples, this aspect becomes very important when minimum "infinite-thickness" samples or maximum collimator geometries are used for enrichment measurements (as discussed in Chapter 3). In order to assure a proper sample centering with respect to the collimator axis in those cases, it is useful to insert the samples to be assayed into a guide ring which is fixed at the collimator surface and which fits closely to the sample diameter, as shown in Fig. 4.8.

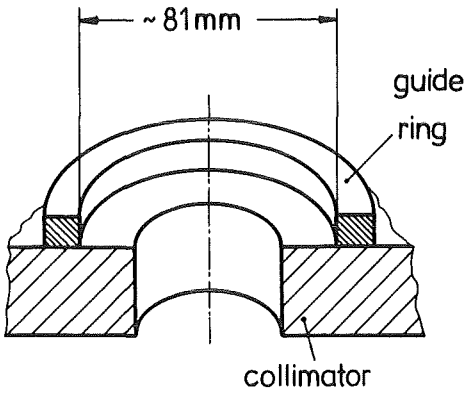

Fig. 4.8
Guide ring for sample positioning.

5. COUNTING EQUIPMENT AND DATA ANALYSIS

This chapter describes in a short form the hardware components required for enrichment assays, and possible errors arising from this part of the measurement. It is assumed that the reader is familiar with the fundamentals of gamma-ray spectrometry regarding the electronic equipment and the techniques for data evaluation techniques. Informations on this subject may be found in many review articles, e.g., in references [5], [13], [14].

A short summary of equipment specifications is given in Section 5.1 of this chapter. It may assist the user in selecting the hardware components required for the enrichment-assay system. In Section 5.2 the errors are discussed that are caused by system dead time and pulse pile-up effects, and possible countermeasures are described. Without claim for completeness, Sections 5.3 and 5.4 give some examples of techniques for net peak area evaluation and calibration procedures.

5.1 Basic counting equipment

Two examples of a counting equipment suitable for enrichment measurements are given in Figs. 5.1 and 5.2. Fig. 5.1 shows the minimum configuration, as realized in some commercially available assay systems. Fig. 5.2 displays an equipment that is close to the optimum choice for high-accuracy gamma spectrometry. The user may select his own equipment in between these two extreme examples according to his needs.

Some criteria for the selection of the various hardware components are summarized here in a condensed form:

- Background radiation shielding

  Necessary. A shielding of a least 2-3 cm lead around the detector is recommended. Radiation shielding is particularly important for in-plant measurements at high ambient gamma-radiation levels.

- Cadmium filter

  Optional. A 0.5 - 1.5 mm thick cadmium sheet between

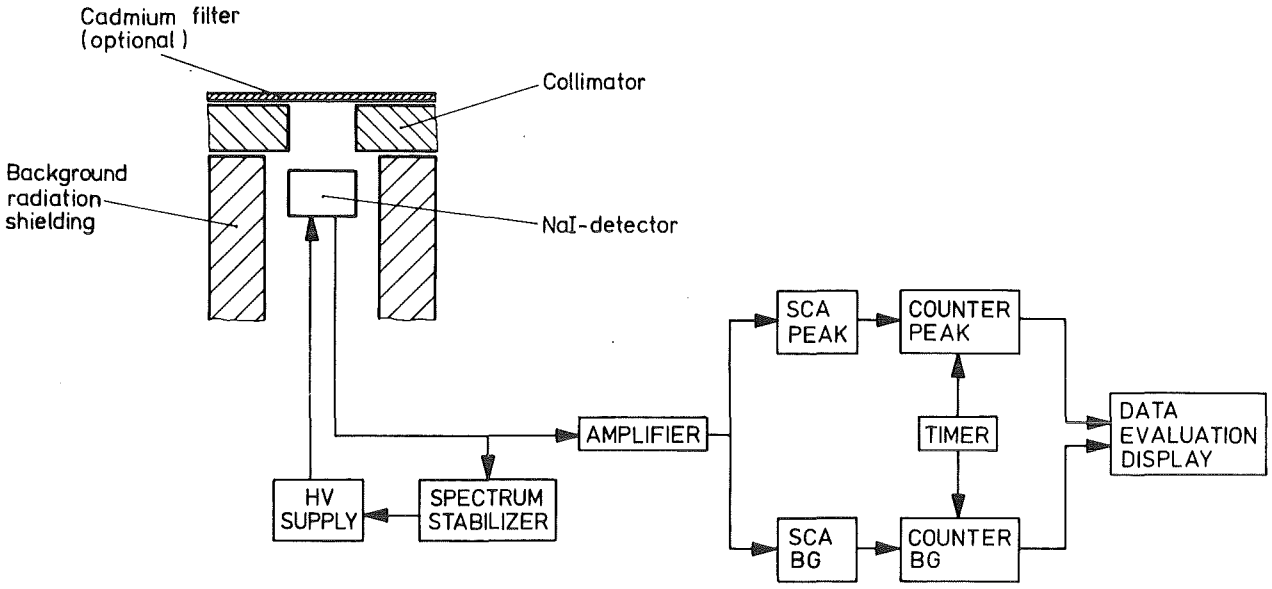

Fig. 5.1 Minimum equipment required for gamma-spectrometric ^{235}U enrichment assays

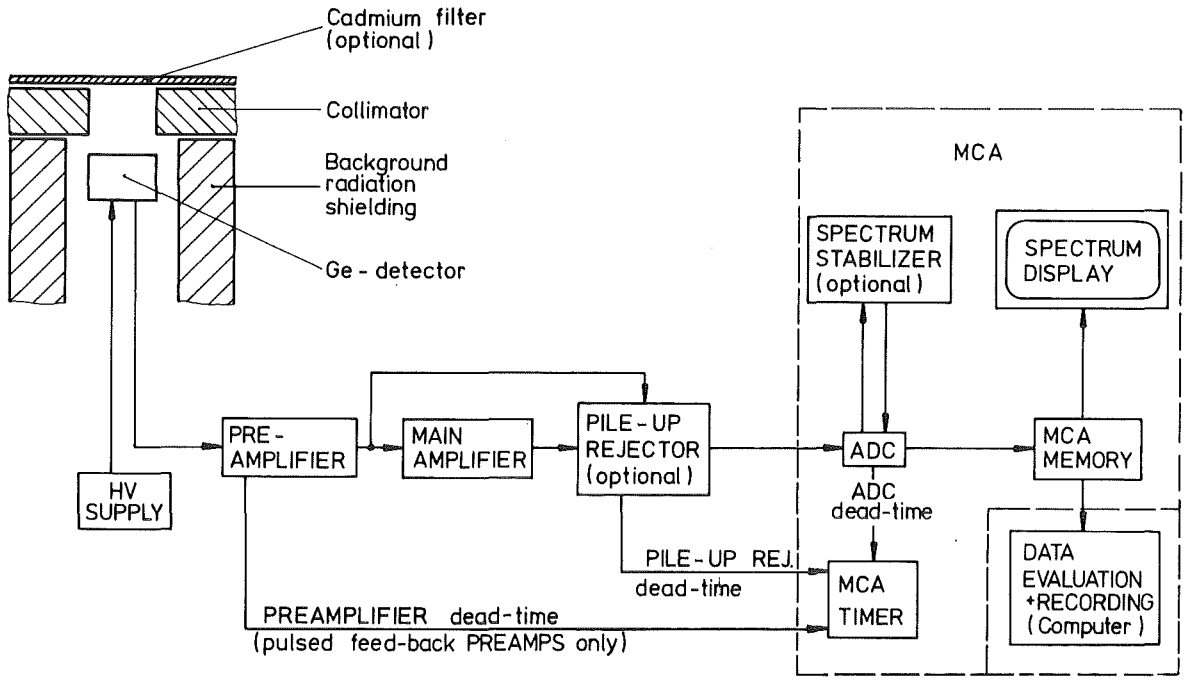

Fig. 5.2 Optimum equipment for high-resolution gamma-ray spectrometry

sample and detector serves as absorber for low-energy gamma rays < 100 keV without significantly affecting the 186 keV photons. The cadmium filter is used to reduce the total detector counting rate and the associated errors (dead time, pile-up). Note: Both the calibration measurements and the assays of unknowns should be performed using the same cadmium filter. The correction factor for bottom-thickness variations discussed in Section 4.1 requires a slight modification when a cadmium filter is used (see Appendix A3).

- Collimator

The diameter and the height of the collimator must be selected according to size and material density of the samples under assay (see Chapter 3).

Caution: The collimator position with respect of the detector must be invariably fixed (see Section 4.3).

- Detector (NaI, Ge)

High resolution Ge detectors are recommended for highly accurate measurements. NaI detectors should not be used, if the sample material is suspected to contain recycled uranium. Detector area: If possible, the active area of the detector should be larger than the collimator cross section.

Detector thickness: The optimum detector thickness is to be selected for high photon efficiency at 186 keV and low compton background from high-energy gamma rays. Rough estimate of optimum detector thickness: 2-3 cm (lower value for NaI detectors - higher value for Ge detectors).

- Preamplifier for Ge detectors

Caution: Pulsed feedback preamplifiers contribute to system dead-time (see Section 5.2).

- Stabilizer

  Necessary for NaI detectors due to instabilities of the photomultiplier. Possible reference peaks: Internal α-particle emitter, internal optical pulser, internal gamma lines of the measured spectrum, or external gamma source.

  Optional for Ge detectors. Reference peaks: Internal gamma lines of the measured spectrum, external gamma source, or precision pulser. Preferably digital stabilizer in connection with the ADC.

  Alternative: Software correction for long-term instabilities, if the gamma spectrum is accessible by a computer for analysis of the peak position.

- Pile-up rejector

  Recommended in case of high counting rates, particularly for Ge-detector systems. The pile-up rejector reduces counting-rate losses due to pulse pile-up. Alternative pile-up correction techniques are described in Section 5.2.

  Caution: Pile-up rejectors contribute to system dead-time (see Section 5.2).

- Multichannel analyzer (MCA) with spectrum display

  Recommended for Ge detectors, useful for NaI detectors. A MCA allows a more sophisticated evaluation of the acquired spectral data as compared to single-channel analyzers (SCA). Moreover, the display is very useful for visual checking of the measured gamma spectrum, and it facilitates the setting the counting windows.

  The FWHM of the 186 keV peak should be 6-10 channels minimum. Thus, the recommended conversion gain of the ADC is $\geq$ 2 K channels for Ge detectors.

Note: The user should follow strictly the advices for adjustments of the electronic instruments given by the manufacturer. This concerns parameters as pole-zero cancellation, baseline restoration, DC-level adjustment, lower-level discriminator settings etc.

5.2 Counting losses introduced by system electronics

Both system dead-time and pulse pile-up effects cause counting losses in the 186 keV gamma-ray peak. Since the gamma-spectrometric ^{235}U enrichment assay is based on the determination of the 186 keV gamma counting rate, we have to consider the problem of counting losses in some more detail. In this section some hardware-oriented countermeasures are described that will help to reduce the problem of dead-time and pulse pile-up. Also various methods are discussed that allow to correct the measured 186 keV net peak counts for counting losses.

5.2.1 Dead-time effects

Counting losses due to dead-time effects are observed when the counting system is not ready to accept incoming gamma pulses while it is busy with the processing of a previous event. These losses increase with increasing total detector counting rate. Therefore, dead-time effects must be corrected for in order to avoid a dependence of the measured enrichment value on the total detector counting rate.

The main components of the electronic equipment that contribute to the system dead-time are:

- the preamplifier (only pulsed feed-back preamplifiers!),
- the pile-up rejector, and
- the ADC.

The counting rate is defined as the number of events per unit time. To determine a counting rate, one normally registers the number of events in an event counter, and, simultaneously, the number of pulses derived from a stable high-frequency clock in a separate time counter (timer). Since the time distribution of the incoming gamma events is random in nature, the simplest and most effective way to eliminate system dead-time effects is to switch off the running measurement timer during all time intervals in which the various components of the measurement system are not ready to accept incoming gamma pulses.

As shown in Fig. 5.2, this can be achieved by feeding the "busy" signals of all components contributing to the system dead-time into an appropriate input at the MCA, that gates off the MCA's measurement timer in the high frequency part of its timer clock (use, e.g., the anti-coincidence input at the ADC). Note that in most cases a pulse conditioning of the busy pulses is necessary (time delay and/or pulse stretching) depending on individual characteristics of the electronic equipment used. Required information can be taken from the manuals of the respective electronic components, or may be obtained from the manufacturer of the instruments.

When a complete elimination of system dead-time effects is not possible, we recommend to correct for these effects by normalizing the measured 186 keV counting rate to the counting rate in a reference peak as described in the following Section 5.2.2.

Note: In most MCA's two operation modes are available: real-time counting and live-time counting. In the latter case the "ADC busy" signal is gated automatically to the system timer. This eliminates dead-time effects introduced by the ADC. Therefore, it is recommended to operate the MCA always in live-time mode.

5.2.2 Pulse pile-up effects

Pulse pile-up (or random pulse summing) occurs, when the time interval between two or more succeeding pulses is so short that the pulses will partly or totally overlap, and the sum of the pulses is treated as one event by the analyzing system. This results in incorrect pulse heights being analyzed and registered in the measurement system. Thus, pile-up events involving 186 keV gamma pulses reduce the counting rate within the 186 keV peak, and consequently falsify the measured ^{235}U enrichment value.

The distribution of the length of time intervals between successive events in random processes is described by Poisson statistics. According to this distribution the probability of observing a random coincidence of pulses within the finite pulse-

pair resolving time τ of the system is given by

$$P_{pile\text{-}up} = 1 - e^{-2 \cdot \tau \cdot \dot{N}}, \qquad (5.1)$$

where $\dot{N}$ is the total detector counting rate. P gives the fractional loss of counting rate in the 186 keV peak as a function of the pulse-pair resolving time and of the total detector counting rate. In a first order approximation, P will linearly increase with increasing total detector counting rate $\dot{N}$:

$$P_{pile\text{-}up} = 2 \cdot \tau \cdot \dot{N} \qquad (5.2)$$

In typical counting arrangements with solid state detectors using Gaussian shaped pulses, the pulse-pair resolving time τ corresponds approximately to the pulse peaking time. This peaking time is typically by a factor of 2 to 2.5 larger than the shaping time selected at the main amplifier. As a rough estimate, we expect from eq. 5.2 that at a shaping time of 2 µs (corresponding to $\tau = 2 \cdot 2.5$ µs = 5 µs) the peak counting rate will decrease by approximately 1 %, if the total detector counting rate is increased by 1000 counts/s. Counting rate differences of this order of magnitude may occur, e.g., if freshly separated and aged sample materials are measured.

Note: The effective pulse-pair resolving time relevant for pile-up effects with 186 keV gamma pulses depends critically on details of the shape of the main-amplifier pulse, and on the discrimination power of the ADC for double pulses. The latter, in turn, is influenced to some degree by the amplitude ratio of the summing pulses. Therefore, the effective pulse-pair resolving time is not an invariable instrument's constant, but depends slightly on the form of the measured gamma spectrum, and on the position of the photo peak of interest in the spectrum.

There are several possibilities to correct for pile-up effects in actual measurements:

1. Use of a pile-up rejector

A pile-up rejector supervises the incoming pulse train and rejects a pulse whenever it detects more than one event in a

pre-selectable time interval. Because the rejector normally uses the fast preamplifier pulses as input, it exhibits a much smaller pulse-pair resolving time (typically 500 ns) than the ADC. Therefore, when a pile-up rejector is integrated into the analog pulse processing chain, and its busy signal is properly gated to the system timer (see Fig. 5.2), the pulse pile-up effects in the measurement system can be reduced to a negligible level. No further pile-up correction is required in this case. Pile-up rejector modules are commercially available.

Note: Due to its own finite resolving time the pile-up rejector does not completely eliminate the random pulse summing. This should be observed at very high detector counting rates. It should be considered also that pile-up rejectors can deform the measured spectrum when they are improperly adjusted. It is therefore recommended to test the operation of the pile-up rejector prior to the final installation using one of the methods described below.

2. Normalization to a reference peak

This technique uses a reference pulse source as a counting rate monitor. Pile-up correction is done by normalizing the net peak area of the 186 keV peak to the net peak area of the reference peak.

Note: Similar energy windows for peak- and background-integration should be used for the 186 keV peak and for the reference peak, respectively, in order to assure a similar pile-up behaviour for both peaks. The reference peak can be also used for the purpose of spectrum stabilization.

a) Use of an external gamma source with constant emission rate.

When selecting the reference gamma source one should take care that the energy of the reference line is not too far away from 186 keV, and that the compton background below the 186 keV peak is not unduely increased by the external gamma source. The gamma source should be sufficiently intense to keep the error additionally introduced by the normalization procedure low, i.e., the reference peak should preferably receive more counts than the 186 keV peak.

Note: A correction for the radioactive decay of the reference source is required, when a gamma emitter with a short half-life is used as a long-term stable reference. Extreme care must be taken to keep the source-to-detector distance fixed (see Section 4.3).

Prior to the enrichment measurements the net peak counting rate $\dot{N}^{o}_{ref}$ of the reference peak is determined from the accumulated gamma spectrum (measurement without uranium sample). In any actual ^{235}U enrichment assay both the net peak counting rate $\dot{N}^{meas}_{186}$ of the 186 keV peak and that of the reference peak $\dot{N}^{meas}_{ref}$ are evaluated. From these three counting rates the 186 keV net peak counting rate $\dot{N}_{185}$ corrected for pile-up can be derived

$$\dot{N}_{186} = \dot{N}^{meas}_{186} \cdot C_{El} \quad . \tag{5.3}$$

Note, that the net peak counts N and the net peak counting rate $\dot{N}$, and their respective errors, are related by

$$\dot{N} = \frac{N}{LT} \quad , \quad \frac{\Delta\dot{N}}{\dot{N}} = \frac{\Delta N}{N} \quad ,$$

where LT is the live-time of the measurement. The live-time is defined as the real measurement time minus the cumulative system dead-time.

The pile-up correction factor C_{El} and its associated error are given by:

$$C_{El} = \frac{N^{o}_{ref}}{LT^{o}} \cdot \frac{LT^{meas}}{N^{meas}_{ref}} \quad , \tag{5.4}$$

$$\frac{\Delta C_{El}}{C_{El}} = \sqrt{\left(\frac{\Delta N^{o}_{ref}}{N^{o}_{ref}}\right)^2 + \left(\frac{\Delta N^{meas}_{ref}}{N^{meas}_{ref}}\right)^2} \quad , \tag{5.4a}$$

where N^{o}_{ref} and N^{meas}_{ref} are the net peak counts in the reference peak measured without and with an uranium sample during the measurement live-times LT^{o} and LT^{meas}, respectively. ΔN^{o}_{ref} and ΔN^{meas}_{ref} are the associated errors introduced by the net peak area evaluation.

b) Use of an electronic pulser

Suitable electronic pulsers with periodic or random triggering are commercially available. Since the pulse shapes of pulser pulses usually differ slightly from that of real gamma pulses generated in the detector, the user should assure himself that the pile-up behaviour of the pulser pulses is not very different from that of detector pulses. Pulsers with adjustable rise- and fall-time are better suited in this respect. A stable pulser frequency and, of course, a highly stable pulse amplitude are required when the pulser peak is used as a reference peak. It is recommended to test these two parameters of a pulser for stability prior to its installation in the measurement system. Frequency instabilities of a pulser, or the use of a randomly triggered pulser, necessitate, in general, the determination of the actual mean frequency of the pulser. This can be done by counting the number of pulser pulses during the measurement time in a separate counter, and by recording the real measurement time. The position of the pulser peak in the spectrum should be not too far away from the 186 keV peak (e.g., at ∿175 keV in case of high resolution spectroscopy with a Ge detector).

Note: A small error is introduced by the fact that, unlike gamma pulses, pulser pulses do not sum with each other. This error is neglected here. In case of switched feed-back preamplifiers the use of a randomly triggered pulser may help to avoid possible interference effects between the pulser frequency and the "FET-reset" frequency.

The pile-up correction (see eq. 5.3) and the associated relative error are given by:

$$C_{El} = \nu \cdot \frac{LT^{meas}}{N^{meas}_{pulser}} \quad , \quad \text{for a periodic pulser, or} \qquad (5.5)$$

$$C_{El} = \frac{N^{counted}_{pulser}}{RT^{meas}} \cdot \frac{LT^{meas}}{N^{meas}_{pulser}} \quad , \quad \text{for a randomly triggered pulser, and}$$

$$\frac{\Delta C_{El}}{C_{El}} = \frac{\Delta N^{meas}_{pulser}}{N^{meas}_{pulser}} \quad . \qquad (5.5a)$$

ν is the fixed frequency of a periodic pulser, $N_{pulser}^{counted}$ is the number of pulser events recorded during the measurement real-time RT^{meas} in a separate pulser counter. (The corresponding counting error is neglected here.) N_{pulser}^{meas} and ΔN_{pulser}^{meas} are the net peak counts in the reference peak and the associated error, respectively, which are obtained from the spectrum accumulated during the measurement live-time LT^{meas}.

3. Correction using total counting rate and pulse-pair resolving time

Pile-up effects can be also corrected for according to eq.5.1, provided both the pulse-pair resolving time of the counting system and the total detector counting rate are known. The effective pulse-pair resolving time τ must be determined prior to the actual ^{235}U enrichment assays. For that purpose, the 186 keV net peak counting rate and the total detector counting rate of a representative uranium sample (e.g., of a Reference Sample) are measured without and with an additional external gamma source.

The effective pulse-pair resolving time τ is calculated from eq. 5.1:

$$2 \cdot \tau = \frac{\ln \left(\frac{N_{186}^{0}}{LT^{0}} \cdot \frac{LT^{Src}}{N_{186}^{SRC}} \right)}{\frac{N_{total}^{Src}}{LT^{Src}} - \frac{N_{total}^{0}}{LT^{0}}} \qquad (5.6)$$

N_{186}^{0}, N_{186}^{Src} are the 186 keV net peak counts without and with external gamma source registered during the measurement live times LT^{0} and LT^{SRC}, respectively, and

N_{total}^{0}, N_{total}^{Src} are the total detector counts accumulated during the measurement live-times LT^{0} and LT^{meas}.

As a practicable approximation of the true total detector counting rate, the total number of events registered in the MCA spectrum during the measurement live-time LT may be used.

Note: When selecting the gamma source, care should be taken not to appreciably disturb the overall pulse height distribution of the uranium gamma spectrum by the external gamma radiation. Furthermore, it is essential that the counting geometry for the 186 keV gamma rays is not changed between the measurements. One possible solution to this problem is to apply the additional gamma radiation through a hole drilled into the background gamma shielding of the detector.

Once the effective pulse-pair resolving time τ is known, only the 186 keV net peak counts and the total detector counting rate must be determined in an actual ^{235}U enrichment assay. The pile-up correction according to eq. 5.3 is then given by:

$$C_{El} = e^{2 \cdot \tau \cdot \frac{N_{total}^{meas}}{LT^{meas}}} , \qquad (5.7)$$

with similar notation as in eq. 5.6.

An error is not given in this case because the uncertainty of the pile-up correction is dominated by the systematic error introduced by the determination of the effective pulse-pair resolving time τ (eq. 5.6), which is, in general, much larger than the error due to counting statistics. The author has observed relative deviations of up to 20 % for the τ values, depending on the type of the external gamma source used, on its position relative to the detector, and on the shape of the measured gamma spectrum. It is therefore recommended to apply this pile-up correction technique only if both the changes of the total detector counting rates and the variations in the overall shapes of the measured gamma spectra are moderate.

Which of the above methods for the pile-up corrections is preferably applied in practice has to be decided according to the equipment available to the user. It should be mentioned that the methods discussed under 1.) and 2.) in this sub-section require additional hardware equipment as, e.g., pile-up rejector, gamma source or electronic pulser. The technique given under 3.) needs only the evaluation of the total detector counting rate,

which may be easily obtained from the gamma spectrum accumulated in the MCA. However, due to the difficulties in determining the effective pulse-pair resolving time, its application should be restricted to those cases in which the pile-up corrections are small.

5.3 Net peak area determination

The "enrichment-meter" principle requires the precise determination of the 186 keV gamma counting rates from the samples under assay. In order to evaluate the true number of 186 keV photons from a measured gamma spectrum, one has to remove the background continuum below the peak, which is mainly caused by the scattering of higher-energy gamma rays from the ^{238}U decay. A large variety of methods is available for this purpose, ranging from simple two-window integration up to very complex non-linear least-squares fitting procedures. The latter techniques are in general not required for the ^{235}U enrichment assays because in most applications the major ^{235}U gamma peaks are well isolated in the gamma spectrum, and no significant interference is expected from gamma emitters other than ^{235}U, so that complex unfolding procedures of gamma multiplets are not necessary. However, this argument is not true for NaI detectors, when recycled uranium or other gamma contaminants are present in the sample material. The use of high-resolution Ge detectors is strongly recommended in these cases.

It is outside the scope of the manual to give a thorough discussion of the various methods of background subtraction. We will describe here only three commonly used, simple techniques for the evaluation of the net-peak area and of the associated errors due to counting statistics. Prior to this, some general rules are outlined that apply to the selection of the counting windows.

5.3.1 Selection of peak- and background windows

The fact that we use always "quasi-infinite" samples in ^{235}U enrichment measurements exhibits an important aspect that is not generally given for other types of gamma sources: the "infinite-sample" condition is not only fulfilled for 186 keV photons, but, obviously, also for ^{235}U photons with lower energies, and it is approximately satisfied for the few weak gamma lines from ^{235}U with energies above 186 keV. Moreover, since the "saturation" of the gamma activity from thick samples discussed in Section 2.2 comprises both the gamma peaks and the continuum due to inelastic gamma scattering, we can expect that the entire gamma spectrum originating from ^{235}U (not only the 186 keV peak) is proportional to the ^{235}U enrichment in case of infinite samples. It should be noted, however, that with decreasing photon energy the ^{235}U gamma counting rate becomes more sensitive to variations of the sample matrix, and of the container wall.

As background we define that portion of the total gamma spectrum (peaks and continuum) which arises from gamma emitters other than ^{235}U, and which is therefore not proportional to the ^{235}U enrichment. The photons causing background originate from the decay of ^{238}U, from minor uranium isotopes, from gamma contaminants present in the sample, or from the ambient background radiation. The amplitude of the background spectrum and, to some extent, its shape may vary as a function of the sample age, of the sample size, of the isotopic composition of the sample etc. In order to arrive at a "true" ^{235}U gamma counting rate, the background portion must be removed from the total number of events registered in the gamma spectrum.

In our particular case of thick samples it is, in principle, not necessary to restrict the evaluation of the ^{235}U gamma counting rate to 186 keV photons only. Any suitable energy window in the ^{235}U gamma spectrum may serve for the purpose of enrichment assays. However, the optimum choice will be an energy region in the gamma spectrum that provides likewise the best "signal-to-background" ratio for ^{235}U gamma radiation and the lowest sensitivity to changes of secondary measurement parameters. In most applica-

tions both requirements are met only for an energy window around the strongest ^{235}U gamma peak at 186 keV. Note, that no detailed peak analysis is necessary. The 186 keV peak just marks the energy window that provides the lowest counting error. In this modified sense the terms "net peak" area and "net peak" counting rate should be interpreted here.

Simple methods for the evaluation of the net area of the 186 keV gamma peak use only the gross counts measured in two or three selected energy windows: one window is set around the 186 keV peak, and one or two windows are placed outside the peak region in order to get an estimate of the background portion within the peak window. The resulting error of the net peak area depends on uncertainties of the gross counts in the selected counting windows.

When selecting the width and the position of the counting windows, the following criteria should be considered:

1. Minimization of the error due to counting statistics.
2. Low sensitivity to electronic instabilities (gain shift, zero shift, change of spectral resolution).
3. Low sensitivity to changes of the shape of the background spectrum.
4. Minimization of gamma interference effects.

Which one of these factors will have the strongest effect on the assay accuracy depends on the properties of the counting equipment used, and on the sample material under assay. Therefore, only some general rules for the selection of the width and of the position of the counting windows are given (the numbers in brackets refer to the afore-mentioned objectives).

Background windows

The width of the selected background windows should be at least of the same size as the width of the peak window, preferably larger (1).

The position of the background windows should be clearly outside the peak region in the flat part of the gamma spectrum (2), but not too far away from the gamma peak of interest (3). Special care must be observed to avoid gamma interference from

isotopes other than ^{235}U (4) (see Section 3.4 and Tables in Appendix B).

Note: The presence of ^{235}U photons in the background window(s) will not introduce a systematic error into the enrichment assay. It only increases the random error in the determination of the net peak area. In particular, when using a NaI detector it may happen that no suitable background window can be found on the high-energy side of the 186 keV peak due to strong gamma interference effects. In this case one may use a background window at the low-energy side of the peak at the expense of an increased random error of the net peak counts.

Peak window

The position of the peak window in a set-up using an MCA should be selected in such a way that the channel contents at the window boundaries are approximately equal (2). For symmetric peaks the window limits are then centered around the 186 keV peak maximum.

The selection of the width of the peak window is always a compromise between optimum "signal-to-background" ratio P/B (1) and low sensitivity to electronic instabilities (2). When using NaI detectors, possible gamma interference effects (4) must be also taken into account. Table 5.1 shows the tolerance limits for electronic instabilities at various window widths that must be observed to keep the impact on the assay result below 0.1 %. The Table also provides error factors for some typical "peak-to-background" ratios P/B. The error factors describe the increase of the random counting error as compared to a background-free measurement using a wide peak window. The values given in Table 5.1 are derived from a simple model assuming a purely Gaussian peak form, a constant background, and equal width of peak- and background windows.

It can be deduced from columns 5, 6 and 7 in Table 5.1 that the best choice for the width of the peak window with respect to the lowest random counting error would be a width corresponding to 1.3 to 1.8 units of FWHM. However, this window setting makes the assay result very sensitive to small drifts of the peak position and to variations of the energy resolution (see columns 3 and 4 in Table 5.1). We therefore recommend to

use a window width of about 2.5 to 3 times the FWHM for the peak. In case of high-resolution Ge spectra one may consider to include the 182.7 keV satellite peak from the ^{235}U decay in the peak window.

Note: It is a good practice to monitor the position and the FWHM of the 186 keV peak during the measurements in order to increase the reliability of the assay results.

Table 5.1 Tolerance values for peak shifts and FWHM variations at the level of 0.1 % assay error, and error factors given for different widths of the peak window and different peak-to-background ratios P/B

Widths of peak window in units of FWHM	% of total net peak area	Tolerable peak shift (in % of FWHM)	Tolerable variation of FWHM (%)	Error factors relative to a background-free measurement		
				P/B=0.1	P/B=1	P/B=10
1	76.16 %	± 2.4 %	+ 0.15 % - 0.17 %	5.81	2.14	1.28
1.5	92.26 %	± 3.4 %	+ 0.29 % - 0.33 %	5.85	2.10	1.19
2	98.15 %	± 5.5 %	+ 0.80 % - 0.87 %	6.33	2.22	1.19
2.5	99.68 %	± 11 %	+ 2.92 % - 3.67 %	6.95	2.39	1.21
3	99.96 %	± 23 %	+ 10.6 % - --	7.58	2.58	1.25
4	99.999 %	± 68 %	+ 43.2 % - --	8.73	2.92	1.32

5.3.2 Background subtraction

In this section three simple methods are discussed which model the background in the peak window from the counts registered in the background window(s). In contrast to the more elaborate peak fitting procedures, these methods do not require any knowledge about details of the peak form.

a) Two-window counting

This is the simplest method to evaluate the net peak area of the 186 keV peak. The "two-window" technique uses only the gross gamma counts registered during the measurement time LT in two selected energy windows, one window for the 186 keV peak, and one window which is representative for the background. The gross counts can be obtained either from two single-channel analyzers connected to two counters (as realized, e.g., in the SAM-2 unit), or by integrating the channel contents in two energy regions of the MCA spectrum. In order to get the true ^{235}U signal, we have to subtract the background portion from the gross counts in the peak window.

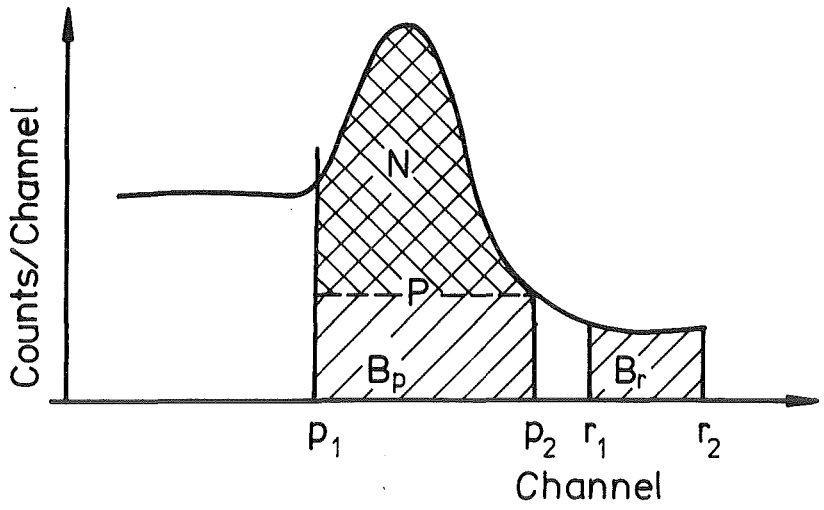

Fig. 5.3 Two-window counting.

As a model for the background part in the peak window we assume that the background portions in both counting windows are always proportional to each other (see Fig. 5.9).

$$B_p = b \cdot B_r \tag{5.8}$$

Note, that the background window needs not necessarily be located at the high energy side of the 186 keV peak, as given in Fig. 5.3.

The peak counts are then calculated from

$$N^{meas} = P - b \cdot B_r \quad , \tag{5.9}$$

where P and B_r denote the gross counts in the peak- and background window, respectively.

When we further simplify the model assuming a constant background, then the proportionality constant b is given as the ratio of the widths of both counting windows (see Fig. 5.3):

$$b = \frac{p_2 - p_1 + 1}{r_2 - r_1 + 1} \quad . \tag{5.10}$$

The standard deviation of the net peak counts is given in this case by

$$\Delta N^{meas} = \sqrt{P + b^2 \cdot B_r} \quad , \tag{5.11}$$

with same notations as used above.

It must be stressed that the assumption of a constant background is not a good model for many observed gamma spectra. Therefore, instead of using eq. 5.10, we recommend to derive the constant b from a calibration run using the Reference Samples. The constant b is then obtained along with the other fit parameters a and c from a least-squares fit of the gamma counting rates to the enrichment values enr according to :

$$enr = a \cdot (\dot{P} - b \cdot \dot{B}_r) + c \quad . \tag{5.12}$$

Details are given in Section 5.4. The counting rates $\dot{P}$ and $\dot{B}_r$ are related to the gross counts P and B_r by

$$\dot{P} = \frac{P}{LT} \quad , \quad \dot{B}_r = \frac{B_r}{LT} \quad ,$$

where LT is the measurement life time, i.e., the real measurement time minus the cumulative system dead-time (see Section 5.2).

Note, that the "two-window" technique described in this paragraph is based on the assumption that the background portions in both counting windows are proportional to each other, or, in other words, that the shape (not the amplitude!) of the background spectrum within the region of interest remains invariant for all samples under assay. This condition may be not fulfilled in case of strong differences with respect to

- sample size (scattering of 1 MeV photons),
- container wall (photon attenuation),
- gamma contaminants in the sample material, and
- ambient background gamma radiation.

The "three-window" methods discussed in the following are less sensitive to variations of these parameters.

b) Three-window counting, linear background

This procedure uses the gross counts acquired in the peak window and in two adjacent background windows on both sides of the peak (see Fig. 5.4). The gross counts are obtained either by using three single-channel analyzers and three counters, or by integrating the channel contents of the measured MCA spectrum in the three regions of interest.

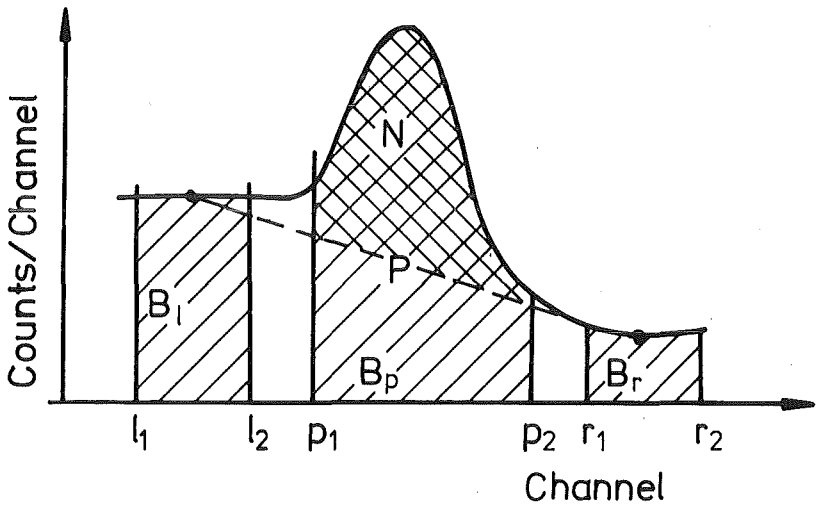

Fig. 5.4 Linear background.

As a model for the background in the peak window we assume here that the background portions within the three counting windows are related by a linear function

$$B_p = e \cdot B_\ell + f \cdot B_r \qquad (5.13)$$

For notations see Fig. 5.4.

When we approximate the background by a straight line going through the midpoints of the two background windows, then we can calculate the constants e and f from the widths and the relative positions of the counting windows. Using the notation of Fig. 5.4 we get

$$e = \frac{p_2 - p_1 + 1}{\ell_2 - \ell_1 + 1} \cdot \frac{r_1 + r_2 - p_1 - p_2}{r_1 + r_2 - \ell_1 - \ell_2} \qquad (5.14a)$$

$$f = \frac{p_2 - p_1 + 1}{r_2 - r_1 + 1} \cdot \frac{p_1 + p_2 - \ell_1 - \ell_2}{r_1 + r_2 - \ell_1 - \ell_2} \quad . \qquad (5.14b)$$

The net counts of the 186 keV peak and the standard deviation are then given by

$$\begin{aligned} N^{meas} &= P - B_p \\ &= P - e \cdot B_\ell - f \cdot B_r \quad , \end{aligned} \qquad (5.15)$$

and

$$\Delta N^{meas} = \sqrt{P + e^2 \cdot B_\ell + f^2 \cdot B_r} \quad , \qquad (5.16)$$

where P, B_ℓ and B_r denote the gross counts in the three counting windows.

Alternatively, the constants e and f can be also obtained from a calibration procedure using the Reference Material. The calibration equation that relates the enrichment values and the observed gross counting rates is given by

$$enr = a \cdot (\dot{P} - e \cdot \dot{B}_\ell - f \cdot \dot{B}_r) + c \quad , \qquad (5.17)$$

with similar notation as used in eq. 5.12.

c) Smoothed step-like background

In gamma spectra obtained from thick samples one observes that the background at the low-energy side of a gamma peak is higher than the background at the high-energy side. This effect is mainly caused by small-angle scattering of the "peak photons" within the sample material. Gunnink [15] has described a method

that removes also this portion of the background from the gamma peak so that only unscattered photons are remaining in the net peak.

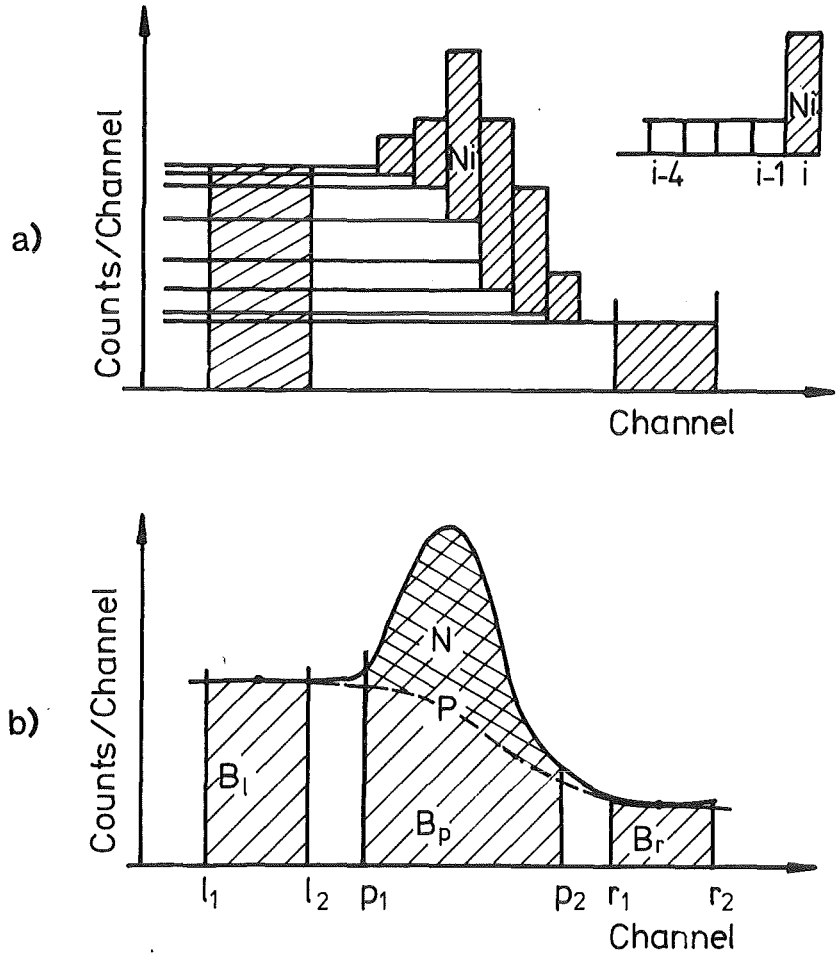

Figs. 5.5a and 5.5b Smoothed step-like background

In general, the small-angle scattering effect has to be taken into account when peak multiplets are to be analyzed, or when small samples with varying sizes are measured resulting in varying contributions to the scattering effect. Both conditions are not given in the particular case of enrichment measurements: the 186 keV peak is normally well isolated in the gamma spectrum, and the quasi-infinite sample size causes the height of the "scattering step" to be always a fixed fraction of the "true" net-peak area. Therefore, the removal of the scattered ^{235}U photons from the 186 keV peak is, in principle, not necessary for enrichment analyses. However, the technique for background subtraction described in this paragraph makes the resulting net peak area less sensitive to electronic shifts and less dependent on the posi-

tion of the counting windows, as can be seen from a comparison of Figs. 5.3, 5.4 and 5.5b.

In contrast to the methods described before under a) and b) this technique requires the use of a MCA and of a computer to perform the necessary calculations and the channel-by channel background subtraction.

As shown in Figs. 5.5a and 5.5b the underlying model assumes in its simplest form that

- the background continuum is constant, and
- any - still unknown - net counts registered in channel i scatter a small, constant fraction of its amplitude N_i into any lower channel $j < i$, as indicated in the insert in Fig. 5.5a.

The "scattering amplitude" is adjusted in such a way that the sum of the scattering events plus the constant background fit to the background in the low-energy window (see Fig. 5.5a). The resulting total background appears as a smoothed step below the peak with a step height proportional to the integral net counts (see Fig. 5.5b). Since both the scattering amplitude and the net counts N_i are unknown, the solution of the problem is to be obtained from an iterative procedure. The iteration equation for the net peak counts N_i is given by

$$N^{(\nu+1)}(i) = Y(i) - \frac{B_\ell}{\ell_2-\ell_1+1} + \frac{\frac{B_\ell}{\ell_2-\ell_1+1} - \frac{B_r}{r_2-r_1+1}}{\sum_{k=\mathrm{INT}(\frac{\ell_1+\ell_2}{2}+1)}^{\mathrm{INT}((r_1+r_2)/2)} N^{(\nu)}(k)} \cdot \sum_{j=\mathrm{INT}(\frac{\ell_1+\ell_2}{2}+1)}^{i} N^{(\nu)}(j) \qquad (5.18)$$

for all channels $i = \mathrm{INT}(\frac{\ell_1+\ell_2}{2}+1), \ldots, \mathrm{INT}(\frac{r_1+r_2}{2})$.
$Y(i)$ denotes the content of channel i, B_ℓ and B_r are the integrated channel contents in the background windows

$$B_\ell = \sum_{i=\ell_1}^{\ell_2} Y(i), \qquad B_r = \sum_{i=r_1}^{r_2} Y(i)$$

with window limits ℓ_1, ℓ_2 and r_1, r_2, respectively (see Fig. 5.5b). The function INT returns the integer number closest to the argument.

When we use the somewhat arbitrary starting condition

$$N^{(0)}(i) \equiv 1 \quad , \tag{5.19}$$

then the first iteration step delivers the solution for the linear background discussed under b). Usually, sufficient convergence of the net count values $N^{(\nu)}(i)$ is obtained after three to four iteration steps.

The net peak counts N^{meas} are calculated from the net counts $N^{(m)}(i)$ in the peak window after m iterations

$$N^{meas} = \sum_{i=p_1}^{p_2} N^{(m)}(i) \quad , \tag{5.20}$$

with peak window limits p_1 and p_2. Denoting the gross counts in the peak window by P

$$P = \sum_{i=p_1}^{p_2} Y(i) \quad ,$$

and introducing the following abbreviations

$$\xi = \frac{r_1+r_2-p_1-p_2}{\ell_2-\ell_1+1} \quad , \qquad \eta = \frac{p_1+p_2-\ell_1-\ell_2}{r_2-r_1+1} \quad ,$$

we get an estimate of the standard deviation of the net peak counts N^{meas}

$$\Delta N^{meas} = \sqrt{P + (P - N^{meas})^2 \cdot \frac{(\xi^2 \cdot B_\ell + \eta^2 \cdot B_r)}{(\xi \cdot B_\ell + \eta \cdot B_r)^2}} \quad , \tag{5.21}$$

with notations given above.

Summary:

The user may select one of the techniques for net peak area evaluation described in this section, or he may apply more elaborate evaluation procedures according to his available equipment for data evaluation. It should be mentioned that even very simple methods

for net peak evaluation can yield highly accurate assay results, provided the model used for the background below the peak is adequate to the "true" background, and the counting-window parameters are carefully selected. In many applications the stability of the counting set-up and the appropriate setting of the width and the position of the counting windows will enter more critically into the accuracy of the assay result than the choice of a particular procedure for the net peak evaluation.

Some MCA's are equipped with programs for net peak area evaluation. Care should be taken in this case, when the background windows are selected automatically, e.g., when only one channel or a few channels directly adjacent to the peak window are used for the background determination. This is possibly not the best evaluation procedure with respect to counting precision and measurement accuracy.

Note: The various techniques for net peak evaluation discussed in this section will, in general, result in different net peak counting rates obtained from the same gamma spectrum, because the "net peak" areas contain different portions of the total ^{235}U gamma spectrum, e.g., including (method a) or excluding (method c) the small-angle scattering portion of the 186 keV photons. Also the choice of the counting windows will influence the resulting net counting rates. However, once a particular evaluation technique is selected and the window settings are fixed, then we can expect that the net peak counting rates obtained from the samples under assay are always <u>proportional</u> to the "pure" ^{235}U gamma counting rates, and, thus, to the ^{235}U enrichment. Obviously, the calibration constants will differ for various methods and various windows settings. Therefore, any change of the data evaluation technique and/or counting parameters requires a recalibration of the counting system.

5.4 Calibration

It has been shown in Section 2.4 of the manual that gamma-spectroscopic measurements of the ^{235}U enrichment cannot be performed at the desirable accuracy level on an absolute basis. Therefore, highly accurate ^{235}U enrichment measurements are usually made relative to reference samples with well known ^{235}U enrichment values. The calibration of a measurement system is defined as a procedure consisting of four steps:

1. The measurement of the reference samples in the counting setup that is to be calibrated.
2. Formulation of a mathematical model that relates the response of the measurement system (186 keV gamma counting rate) to the parameter of interest (^{235}U enrichment).
3. Determination of the parameters of the model from the measurements.
4. Determination of the standard deviations of these parameters.

With the set of calibration parameters it is possible to determine the ^{235}U enrichment of an unknown sample from a gamma-spectroscopic measurement, using additional informations about wall thickness, matrix composition etc. It is essential, that also the error limits of the predicted enrichment value can be obtained, since, in general, a measured value given without an error estimate is only of limited value.

In this section a calibration procedure is described that assumes a linear relation between the 186 keV gamma counting rate and the ^{235}U enrichment. The calibration constants and their standard deviations are derived from a least-squares fit taking into account that both the gamma counting rates and the enrichment values are subject to errors. Also some hints are given how to test the quality of the fit.

5.4.1 The calibration equation

Under well defined conditions, as described in the previous chapters, the relation of the 186 keV gamma counting rate $\dot{N}^{meas}$ and the ^{235}U enrichment enr can be expressed by

$$enr = a \cdot \dot{N}^{meas} \cdot C_{Ma} \cdot C_{Wa} \cdot C_{El} + C_{Int} \qquad (5.22a)$$

where the C's denote the correction terms for matrix attenuation, container wall attenuation, counting rate losses and gamma interference, respectively, described in Sections 4.1, 4.2, 4.4 and 5.2. $\dot{N}^{meas}$ is the observed 186 keV net peak counting rate, and a is a proportionality factor that is determined from the calibration experiment using the Reference Material.

When the "two-window" technique is used for the determination of the ^{235}U enrichment, the 186 keV net peak counting rate is not evaluated explicitely. Eq. 5.22a is then modified to

$$enr = (a \cdot \dot{P}^{meas} + b \cdot \dot{B}^{meas}) \cdot C_{Ma} \cdot C_{Wa} \cdot C_{El} + C_{Int}. \qquad (5.22b)$$

$\dot{P}^{meas}$ and $\dot{B}^{meas}$ are the observed gross counting rates in the peak- and background window, respectively. In this case the parameters a and b are determined from the calibration run using the Reference Material. Note that in eq. 5.22b the same photon attenuation corrections C_{Ma} and C_{Wa} are used for both windows. This approximation is acceptable if the mean energies of the two counting windows are not very different, and/or if the attenuation corrections are small.

The correction factors C_{Ma} and C_{Wa}, as defined in this manual, are equal to 1 for the Reference Material, i.e., for U_3O_8 samples contained in the reference cans with 2 mm aluminium bottom. The calibration equations for the Reference Samples are then given by

$$enr = a \cdot \dot{N}^{meas} \cdot C_{El} + C_{Int}, \qquad (5.23a)$$

and

$$enr = (a \cdot \dot{P}^{meas} + b \cdot \dot{B}^{meas}) \cdot C_{El} + C_{Int}. \qquad (5.23b)$$

To further simplify the notation, we define the counting rates corrected for electronic losses by

$$\dot{N} =: \dot{N}^{meas} \cdot C_{El} \quad ,$$

$$\dot{P} =: \dot{P}^{meas} \cdot C_{El} \quad ,$$

$$\dot{B} =: \dot{B}^{meas} \cdot C_{El} \quad ,$$

and change the notation for the enrichment and for the gamma interference term to

$$E =: enr$$

$$C =: C_{Int} \quad .$$

Then we finally arrive at the equations

$$E = a \cdot \dot{N} + C \quad , \qquad (5.24a)$$

and

$$E = a \cdot \dot{P} + b \cdot \dot{B} + C \quad , \qquad (5.24b)$$

which present in a compressed form our assumed linear model for the relation between the 186 keV gamma counting rate and the enrichment value.

An estimate of the gamma interference term C can be obtained from eq. 3.26 in Section 3.4 using the Tables in Appendix B, provided the relative abundances of the isotopes producing the interference are known. This requirement is met for the Reference Material.

The interference term C can be also treated as a free parameter in the fit procedure. The comparison of the fitted value and the expected value of C may then serve as an indicator of the goodness of the fit or of the validity of the underlying linear model (see Section 5.4.4).

Once the gamma interference term C is known (or, if it can be forced to zero by a suitable selection of the counting windows (see section 3.4)), we arrive at the homogeneous form of the calibration equations

$$E' = E - C = a \cdot \dot{N} \quad , \qquad (5.24c)$$

and

$$E' = E - C = a \cdot \dot{P} + b \cdot \dot{B} \quad . \tag{5.24d}$$

If the parameters of the "three-window counting" technique are determined from the calibration procedure (see eq. 5.17), then the corresponding calibration equations are given by

$$E = a \cdot \dot{P} + e \cdot \dot{B}_{\ell} + f \cdot \dot{B}_{r} + C \quad , \tag{5.24e}$$

and

$$E' = E - C = a \cdot \dot{P} + e \cdot \dot{B}_{\ell} + f \cdot \dot{B}_{r} \quad . \tag{5.24f}$$

We restrict the further discussion on eqs. 5.24a and 5.24d. However, the considerations outlined in the following sections can be easily transferred to other cases.

5.4.2 Observation errors

The corrected counting rates $\dot{N}$, $\dot{P}$, $\dot{B}$ of the Reference Samples are products of the form

$$\dot{N} = \dot{N}^{meas} \cdot C_{EL} \quad , \tag{5.25}$$

In the more general case of samples with a matrix composition and a container wall which differs from that of the Reference Samples we get

$$\dot{N} = \dot{N}^{meas} \cdot C_{MA} \cdot C_{Wa} \cdot C_{El} \quad . \tag{5.25a}$$

It should be noted that besides the random error $\Delta\dot{N}^{meas}$ introduced by the random nature of the radioactive decay, also the uncertainties of the various corrections will contribute to the total error of the net peak counting rate $\dot{N}$. Therefore, the standard deviation of $\dot{N}$ is given by

$$\Delta\dot{N} = \dot{N} \cdot \sqrt{\left(\frac{\Delta\dot{N}^{meas}}{\dot{N}^{meas}}\right)^2 + \left(\frac{\Delta C_{El}}{El}\right)^2} \quad , \text{ and} \tag{5.26}$$

$$\Delta\dot{N} = \dot{N} \cdot \sqrt{\left(\frac{\Delta\dot{N}^{meas}}{\dot{N}^{meas}}\right)^2 + \left(\frac{\Delta C_{Ma}}{C_{Ma}}\right)^2 + \left(\frac{\Delta C_{Wa}}{C_{Wa}}\right)^2 + \left(\frac{\Delta C_{El}}{C_{El}}\right)^2} \quad , \tag{5.26a}$$

respectively. The various error components are discussed in the

previous sections of the manual. We have assumed here that the individual error contributions are not correlated, which is a reasonable approach, since the various corrections are based on independent observations. Similar equations apply to the standard deviations of the counting rates $\dot{P}$ and $\dot{B}$, which are omitted here.

We have to consider that also the enrichment values of the reference samples determined by mass spectrometry are subject to errors. When using the Reference Material EC-NRM-171/NBS-SRM-969 as calibration standards these errors are negligibly small, but in general they must be included in the error analysis. Note that the enrichment uncertainties of the RM are given in the certificate at the 2σ level or 95 % confidence level. Since in our data analysis we refer to the standard deviation ΔE or its square, the variance var(E), those values must be divided by a factor of 2.

It should be noted that the stated enrichment uncertainties comprise random and systematic errors as well. That portion of the systematic deviations between the true ^{235}U enrichment and the quoted mass-spectrometric values which appears as offset or which is proportional to the ^{235}U enrichment, is not recognized in our error analysis,since we fit the data to a general linear relation between gamma counting rate and ^{235}U enrichment. This part, if identifiable, should be removed from the stated enrichment error prior to entering into the data evaluation procedure described below, and should then be added to the final enrichment error.

We assume that a set of n reference samples has been measured in the counting set-up to be calibrated, and that the necessary corrections have been applied to the counting rates. The result of the calibration measurements is then a set of n pairs of observations $(E_i, \dot{N}_i)$, or, in case of the "two-window counting" technique, a set of n tripels of observations $(E_i, \dot{P}_i, \dot{B}_i)$. Each of these observations has its own individual error. In our data analysis we make the following assumptions for the structure of the observation errors:

1. The errors of each observation are randomly distributed with zero mean around its (unknown) true value,
2. The errors in all observations are independent and not correlated.
3. The standard deviations (or the corresponding variances) of all observations are known:

$$\text{var}\ (\dot{E}_i) = (\Delta\dot{E}_i)^2$$
$$\text{var}\ (\dot{N}_i) = (\Delta\dot{N}_i)^2$$
$$\text{var}\ (\dot{P}_i) = (\Delta\dot{P}_i)^2$$
$$\text{var}\ (\dot{B}_i) = (\Delta\dot{B}_i)^2$$

Note: This approach does not account for systematic errors and those random errors that have not been identified, or that cannot be easily quantified in real applications, as, e.g., environmental conditions, sample positioning, inhomogeneity of sample enrichment, etc.

When determining the gamma counting rates one should try to eliminate, whenever possible, known systematic deviations by a careful experimental design and by using the various correction terms that are to be applied to the measurements with both the reference samples and the unknown samples. This procedure should be preferred to the introduction of non-linear terms in the calibration equation.

In order to assess unidentified random errors of the corrected gamma counting rates it is useful to repeat the cycle of calibration measurements several times, to calculate the standard deviation of the measured counting rates for each reference sample, and to compare it to the error estimate obtained from a single measurement. A disagreement between the two values may indicate that the error estimates are wrong. Comparing the counting rates obtained from calibration runs performed at distinct times will also help to check the correctness of the assumed errors. Though time-consuming, the validation of the error estimates is strongly recommended, in particular, when a new counting set-up is used, or when relevant measurement parameters are changed.

5.4.3 Solution of the linear least-squares fitting problem

Several solutions to the problem of linear least-squares fits are reported in the literature for our case that all observations are subject to errors. Two recent publications are related to this problem [16, 18]. Also the FORTRAN program 'COMFIT' [19] is available for use on main-frame computers.

The solution given in this section is a simple linear approach that will run on small computers or even on programmable pocket calculators. For the user's convenience a program example written in 'BASIC' language is added to the manual in Appendix E.

The calculation of the fit parameters and their associated errors is demonstrated in this section only for the calibration eqs. 5.24a and 5.24d discussed in Section 5.4.1. The other cases can be derived following the same procedures as given below.

We recall the assumptions required for the validity of our data evaluation model:

1. The relation between observed counting rates and ^{235}U enrichment is linear

$$E = a \cdot \dot{N} + C \quad , \qquad (5.24a)$$

$$E = a \cdot \dot{P} + b \cdot \dot{B} \quad . \qquad (5.24d)$$

2. The observations E, $\dot{N}$, and E, $\dot{P}$, $\dot{B}$, respectively, are made with independent errors.

3. The variances of all observations are known.

In case that one of the conditions is not satisfied, a more elaborate data evaluation will be necessary. A thourough discussion of these problems is given in [17]. Note that the solution described in this section is identical to the "maximum likelihood" estimate, when the errors follow the normal distribution.

a) Solution for the calibration equation $E = a \cdot \dot{N} + C$

We assume that n calibration measurements have been performed using n different reference samples i. We then have n pairs of observations $(E_i, \dot{N}_i)$ and the estimates for the corresponding variances $var(E_i)$, $var(\dot{N}_i)$. We define the residuals Δ_i as

$$\Delta_i =: E_i - a \cdot \dot{N}_i - C \quad , \tag{5.27}$$

and the generalized weight factors [18] G_i as

$$G_i =: \frac{1}{var(E_i) + a^2 \cdot var(\dot{N}_i)} \tag{5.28}$$

According to the principle of least-squares fitting the fit parameters a and C are determined in a way that the sum of the weighted squares of the residuals becomes a minimum:

$$\sum_{i=1}^{n} G_i \cdot \Delta_i^2 = \min \quad , \tag{5.29}$$

where the summation is performed over all n measurements. In the following equations we omit the summation limits.

Setting the partial derivatives with respect to the parameters a and C equal to zero:

$$\sum \frac{\partial G_i}{\partial a} \cdot \Delta_i^2 + \sum G_i \cdot \frac{\partial \Delta_i^2}{\partial a} = 0 \quad , \tag{5.30}$$

$$\sum G_i \cdot \frac{\partial \Delta_i^2}{\partial C} = 0 \quad , \tag{5.31}$$

delivers a system of linear equations for a and C:

$$a \cdot [\Sigma\, G_i \dot{N}_i^2 - \Sigma\, var(\dot{N}_i)\, G_i^2\, \Delta_i^2] + C \cdot \Sigma\, G_i \dot{N}_i = \Sigma\, G_i E_i \dot{N}_i \tag{5.32}$$

$$a \cdot \Sigma\, G_i \dot{N}_i + C \cdot \Sigma\, G_i = \Sigma\, G_i E_i \quad . \tag{5.33}$$

Introducing the abbreviation DET for the determinant of the coefficient matrix of the parameters a and C:

$$DET = \Sigma\, G_i\, [\Sigma\, G_i \dot{N}_i^2 - \Sigma\, var(\dot{N}_i)\, G_i^2 \Delta_i^2] - (\Sigma\, G_i \dot{N}_i)^2 \quad , \tag{5.34}$$

the solution of the system can be written as

$$a = \frac{1}{DET} \left(\Sigma G_i E_i \dot{N}_i \cdot \Sigma G_i - \Sigma G_i E_i \cdot \Sigma G_i \dot{N}_i\right) \tag{5.35}$$

$$C = \frac{1}{DET} \left[\left(\Sigma G_i \dot{N}_i^2 - \Sigma var(\dot{N}_i) G_i^2 \Delta_i^2\right) \cdot \Sigma G_i E_i - \Sigma G_i E_i \dot{N}_i \cdot \Sigma G_i \dot{N}_i\right] \tag{5.36}$$

Note that Δ_i and G_i still depend on the unknown parameters a and C. Inserting a and C will lead to a system of high order equations in a and C which cannot be solved analytically. Instead of this one can get the solution from an iterative approach. The iteration procedure is given below in a schematic form. Simple arbitrary starting values are used.

1) Start values G_i and Δ_i:

$$G_i^{(0)} =: 1 , \quad \Delta_i^{(0)} =: 0 \qquad (i = 1, \ldots, n). \tag{5.37}$$

2) Solution for a and C (Iteration steps $\nu = 0, 1, \ldots.$) :

$$DET^{(\nu+1)} =: \Sigma G_i^{(\nu)} \left\{\Sigma G_i^{(\nu)} \dot{N}_i^2 - \Sigma var(\dot{N}_i) [G_i^{(\nu)}]^2 [\Delta_i^{(\nu)}]^2\right\} - [\Sigma G_i^{(\nu)} \dot{N}_i]^2 \tag{5.38}$$

$$a^{(\nu+1)} = \frac{1}{DET^{(\nu+1)}} \left[\Sigma G_i^{(\nu)} E_i \dot{N}_i \; \Sigma G_i^{(\nu)} - \Sigma G_i^{(\nu)} E_i \; \Sigma G_i^{(\nu)} \dot{N}_i\right] \tag{5.39}$$

$$C^{(\nu+1)} = \frac{1}{DET^{(\nu+1)}} \left[\left(\Sigma G_i^{(\nu)} \dot{N}_i^2 - \Sigma var(\dot{N}_i) [G_i^{(\nu)}]^2 [\Delta_i^{(\nu)}]^2\right) \cdot \Sigma G_i^{(\nu)} E_i - \right. \tag{5.40}$$

$$\left. - \Sigma G_i^{(\nu)} E_i \dot{N}_i \cdot \Sigma G_i^{(\nu)} \dot{N}_i\right]$$

3) Refined values G_i and Δ_i

$$G_i^{(\nu+1)} = \frac{1}{var(E_i) + [a^{(\nu+1)}]^2 \cdot var(N_i)} \tag{5.41}$$

$$\Delta_i^{(\nu+1)} = E_i - a^{(\nu+1)} \dot{N}_i - C^{(\nu+1)} \qquad (5.42)$$

Iteration steps 2 and 3 are repeated until convergence is achieved. Under normal conditions the iteration converges quite rapidly, three to four iteration steps will be sufficient.

Estimates for the variances of the fitted parameters a and C are obtained from the reduced cofactors of the coefficient matrix of the parameters after m iteration steps:

$$\mathrm{var}(a^{(m)}) = \frac{\Sigma\, G_i^{(m)}}{DET^{(m)}} \qquad (5.43)$$

$$\mathrm{var}(C^{(m)}) = \frac{1}{DET^{(m)}} \left[\Sigma\, G_i^{(m)}\, \dot{N}_i^2 - \Sigma\, \mathrm{var}(\dot{N}_i) [G_i^{(m)}]^2 [\Delta_i^{(m)}]^2 \right] \qquad (5.44)$$

Note, that the parameters a and C are correlated. We have therefore a non-vanishing covariance term:

$$\mathrm{cov}(a^{(m)}, C^{(m)}) = \frac{-\Sigma\, G_i^{(m)}\, \dot{N}_i}{DET^{(m)}} \qquad (5.45)$$

The quantity ω^2 may be used as an indicator of the quality of the fit (see Section 5.4.4). It is the χ^2 value devided by the degrees of freedom (DOF):

$$\omega^2 = \frac{\chi^2}{DOF} = \frac{1}{n-2} \Sigma\, G_i^{(m)} [\Delta_i^{(m)}]^2 . \qquad (5.46)$$

The best estimate of the ^{235}U enrichment of an unknown sample from the measured 186 keV peak counting rate $\dot{N}_U$ and its associated variance $\mathrm{var}(\dot{N}_U)$ is then given by

$$\bar{E} = a^{(m)} \cdot \dot{N}_U + C^{(m)} \quad , \qquad (5.47)$$

and the estimated standard deviation of this value is

$$\Delta\bar{E} = \sqrt{a^{(m)^2} \cdot \mathrm{var}(\dot{N}_U) + \dot{N}_U^{\,2} \cdot \mathrm{var}(a^{(m)}) + 2 \cdot \dot{N}_U \cdot \mathrm{cov}(a^{(m)}, C^{(m)}) + \mathrm{var}(C^{(m)})}, \tag{5.48}$$

where the first term in eq. 5.48 represents the error introduced by the measurement of the unknown sample, and the remaining three terms represent the calibration error. Note that the variance of the counting rate comprises the error due to the net peak area evaluation as well as the errors introduced by the various corrections (matrix, container wall, counting rate losses).

b) Solution for the calibration equation $E = a \cdot \dot{P} + b \cdot \dot{B}$

We assume again that n calibration measurements have been performed using n different reference samples. Then we have a set of n observation tripels $(E_i, \dot{P}_i, \dot{B}_i)$ with the associated variances $\mathrm{var}(E_i)$, $\mathrm{var}(\dot{P}_i)$ and $\mathrm{var}(\dot{B}_i)$. We proceed as in case a) discussed above, giving only the main equations and suppressing corresponding comments.

Residuals Δ_i:

$$\Delta_i = E_i - a \cdot \dot{P}_i - b \cdot \dot{B}_i \tag{5.27a}$$

Generalized weight factors G_i:

$$G_i = \frac{1}{\mathrm{var}(E_i) + a^2 \cdot \mathrm{var}(\dot{P}_i) + b^2 \cdot \mathrm{var}(\dot{B}_i)} \,. \tag{5.28a}$$

Least-squares fit principle:

$$\sum_{i=1}^{n} G_i \cdot \Delta_i^2 = \min \tag{5.29a}$$

Setting the partial derivatives with respect to the parameters a and b equal to zero

$$\Sigma \frac{\partial G_i}{\partial a} \Delta_i^2 + \Sigma\, G_i \cdot \frac{\partial \Delta_i^2}{\partial a} = 0 \quad , \tag{5.30a}$$

$$\Sigma \frac{\partial G_i}{\partial b} \cdot \Delta_i^2 + \Sigma G_i \cdot \frac{\partial \Delta_i^2}{\partial b} = 0 \quad , \tag{5.31a}$$

delivers a system of linear equations for a and b:

$$a \cdot (\Sigma G_i \dot{P}_i^2 - \Sigma \operatorname{var}(\dot{P}_i) G_i^2 \Delta_i^2) + b \cdot \Sigma G_i \dot{P}_i \dot{B}_i = \Sigma G_i E_i \dot{P}_i , \tag{5.32a}$$

$$a \cdot \Sigma G_i \dot{P}_i \dot{B}_i + b \cdot (\Sigma G_i \dot{B}_i^2 - \Sigma \operatorname{var}(\dot{B}_i) G_i^2 \Delta_i^2) = \Sigma G_i E_i \dot{B}_i . \tag{5.33a}$$

Since both G_i and Δ_i still depend on a and b, the system of equations is solved by iteration:

1) Start values G_i and Δ_i:

$$G_i^{(0)} =: 1, \qquad \Delta_i^{(0)} =: 0 \quad (i = 1,\ldots n) . \tag{5.37a}$$

2) Solution for a and b ($\nu = 0,1,\ldots$):

$$\begin{aligned} DET^{(\nu+1)} =: {} & [\Sigma G_i^{(\nu)} \dot{P}_i^2 - \Sigma \operatorname{var}(\dot{P}_i) [G_i^{(\nu)}]^2 [\Delta_i^{(\nu)}]^2] \cdot \\ & \cdot \{\Sigma G_i^{(\nu)} \dot{B}_i^2 - \Sigma \operatorname{var}(\dot{B}_i) [G_i^{(\nu)}]^2 [\Delta_i^{(\nu)}]^2\} - \\ & - [\Sigma G_i^{(\nu)} \dot{P}_i \dot{B}_i]^2 \end{aligned} \tag{5.38a}$$

$$\begin{aligned} a^{(\nu+1)} = \frac{1}{DET^{(\nu+1)}} \Big[& \Sigma G_i^{(\nu)} E_i \dot{P}_i \cdot \{\Sigma G_i^{(\nu)} \dot{B}^2 - \Sigma \operatorname{var}(\dot{B}_i) [G_i^{(\nu)}]^2 [\Delta_i^{(\nu)}]^2\} - \\ & - \Sigma G_i^{(\nu)} E_i \dot{B}_i \Sigma G_i^{(\nu)} \dot{P}_i \dot{B}_i \Big] \end{aligned} \tag{5.39a}$$

$$\begin{aligned} b^{(\nu+1)} = \frac{1}{DET^{(\nu+1)}} \Big[& \Sigma G_i^{(\nu)} E_i \dot{B}_i \cdot \{\Sigma G^{(\nu)} \dot{P}^2 - \Sigma \operatorname{var}(\dot{P}_i) [G_i^{(\nu)}]^2 [\Delta_i^{(\nu)}]^2\} - \\ & - \Sigma G_i^{(\nu)} E_i \dot{P}_i \cdot \Sigma G_i^{(\nu)} \dot{P}_i \dot{B}_i \Big] \cdot \end{aligned} \tag{5.40a}$$

3) Refined values G_i and Δ_i

$$G_i^{(\nu+1)} = \frac{1}{\mathrm{var}(E_i) + [a^{(\nu+1)}]^2 \cdot \mathrm{var}(\dot{P}_i) + [b^{(\nu+1)}]^2 \cdot \mathrm{var}(\dot{B}_i)} \tag{5.41a}$$

$$\Delta_i^{(\nu+1)} = E_i - a^{(\nu+1)} \cdot \dot{P}_i - b^{(\nu+1)} \cdot \dot{B}_i \tag{5.42a}$$

Repeat iteration steps 2 and 3 until convergence is achieved (normally three to four iteration steps will be sufficient).

Variations and covariance of the fitted parameters a and b from the reduced cofactors of the coefficient matrix of the parameters after m iteration steps:

$$\mathrm{var}(a^{(m)}) = \frac{1}{\mathrm{DET}^{(m)}} \left[\Sigma\, G_i^{(m)} \dot{B}_i^2 - \Sigma\, \mathrm{var}(\dot{B}_i) [G_i^{(m)}]^2 [\Delta_i^{(m)}]^2 \right] \tag{5.43a}$$

$$\mathrm{var}(b^{(m)}) = \frac{1}{\mathrm{DET}^{(m)}} \left[\Sigma\, G_i^{(m)} \dot{P}_i^2 - \Sigma\, \mathrm{var}(\dot{P}_i) [G_i^{(m)}]^2 [\Delta_i^{(m)}]^2 \right] \tag{5.44a}$$

$$\mathrm{cov}(a^{(m)}, b^{(m)}) = \frac{-\Sigma\, G_i^{(m)} \dot{P}_i \dot{B}_i}{\mathrm{DET}^{(m)}} \tag{5.45a}$$

Indicator of the quality of the fit ω^2 (see sub-section 5.4.4):

$$\omega^2 = \frac{\chi^2}{\mathrm{DOF}} = \frac{1}{n-2} \Sigma\, G_i^{(m)} [\Delta_i^{(m)}]^2 \tag{5.46a}$$

(DOF = degrees of freedom)

The best estimate of the ^{235}U enrichment of an unknown sample from the measured counting rates $\dot{P}_U$ in the peak-, and $\dot{B}_U$ in the background window with corresponding variances $\mathrm{var}(\dot{P}_U)$ and $\mathrm{var}(\dot{B}_U)$ is given by:

$$\bar{E} = a^{(m)} \cdot \dot{P}_U + b^{(m)} \cdot \dot{B}_U \quad , \tag{5.47a}$$

and the estimated standard deviation of this value is

$$\Delta\bar{E} = \sqrt{a^{(m)2}\,\mathrm{var}(\dot{P}_U) + b^{(m)2}\,\mathrm{var}(\dot{B}_U) + \dot{P}_U^2\,\mathrm{var}(a^{(m)}) + 2\dot{P}_U\dot{B}_U\,\mathrm{cov}(a^{(m)}, b^{(m)}) + \dot{B}_U^2\,\mathrm{var}(b^{(m)})} \qquad (5.48a)$$

The first two terms of eq. 5.48a represent the errors introduced by the measurement of the unknown sample, the remaining three terms represent the calibration error. Note that the variances of the counting rates comprise the errors due to the counting statistics as well as the errors introduced by the various corrections (matrix, container wall, counting rate losses).

Remark:

The solution of the least-square fit problem for the other calibration equations discussed in Section 5.4.1 is left to the user. Note that, in general, all fit parameters are correlated to each other. Therefore, besides the variance terms, three or six covariance terms will appear in the equation of the error estimate of the ^{235}U enrichment (corresponding to eqs. 5.48 and 5.48a) in case of three or four calibration parameters, respectively.

5.4.4 Test of the quality of the fit

The quality of the fit can be tested by various statistical methods. The measure ω^2, as defined in eqs. 5.46 and 5.46a, may serve as a suitable test statistics. It tests the hypothesis that the deviations of the data from the fitted straight line are in agreement with the estimated standard deviations of the observations. The ω^2-test statistics is tabulated in Table D1 in Appendix D for various degrees of freedom at selected probability levels. If the measured data and the associated errors are consistent with the assumed linear model, then we expect ω^2 values around 1 (see Table D1). ω^2 values which are significantly smaller than 1 indicate "too good" data, i.e., the deviations from the straight line are smaller than the quoted uncertainties. The error estimates may be too large in this case. Unlikely high ω^2 values indicate

that either the assumed linear model is not adequate, or that the quoted errors are underestimated.

Numerical examples of two calibration runs are given in Appendix E. The ω^2 values of the two data sets are:

Data set I	Data set II
$\omega^2 = 0.64$	$\omega^2 = 15.76$

The first data set is in good agreement with the assumed linear model within the quoted error limits. In contrast to this the very high ω^2 value of the second data set indicates that our model is highly suspect in this case. This may be caused by non-linear effects or by unrealistically low error estimates.

In order to further investigate the structure of the deviations it is very useful to make a plot of the residuals or, equivalently, of the relative deviations from the fitted straight line, so that one can inspect visually the distribution of the deviations. Figs. 5.6a and 5.6b display the relative differences between the stated mass-spectrometric ^{235}U enrichment values enr_i^{RM} and the fitted ^{235}U enrichment values enr_i^{Fit}:

$$Diff_I\ \% = \frac{enr_i^{Fit} - enr_i^{RM}}{enr_i^{RM}} \cdot 100 \quad , \tag{5.49}$$

for the two sets of calibration data given in Appendix E as a function of the ^{235}U enrichment. The error bars represent the assumed relative error of each measurement

$$Err_i\ \% = \frac{100}{enr_i^{RM}} \cdot \sqrt{\frac{1}{G_i}} \quad , \tag{5.50}$$

with the generalized weight factor G_i defined in eq. 5.28. The Figs. 5.6a and 5.6b also give the confidence limits of the relative calibration error at the 1σ level. Note that here and in the program example given in Appendix E the final variances and the covariance are multiplied by ω^2, and that, accordingly, the confidence limits of the fit are multiplied by ω. Though this approach is not justified by our model which assumes known variances in all observations, it may provide more realistic error

estimates in case of a bad fit, as, e.g., for the calibration data set II.

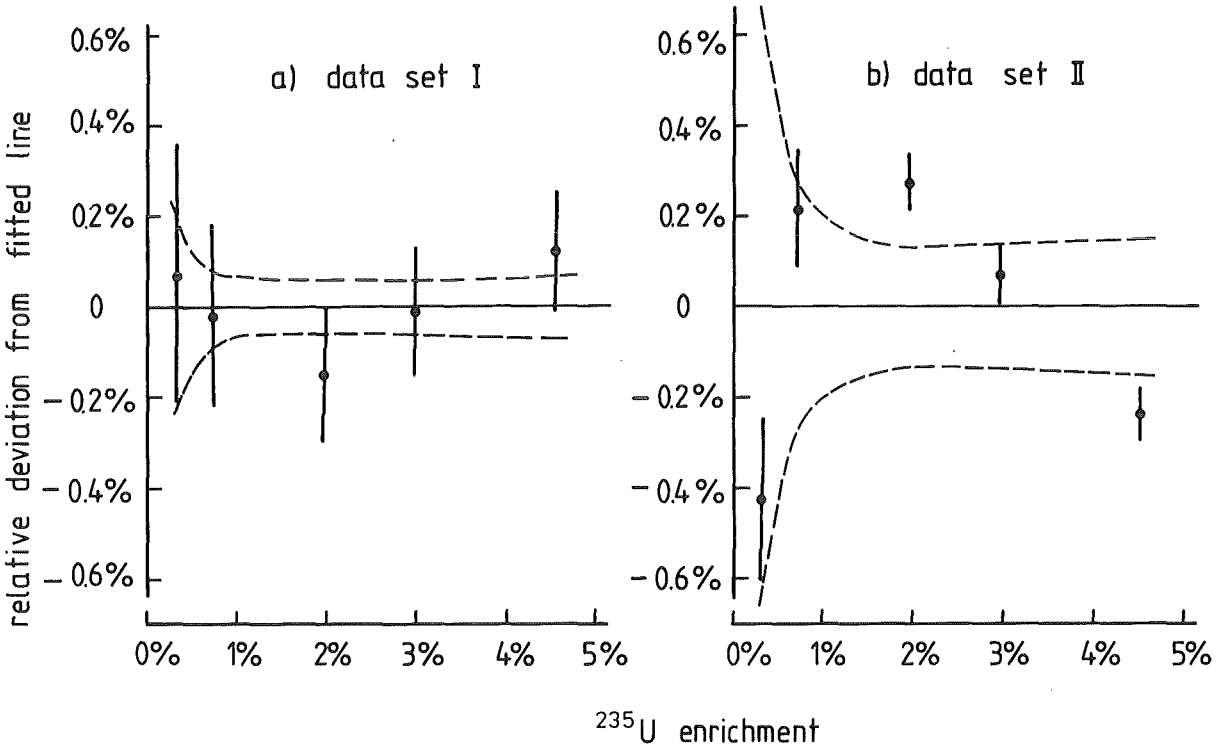

Figures 5.6a and 5.6b
Relative deviations of measured ^{235}U enrichment values from the fitted straight line. The dashed lines indicate the confidence limits of the relative calibration error at the 1σ level.

The visual inspection of the relative deviations and of the associated relative errors plotted in Fig. 5.6a gives no indication that our assumed linear model is suspect or that the error estimates are wrong. In contrast to this, Fig. 5.6b demonstrates an unsatisfactory calibration, as expected from the ω^2 test. The pattern of the deviations suggests that the linear model is not in a good agreement with the measured data in this case. There seems to be a non-linear component in the relation between the 186 keV net peak counting rate and the ^{235}U enrichment. Such non-linearities may arise, e.g., from uncorrected pulse losses (see Sections 5.1 and 5.2), or from a non-adequate technique for net peak area evaluation (see Section 5.3). Note

that strongly underestimated random measurement errors may also be responsible for a bad calibration result with abnormally high ω^2 values. A careful check of the counting equipment, a thorough examination of the data evaluation procedures, and repeated calibration measurements may help to identify and to remove the sources of the systematic deviations. The user should be warned not to try to remove the deviations by introducing non-linear terms into the calibration equation. This may lead to erroneous enrichment measurements when the non-linearity is not a unique function of the ^{235}U enrichment, but is caused, e.g., by variations of the total counting rate, which can be significantly different for the Reference Samples and the unknown samples.

In case of inhomogeneous calibration equations (see Section 5.4.1) the comparison of the fitted offset C with the predicted gamma interference term C can serve as an additional test of the quality of the fit. The predicted value of C for aged sample material measured with a high resolution detector is about -0.001 (in units of % ^{235}U enrichment, see Section 3.4). The fitted C values of the two sets of calibration data given in Appendix E are:

Data set I	Data set II
$C = (-0.0018 \pm 0.008)$,	$C = (-0.0042 \pm 0.0023)$.

The measure

$$t = \sqrt{\frac{(C_{Fit} - C_{predicted})^2}{var(C_{Fit})}} \qquad (5.51)$$

follows a t- distribution and may be used as a method to test the hypothesis that the true offset of the calibration line is - 0.001. The test statistics of the t-test is tabulated in Table D2 in Appendix D. For our particular calibration examples both t-values

$$t_I = 1 \quad \text{and} \quad t_{II} = 1.4$$

will not reject this hypothesis (see Table D2). Though this test is much less sensitive to deviations from the linearity than the ω^2 test, it may be useful as a rapid quality check when unlikely offset values will result from a calibration run.

Note, that the predicted value of the interference term C is based on nuclear data [12] which are not known very precisely. Therefore, a careful experimental verification of the gamma interference effect would be desirable.

6. USER'S GUIDE: A SUMMARIZING SURVEY

Applications of the ^{235}U enrichment assay technique are restricted, for principal and practical reasons, to relatively large samples. From materials presented in Chapter 3 we deduce, for example, that about 250 g of low enriched uranium oxide powder are required for the enrichment analysis, when reasonably dimensioned collimator sizes are used in order to achieve a high measurement accuracy within acceptable counting times.

The disadvantage of requiring larger samples, however, is compensated by the benefits of the technique: the response of the enrichment assay system is almost completely independent of the sample geometry, the sample density, and the amount of sample material used, provided the sample is thick enough. In addition, the enrichment is measured non-destructively, requiring no chemical preparation and only minimum handling of the sample material.

The measured enrichment is susceptible to a number of factors. Possible systematic errors that may arise from properties of the sample material, of the sample container and of the gamma counting arrangement are thoroughly discussed in this user's manual. Whenever possible, quantitative correction terms have been given for the various measurement parameters affecting the enrichment assay accuracy. In the following Table 6.1 the salient points are summarized for the user's convenience in a tabulated form.

Three major prerequisites for accurate enrichment measurements deserve to be mentioned specifically. They should be carefully observed before starting a measurement:

1. The sample must be thick enough to be opaque for 186 keV gamma radiation.
2. The sample material must be highly uniform with respect to the ^{235}U enrichment.
3. The wall thickness of the sample container must be known precisely to allow an accurate correction for gamma attenuation.

Table 6.1 Sources of systematic errors in gamma-ray measurements of the ^{235}U enrichment (tolerance values are given with reference to a relative error of 0.1 %).

	Parameter	Effect on enrichment determination	Correction given in	Remarks
1.	Interfering gamma radiation from uranium isotopes and their descendants.	Small to negligible for Ge detectors, crucial for NaI detectors.	Sections 3.3.3 and 5.4	Effect depends on time after chemical separation. NaI detectors should not be used for analysis of recycled uranium.
2.	Chemical composition of the sample:			
	Different U compounds and stoichiometry	Up to a few %, usually correction required	Section 3.3.1	
	Sample Impurities	Correction required if impurity mass fraction > 1 % (matrix of low Z) or > 0.1 % (matrix of high Z) of uranium content	Section 3.3.2	
	Water content	Correction required if mass fraction > 1 % of uranium content	Section 3.3.3	
3.	Sample density	No effect for "quasi-infinite" samples.	-	

Table 6.1 (continued)

	Parameter	Effect on enrichment determination	Correction given in	Remarks
4.	Sample inhomogeneities:			
	Enrichment	Assay result is very sensitive to this parameter. Local variations must be < 0.1 % relative.	Not given in an analytical form. (see Section 3.2)	Correction would require exact knowledge of absolute value and distribution of the respective inhomogeneities. Difficult to treat mathematically.
	Matrix composition	Small influence. Negligible if local variations < 1 wt% of uranium for low Z matrix		
	Density	No effect for "quasi"-infinite" samples		
5.	Sample size	No influence for "quasi-infinite" samples. Significant effects for non-infinite thickness geometry (samples too small, collimators too large, material density too low)	- Not given in an analytical form.	Recommendations for minimum sample size and maximum collimator dimension given in Section 3.1 for different material densities.
6.	Sample positioning	No effect for "quasi-infinite" samples.	-	Proper positioning required when samples of minimum size are used.

Table 6.1 (continued)

	Parameter	Effect on enrichment determination	Correction given in	Remarks
7.	Sample container:			
	Wall thickness	Significant influence. Thickness must be known with accuracy of ∿20 μm for aluminium and ∿5 μm for steel.	Section 4.2	Container wall thickness must be uniform over area viewed by the detector.
	Wall deformation	Negligible in most applications. Angle between surface of collimator and container not to exceed a few degrees (∿3° to 5°).	- (see Section 4.3)	
8.	Distance variations between collimator and detector	No effect if detector diameter >> collimator diameter. Otherwise distance variations not to exceed 20 - 30 μm.	Not given in an analytical form. (see Section 4.1)	Collimator to be rigidly fixed with respect to detector cap, or large detectors to be used.
9.	Ambient background radiation	Significant effects for in-plant applications.	-	Careful shielding of detector against background radiation required.
10.	System dead-time and and pulse pile-up	Significant effects.	Section 5.2	Countermeasures by electronic hardware. Pile-up rejector recommended.

REFERENCES

[1] P. de Bièvre, B.S. Carpenter et al.,
"^{235}U Isotope Abundance Certified Reference Material for Gamma Spectrometry, Certification Report",
CEC, JRC: Eur....., NBS Special Publication 260-.....

[2] R.J.S. Harry,
"Enrichment Standards for Gamma Spectrometry, Historical Overview of the Project to Produce CRM's for ^{235}U Abundance Determination by Gamma-Spectrometry", Proceedings of the Sixth Annual Symposium on Safeguards and Nuclear Material Management, May 14-18, 1984,Venice, Italy, JRC Ispra (VA), Italy (1984), ESARDA-17, p. 187-194.

[3] R.P. Debeir, F. Violin, R. Denis, S. Crutzen,
"Experience Gained with the Unique Identification of 640 Standard of Uranium Enrichment",
Proceedings of the Fifth Annual Symposium on Safegurads and Nuclear Material Management, April 19-21, 1983, Versailles, France,
JRC Ispra (VA), Italy (1983), ESARDA-16, p. 139-144.

[4] T.D. Reilly, R.B. Walton, J.L. Parker,
"The 'Enrichment Meter' - A Simple Method for Measuring Isotopic Enrichment",
Los Alamos Scientific Laboratory Report LA-4605-MS (1970), p. 19-21.

[5] L.A. Kull, R.O. Ginaven,
"Guidelines for Gamma-Ray Spectroscopy Measurements of ^{235}U Enrichment",
Brookhaven National Laboratory Report BNL-50417 (1974).

[6] W.G. Winn,
"Nondestructive Assay of Uranium Enrichment with Gamma Rays", Savannah River Laboratory Report DP-1654 (1983).

[7] R. Vaninbroukx, B. Denecke,
"Determination of Gamma-Ray Emission Probabilities in the Decay of ^{235}U and ^{231}Th",
Nuclear Instruments and Methods 193 (1982), p. 191-196.

[8] A. Lorenz,
"Proposed Recommended List of Transactinium Isotope Decay Data, Part 1, Half-Lifes",
INDC(NDS) - 121 / NE (1980).

[9] E. Storm, H.I. Israel,
"Photon Cross Sections from 1 keV to 100 MeV for Elements Z = 1 to Z = 100",
Nuclear Data Tables A, Vol. 7, Nr. 6 (1970).

[10] R.J.S. Harry, J.K. Aaldijk, J.P. Braak,
"Gamma-Spectrometric Determination of Isotopic Compositions without Use of Standards",
Safeguarding Nuclear Materials, Proceedings of a Symposium, Vienna, Oct. 20-24, 1975, IAEA, Vienna, Austria (1976), Vol. II, p. 235-245.

[11] T.N. Dragnew, B.P. Damjanow,
"Methods for Precise Absolute Gamma-Spectrometric Measurements of Uranium and Plutonium Isotopic Ratios",
Nuclear Safeguards Technology 1978, Proceedings of a Symposium, Vienna, Oct. 2-6, 1978, IAEA, Vienna, Austria (1979), Vol. I, p. 739-753.

[12] C.M. Lederer, V.S. Shirley et al.,
"Table of Isotopes", Seventh Edition
John Wiley & Sons, Inc., New York (1978).

[13] D.H. Augustson, T.D. Reilly,
"Fundamentals of Passive Nondestructive Assay of Fissionable Material",
Los Alamos Scientific Laboratory Report LA-5651-M (1974).

[14] T.D. Reilly, J.L. Parker,
"A Guide to Gamma-Ray Assay for Nuclear Material Accountability", Los Alamos Scientific Laboratory Report LA-5794-M (1974).

[15] R. Gunnink, J.B. Niday, P.D. Siemens,
"A System for Plutonium Analysis by Gamma-Ray Spectrometry, Part 1: Techniques for Analysis of Solutions",
Lawrence Livermore Laboratory Report UCRL-51577 (1974).

[16] J. Mandel,
"Fitting Straight Lines when Both Variables are Subject to Error",
Journal of Quality Technology, Vol. 16, Nr. 1 (1984) p.1.

[17] W. Ligget,
"Calibration for Measurements with Background Correction Applied to Uranium-235 Enrichment",
Nuclear Instruments and Methods 216 (1983), p. 455-470.

[18] W.L. Zijp,
"Generalized Least Squares Principle for Straight Line Fitting", Netherlands Energy Research Foundation Report ECN-154, Petten (1983).

[19] W.L. Zijp, J.K. Aaldijk,
"COMFIT, a Computer Program for Determining Best Fitting Curves", Netherlands Energy Research Foundation Report ECN-117, Petten (1982).

[20] J.H. Hubbel et al.,
"Atomic Form Factors, Incoherent Scattering Functions, and Photon Scattering Cross Sections",
Journal of Physical and Chemical Reference Data, Vol. 4, No. 3, (1975), p. 471-538.

[21] R.C. Weast, M.J. Astle, W.H. Beyer,
"CRC Handbook of Chemistry and Physics", 65th Edition,
CRC Press Inc., Boca Raton, Florida (1984).

APPENDIX A

Derivation of basic formulae for gamma-spectrometric ^{235}U enrichment assays

Appendix A

Appendix A comprises the derivation of the basic formulae used in the present manual. In particular, it describes the surface gamma radiation of large absorbing radioactive samples (Section A1), the photon transmission through cylindrical and conical collimators (Section A2), and the influence of cladding materials and of the size of the gamma detector on the observed gamma counting rate (Section A3).

A.1 Surface gamma radiation of large ^{235}U-bearing samples

For gamma-spectroscopic ^{235}U enrichment assays the parameter of interest is the flux of 186 keV gamma rays at the surface of large ^{235}U-bearing samples. The 186 keV gamma radiation may interact with the sample matter (and also with the materials of the sample container)in several ways. Here we summarize by definition all interaction processes, regardless of their physical nature, as "attenuation", which do change the energy of the 186 keV gamma quanta and thus remove them from the 186 keV peak observed in the gamma spectrum. Coherent gamma scattering, which changes only the direction of the scattered gamma quantum but not its energy, can be ignored for the photon energies considered, because

1) the angular distribution of the coherently scattered gamma quanta is strongly forward peaked, i.e. the direction of the photon is not significantly changed in most of the coherent scattering events [20], and
2) the probability for coherent scattering is low compared to the gamma attenuation defined above. Hence, larger scattering angles due to multiple coherent scattering are very unlikely.

For the above reasons we can in fact neglect the contribution of coherent scattering to the total scattering in the applications considered here. Therefore, the attenuation cross section for 186 keV gamma rays that has to be used in our case is given by:

Total narrow-beam cross section minus coherent cross section.

The same arguments apply to the mass attenuation coefficient and the linear attenuation coefficient, which are related to the photon attenuation cross section (see Appendix C).

For the quantitative determination of the gamma flux and its angular distribution at the sample surface we consider a half-space filled with ^{235}U-bearing material. Then we calculate the number of 186 keV gamma rays, which penetrate the surface element dF through the differential solid angle $d\Omega$ per unit time (see Fig. A1)

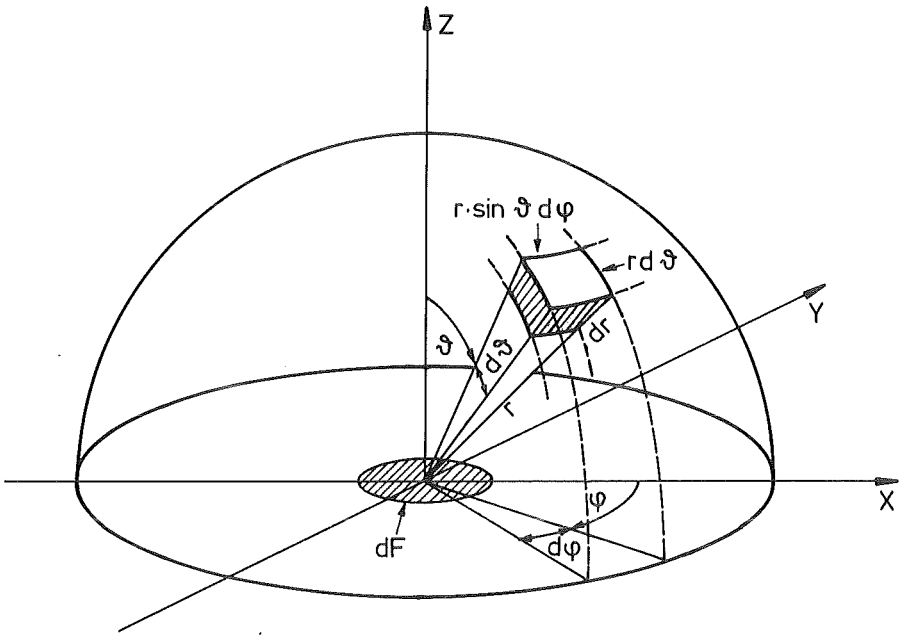

Fig. A 1 Gamma radiation at the surface of a thick sample.

The radiation S emitted from the volume element dV at location r per unit time is given by

$$d^3S(r,\theta,\phi) = N_{235_U}(r)\cdot\dot{n}_{186}\cdot\underbrace{r^2\cdot\sin\theta\cdot d\theta\cdot d\phi\cdot dr}_{dV}$$

or

$$d^2S(r,\Omega) = N_{235_U}(r)\cdot\dot{n}_{186}\cdot r^2\cdot dr\cdot d\Omega \quad , \tag{A1}$$

where $N_{235_U}(r)$ denotes the number of ^{235}U atoms per volume unit at location r, and $\dot{n}_{186}$ is the number of 186 keV gamma quanta

emitted by a single ^{235}U atom per unit time (see Chapter 2.1).

The surface element dF is seen from dV under the angle θ. Its visible area is thus $\cos\theta \cdot dF$. Without absorption the number of 186 keV gamma rays emitted from dV penetrating dF would be

$$d^3I_\gamma = d^2S(r,\Omega) \cdot \frac{\cos\theta}{4\pi r^2} \cdot dF \quad . \tag{A2}$$

On the way through the sample matter to the surface the gamma radiation is attenuated. The attenuation factor is given by

$$B_{abs} = e^{-\lambda r} \quad , \tag{A3}$$

or in the more general case of heterogeneous sample material by

$$B_{abs} = e^{-\int_0^r \lambda(s)\,ds} \quad , \tag{A3a}$$

where $\lambda(r)$ denotes the linear attenuation coefficient of the material at location r. $\lambda(r)$ is connected to the particle density $N_i(r)$ of the chemical element i and its associated attenuation cross section σ_i by

$$\lambda(r) = \sum_i N_i(r) \cdot \sigma_i \quad . \tag{A4}$$

Summation has to be performed over all different elements present in the sample. Using $N_U(r)$ for the particle density of uranium atoms, eq. A4 can be transformed to

$$\lambda(r) = N_U(r) \cdot \sigma_U \cdot \left(1 + \sum_{i \neq U} \frac{N_i(r) \cdot \sigma_i}{N_U(r) \cdot \sigma_U}\right) \quad , \tag{A5}$$

summing now over all elements of the sample matrix, i.e., over all elements other than uranium. We define a correction factor for the matrix attenuation as

$$\beta(r) =: \frac{1}{1 + \sum_{i \neq U} \frac{N_i(r) \cdot \sigma_i}{N_U(r) \cdot \sigma_U}} \quad . \tag{A6}$$

Since the matrix composition is often given as mass fraction of uranium, eq. A6 can be also expressed in terms of element density

ρ_i (in units of mass per volume unit), and of mass attenuation coefficients μ_i (in units of area per mass unit). Using the identity

$$N_i(r) \cdot \sigma_i \equiv \rho_i(r) \cdot \mu_i \quad , \tag{A7}$$

the matrix attenuation factor can be written equivalently

$$\beta(r) = \frac{1}{1 + \sum_{i \neq U} \frac{\rho_i(r) \cdot \mu_i}{\rho_U(r) \cdot \mu_U}} \quad . \tag{A8}$$

Note, that the mass attenuation coefficient μ of an element varies with its isotopic composition (e.g. for uranium by -1.3 % from pure ^{235}U to pure ^{238}U), whereas the product $\mu \cdot \rho$ is independent from the isotopic composition.

To simplify the calcultion we assume a uniform sample matrix composition, i.e., constant ratios N_i/N_U of matrix atoms to uranium atoms throughout the sample volume. Then the matrix attenuation factor β becomes a material constant. The linear attenuation coefficient given in eq. A5 takes the form:

$$\lambda(r) = \frac{N_U(r) \cdot \sigma_U}{\beta} \quad . \tag{A9}$$

We define the ^{235}U enrichment enr in terms of atom fraction as the ratio of ^{235}U atoms to total uranium atoms in a unit volume:

$$enr(r) = \frac{N_{^{235}U}(r)}{N_U(r)} \quad . \tag{A10}$$

If we assume a constant ^{235}U enrichment in the sample, then the total uranium particle density $N_U(r)$ can be expressed in terms of the ^{235}U particle density:

$$N_U(r) = \frac{N_{^{235}U}(r)}{enr} \quad . \tag{A11}$$

The linear attenuation coefficient becomes then

$$\lambda(r) = \frac{N_{^{235}U}(r) \cdot \sigma_U}{\beta \cdot enr} \quad . \tag{A12}$$

Combining eqs. A2, A3a and A12 we arrive at the number of 186 keV

gammas emitted by the volume element dV going through the surface area dF:

$$d^3I_\gamma(r,\Omega,F) = \frac{\dot{n}_{186}}{4\pi}\cdot N_{235_U}(r)\cdot e^{-\frac{\sigma_U}{\beta\cdot enr}\int_o^r N_{235_U}(s)\cdot ds}\cdot\cos\cdot\theta dr\cdot d\Omega\cdot dF. \tag{A13}$$

Now, only the ^{235}U particle density N_{235_U} depends on the location variable r.

We can perform the integration of eq. A.13 over r using the following relation for the fundamental function of the integrand:

$$\frac{d}{dr}\left(e^{-a\int_o^r f(x)\cdot dx}\right) = -a\cdot f(r)\cdot e^{-a\int_o^r f(x)\,dx} \tag{A14}$$

We finally get the contribution of all volume elements from 0 to R to the 186 keV gamma radiation penetrating dF through $d\Omega$:

$$d^2I_\gamma(R,\Omega,F) = enr\cdot\frac{\dot{n}_{186}\cdot\beta}{4\pi\cdot\sigma_U}\cdot\left(1-e^{-\int_o^R\lambda(s)\cdot ds}\right)\cdot\cos\theta\cdot d\Omega\cdot dF. \tag{A15}$$

For infinitly thick samples ($r\to\infty$) the exponential term in eq. A15 vanishes, and the differential gamma-ray flux at the surface can be written in a very simple form:

$$d^2I_\gamma(\infty,\Omega,F) = enr\cdot\frac{\dot{n}_{186}}{4\pi\cdot\sigma_U}\cdot\frac{1}{1+\sum_{i\neq U}\frac{N_i}{N_U}\cdot\frac{\sigma_i}{\sigma_U}}\cdot\cos\theta\cdot d\Omega\cdot dF,$$

or

$$\boxed{d^2I_\gamma(\infty,\Omega,F) = enr\cdot A\cdot\cos\theta\cdot d\Omega\cdot dF}, \tag{A16}$$

where the proportionality constant

$$A =: \frac{\dot{n}_{186}}{4\pi\sigma_U}\cdot\frac{1}{1+\sum_{i\neq U}\frac{N_i}{N_U}\cdot\frac{\sigma_i}{\sigma_U}} \tag{A16a}$$

is determined by nuclear and atomic constants, and by the matrix composition of the sample material.

Eq. A16 forms the basis of the "enrichment meter" principle. It shows that in case of an infinite sample the 186 keV gamma-ray flux at the sample surface is directly proportional to the ^{235}U enrichment. Only the influence due to sample matrix material, which is small in most applications, has to be corrected for. The angular characteristic of the surface radiation of thick absorbing samples follows a cosine law (Lamberts law).

The only restrictive assumptions we have made in the derivation of the above equation were:

1. uniform matrix composition, and
2. uniform ^{235}U enrichment

throughout the sample. Note in particular, that the 186 keV gamma-ray flux at the surface of a large sample is completely independent of the physical distribution of the material within the sample. Thus, local density variations in the material, even cavities in the sample, do not affect the observed 186 keV gamma counting rate, provided the sample is thick enough in direction of observation, and the uniformity requirements with respect to sample matrix and ^{235}U enrichment are met.

It should be notized that gamma-spectrometric enrichment measurements deliver the ^{235}U enrichment values in units of atom fraction, and <u>not</u> in units of mass fraction.

A.2 Gamma-ray transmission through a collimator

In order to translate the gamma-ray flux of 186 keV photons at the sample surface into counting rates observable in a measurement set-up, one normally uses a collimator for the definition of a fixed viewing solid angle. A collimator can be considered as a hole in a strongly gamma absorbing material, usually made of lead or tungsten. The collimator material must be thick enough to be opaque for 186 keV gamma rays. Particularly for measurements with low-enriched uranium samples, it is desirable to protect the gamma detector also against the highly penetrating gamma radiation originating from the ^{238}U decay to reduce the Compton background below the 186 keV peak. This leads to a recommended minimum thickness of about 2 cm for a lead collimator, and of about 1.5 cm for a tungsten collimator.

The considerations are restricted here to the most commonly used collimator types with cylindrical and conical shaped collimator holes (see Fig. A.2).

As shown in Appendix A1, the differential gamma radiation penetrating a surface element dF of an infinitely thick sample is described by

$$d^2I_\gamma = enr \cdot A \cdot \cos\theta \cdot d\Omega \cdot dF \ , \qquad (A17)$$

where θ is the angle between the differential solid angle $d\Omega$ and the axis normal to the sample surface, and A is the number of 186 keV gamma quanta penetrating the unit surface area per time unit and per steradian in forward direction $\theta = 0°$ in case of a pure ^{235}U sample.

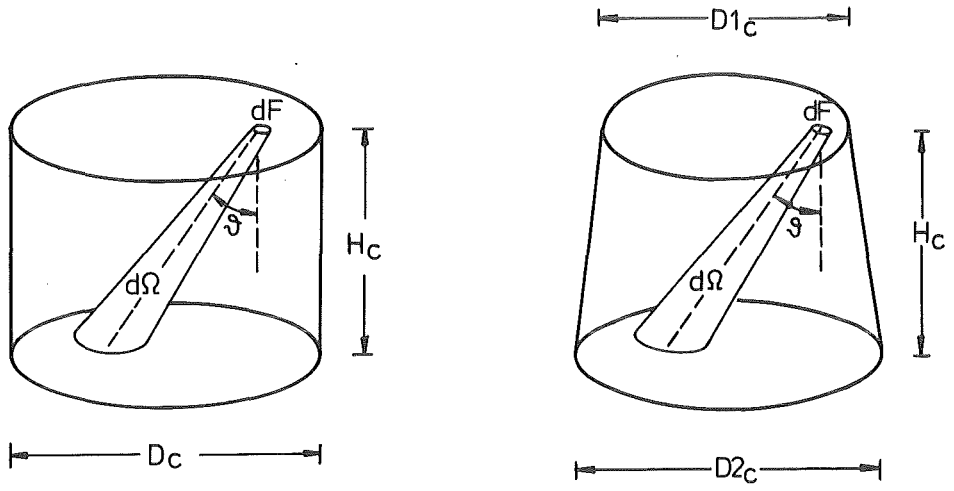

Fig. A2 a) cylindrical and b) conical collimator.

The total number of 186 keV gamma rays passing through the collimator (see Fig. A2) per unit time is expressed by the integral

$$I_\gamma = enr \cdot A \cdot \iint_{F\ \Omega} \cos\theta \cdot d\Omega \cdot dF \ , \qquad (A18)$$

where the integration is to be performed over all surface elements dF of the collimator entrance area F, and over all possible differential solid angles $d\Omega$ seen from each differential area dF.

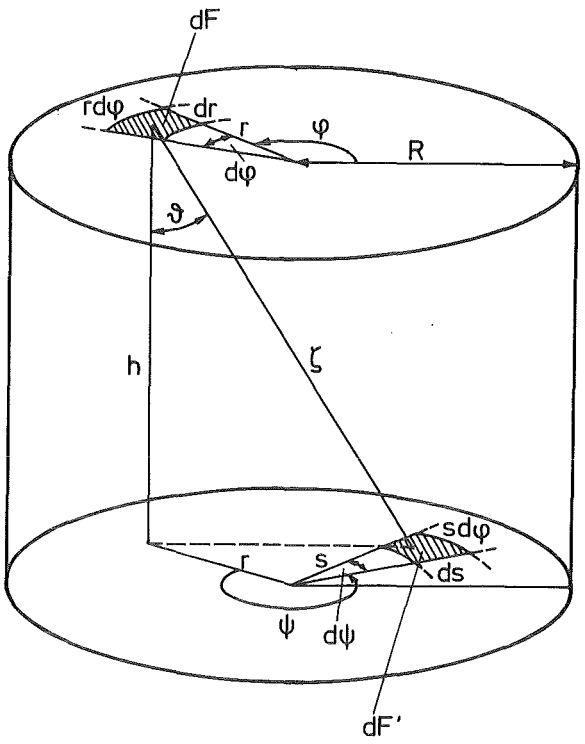

Fig. A3 Radiation penetrating a cylindrical collimator.

Using the relation

$$d\Omega = \frac{\cos\theta}{\zeta^2}\, dF' \qquad \text{(A19)}$$

from Fig. A3, we can substitute the integration over the solid angle Ω by an integration over the collimator exit area F'.

One can easily see in Fig. A3 that the integration over the collimator exit area is not depending on the angle ϕ. Inserting eq. A19 and executing the integration over ϕ, eq. A18 becomes:

$$I_\gamma = enr \cdot A \cdot 2\pi \int_0^R \int_0^{R'} \int_0^{2\pi} \frac{\cos^2\theta}{\zeta^2} \cdot r \cdot s \cdot d\psi \cdot ds \cdot dr \qquad \text{(A20)}$$

Here R and R' denote the radii of the collimator entrance- and exit areas, respectively. h denotes the collimator height.

Having

$$\zeta = \sqrt{h^2+r^2+s^2-2 \cdot r \cdot s \cdot \cos\psi} \quad \text{and} \quad \cos\theta = \frac{h}{\zeta} \ ,$$

(see Fig. A3) we finally obtain:

$$I_\gamma = enr \cdot A \cdot 2\pi \int_0^R \int_0^{R'} \int_0^{2\pi} \frac{h^2 \cdot r \cdot s}{(h^2+r^2+s^2-2 \cdot r \cdot s \cdot \cos\psi)^2} \, d\psi \cdot ds \cdot dr \qquad (A21)$$

This integral can be solved to a closed form.

For a cylindrically shaped collimator with a diameter D_c and a height H_c, we get the number of 186 keV photons penetrating this collimator per unit time:

$$I_\gamma^{cyl} = enr \cdot \pi \cdot A \cdot \underbrace{(\pi \frac{D_c^2}{4})}_{\substack{\text{collimator-} \\ \text{entrance} \\ \text{area}}} \cdot \left[\frac{2H_c^2}{D_c^2} \left(1 + \frac{D_c^2}{2H_c^2} - \sqrt{1 + \frac{D_c^2}{H_c^2}}\right)\right] \qquad (A22)$$

For a conical collimator form with $D1_c$ and $D2_c$ being the diameters of the collimator entrance- and exit areas, respectively, and with the collimator height H_c, the resulting number of 186 keV gamma rays passing the collimator per unit time is given by

$$I_\gamma^{cone} = enr \cdot \pi \cdot A \cdot \underbrace{(\pi \frac{D1_c^2}{4})}_{\substack{\text{collimator-} \\ \text{entrance} \\ \text{area}}} \cdot \left[\frac{2H_c^2}{D1_c^2} \left(1 + \frac{D1_c^2}{4H_c^2} + \frac{D2_c^2}{4H_c^2} - \right.\right. \qquad (A23)$$

$$\left.\left. - \sqrt{\left(1 + \frac{D1_c^2}{4H_c^2} + \frac{D2_c^2}{4H_c^2}\right)^2 - \frac{D1_c^2 \cdot D2_c^2}{4H_c^2}}\right)\right]$$

Eqs. A22 and A23 represent the maximum 186 keV counting rate that could be ideally obtained using these collimators. However, they do not account for the photon attenuation due to material between sample and detector (sample container wall, detector cover, etc.), and for the limited detection efficiency of the gamma detector (detector size, type of detector material, detector positioning, etc.). These effects are discussed in the following Section A3. It should be also mentioned that minor effects have been neglected here, such as penetration of the

186 keV gamma rays through the collimator edges and coherent gamma scattering at the inner walls of the collimator.

A.3 Gamma absorbing material between sample and detector

In a real gamma counting set-up one will always find some gamma-absorbing material between sample and detector, as, e.g., the sample containment or, at least, the detector cover. It is of interest here to quantify the influence of such absorber materials on the observed gamma counting rate. We assume that it is possible to combine all absorbers to a layer of uniform thickness, which is oriented in parallel to the collimator surface. As can be seen from Fig. A4, the path length of an 186 keV photon through the absorber layer depends on the inclination angle θ between the direction of the radiation and the collimator axis. The photon attenuation increases with increasing angle θ.

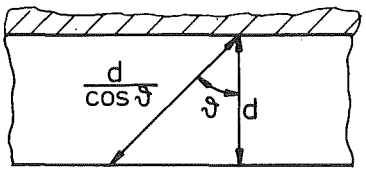

Fig. A4
Path length of gamma rays through an absorber layer.

The mean path length through the absorber with respect to the photons, which are observed in the gamma detector, depends on the angular distribution of the radiation source and on the angular acceptance of the counting geometry. It will be shown below that the effective gamma attenuation is not solely determined by the thickness and the type of the absorbing layer, but also by the properties of the counting set-up.

When an absorbing layer is present in between sample and collimator, then the number of 186 keV gamma rays penetrating the collimator per unit time is given by

$$I_\gamma^{abs} = enr \cdot A \cdot \int_F \int_\Omega \cos\theta \cdot e^{-\frac{\lambda \cdot d}{\cos\theta}} \cdot d\Omega \cdot dF \,, \qquad (A24)$$

where d is the thickness of the absorber layer, and λ is the linear photon attenuation coefficient of the absorber material

at 186 keV. For notations, integration limits and further evaluation of the integral see the previous Section A2.

No closed form has been found for the integral in eq. A24. The calculations have been performed by numerical integration. In this manual eq. A24 has been used to calculate the 186 keV photon flux at the collimator exit for the Reference Samples with a 2 mm thick aluminium container wall (see Fig. 3.7 in Section 3.1.5).

Eq. A24 describes the maximum 186 keV gamma counting rate that could be ideally obtained from a detector with 100 % peak detection efficiency. However, in a real counting arrangement the limited detection efficiency of the gamma detector must be taken into account. This comprises the "geometrical" efficiency (i.e., size and position of the detector) and the intrinsic efficiency of the detector. A schematic cross section through a typical gamma counting setup is shown in Fig. A5.

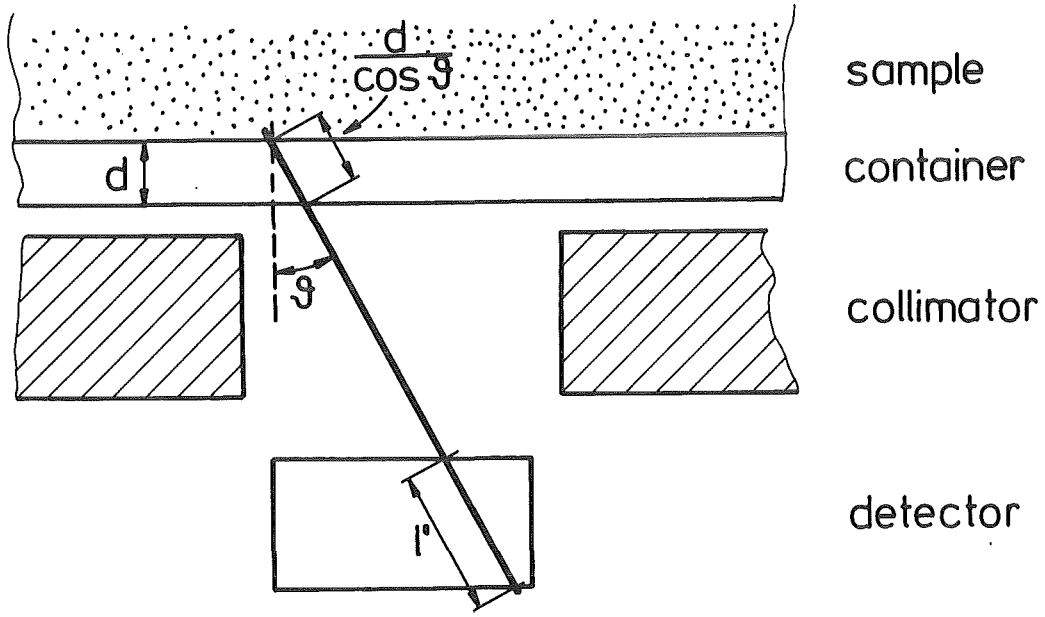

Fig. A5 Schematic cross section through a typical gamma counting set-up.

We use here a very simple model for the intrinsic efficiency ε of the gamma detector, described by

$$\varepsilon = \varepsilon_o \, (1 - e^{-\lambda' \ell'}) \quad , \qquad \text{(A25)}$$

where λ' is the linear photo-absorption coefficient of the detector material, ℓ' is the unscattered path length of the incident photon within the detector (see Fig. A5), and ε_o is the peak efficiency of an infinite detector of this type for 186 keV photons. Photon scattering effects are neglected. Note that ℓ' is dependent on the incidence angle and on the incidence location of the incoming photon at the detector surface.

Using eqs. A24 and A25 we finally arrive at a formula that describes the 186 keV gamma counting rate observed from a detector in a real counting arrangement:

$$\dot{N}_{186} = enr \cdot A \int_F \int_\Omega \cos\theta \cdot \varepsilon_o \cdot (1-e^{-\lambda'\ell'}) \cdot e^{-\frac{\lambda \cdot d}{\cos\theta}} \, d\Omega dF \, . \qquad (A26)$$

The integration is to be performed over all elements dF of the collimator entrance area F and over the solid angles $d\Omega$ defined by the collimator exit area seen from each areal element dF (see Section A2). Note, that the efficiency becomes zero, when the photon doesn't strike the detector ($\ell' = 0$). We omit here the further evaluation of the integral. The solution normally requires the application of numerical integration techniques.

When we ask for photon attenuation by an absorbing layer in context with gamma-ray measurements, we are primarily interested in those effects which influence the gamma counting rate really observed from the detector, rather than in the transmission through the collimator. It can be deduced from eq. A26 that the effective gamma attenuation in an absorbing layer is not only determined by the thickness and the type of the layer alone, but also by the collimator geometry (integration limits!) and, in addition to this, by the size, the position and the intrinsic efficiency of the gamma detector (λ' and ℓ'!). To give an example: it can be seen from Fig. A5 that the range of accepted "penetration" angles θ decreases with decreasing detector size, which will result in a lower effective gamma attenuation for small detectors as compared to large-area detectors.

The photon attenuation in an absorbing layer is usually given as the ratio of photon counting rates observed with and without the absorber. In order to simplify the presentation of

the attenuation correction required for varying container wall thickness d, we define a wall thickness correction factor K_{abs} by:

$$\frac{\dot{N}_{186}(d)}{\dot{N}_{186}(d=0)} =: e^{-\lambda \cdot K_{abs} \cdot d}$$

or

$$K_{abs} =: \frac{\ln \dot{N}_{186}(d=0) - \ln \dot{N}_{186}(d)}{\lambda \cdot d} \quad . \tag{A27}$$

Then the term

$$K_{abs} \cdot d = d_{eff}$$

describes the effective mean path length d_{eff} of the photons through the absorbing layer with a thickness d. It should be noted that the value of K_{abs} depends on the specific parameters of the particular counting geometry and on properties of the canning of the samples under assay.

To allow a more simple calculation of the effective gamma attenuation, at least for a limited range of absorber thicknesses d around a mean thickness d_o in a given counting set-up, we further define a differential wall thickness correction factor DK_{abs} by

$$DK_{abs}(d_o) =: \left. \frac{\partial K_{abs}(d)}{\partial d} \right|_{d=d_o} . \tag{A28}$$

The gamma attenuation within an absorbing layer of thickness d is then given by

$$A_{abs} \approx e^{-\lambda \cdot K_{abs}(d_o) \cdot d_o} \cdot e^{-\lambda \cdot DK_{abs}(d_o) \cdot (d-d_o)} \tag{A29}$$

Here $K_{abs}(d_o)$ and $DK_{abs}(d_o)$ can be considered as constants for a limited range of absorber thickness around d_o, being valid for a particular absorber material and for a particular counting arrangement. The differential wall thickness correction factor DK_{abs} defined in eq. A28 has been used in Section 4.3 of the manual.

It is of interest to examine the range of variations of K_{abs} as a function of the various measurement parameters. For this we have first calculated the dependence of K_{abs} on the detector size, assuming an absorber layer of 2 mm aluminium (as given for the Reference Samples). Three extreme types of gamma detectors have been considered:

1. a large-area, infinitely thick detector,
2. a large-area, infinitely thin detector, and
3. a point detector.

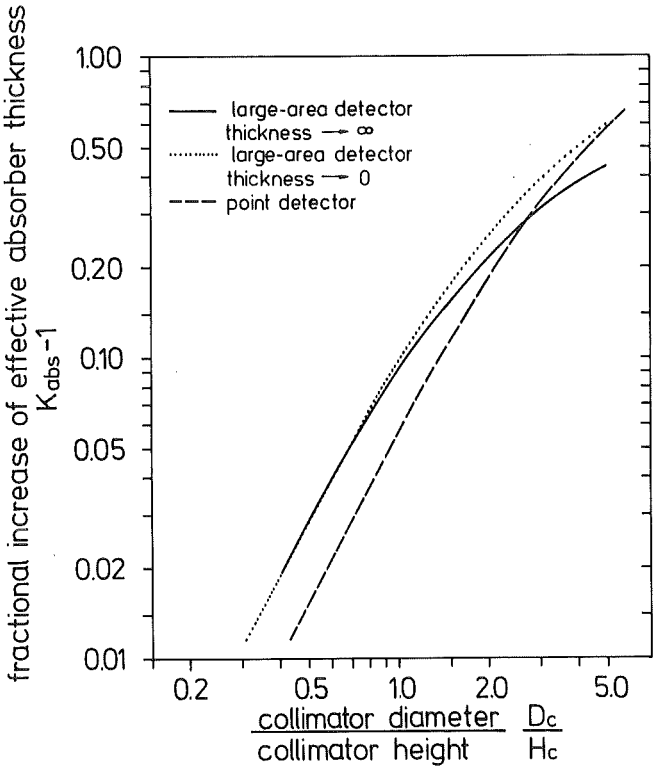

Fig. A6 Fractional increase of the effective absorber thickness (K_{abs} - 1) relative to a very narrow collimator as a function of the collimator geometry, given for three types of gamma detectors.

Fig. A6 gives the calculated values of (K_{abs} - 1) as a function of the collimator geometry in a double logarithmic scale. For very narrow collimators K_{abs} reaches values near unity. For broad and flat collimators the values of K_{abs} increase to about 1.5, indicating that in these cases the effective mean path length of

the photons in the absorber layer may be about 50 % higher than in case of a narrow collimator. Further, it can be seen in Fig. A6 that the effective gamma attenuation is highest for thin large-area detectors.

In order to demonstrate the dependence of K_{abs} on the thickness of the absorbing layer,we have calculated K_{abs} as a function of the absorber material and of the absorber thickness, expressed by the product $\lambda \cdot d$ of the linear attenuation coefficient λ and the thickness d of the absorber, assuming here a thick large-area detector. The results are displayed in Fig. A7. The upper scale shows the linear photon transmission $(1 - \exp(-\lambda \cdot d))$ that corresponds to the $\lambda \cdot d$ values given on the lower scale.

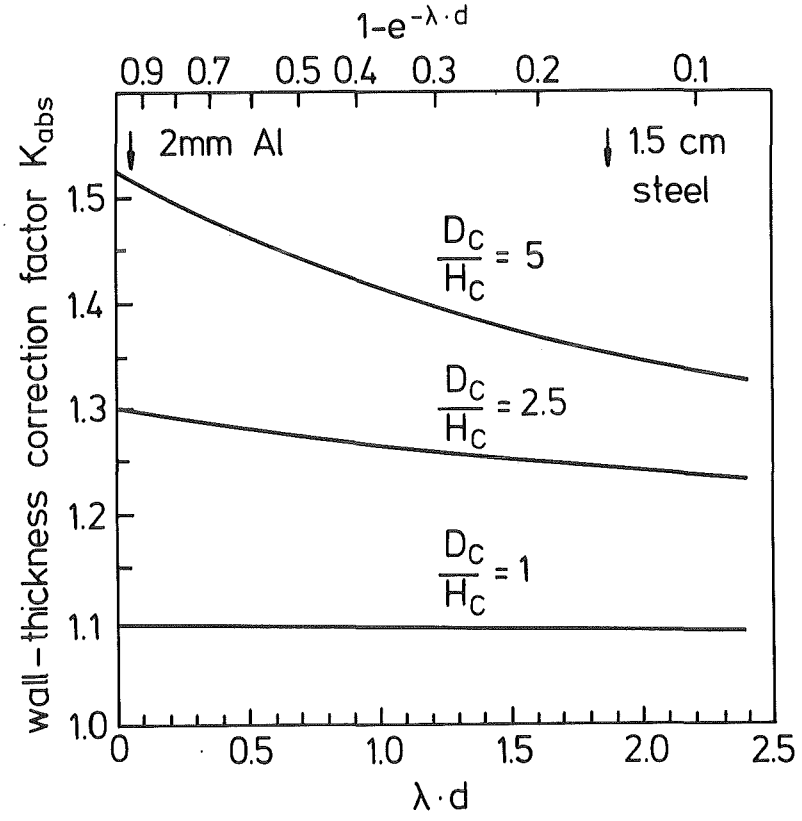

Fig. A7 Thickness correction factor K_{abs} versus thickness d and linear attenuation coefficient λ of the absorber, given for selected cylindrical collimator geometries: D_c = collimator diameter, H_c = collimator height.

Fig. A7 shows that the thickness correction factor K_{abs} decreases with increasing absorber thickness. This can be understood considering the fact that the angular distribution of the

observed photons becomes more forward-peaked with increasing absorber thickness: in case of an extremely thick container wall only those gamma rays are observed from a sample which penetrate the wall approximately perpendicular to its surface.

Fig. A7 also shows that the dependence of K_{abs} on the container wall thickness is higher for broad and flat collimators than for narrow ones. The arrows in Fig. A7 indicate the $\lambda \cdot d$ values of a 2 mm thick aluminium absorber (representing the wall thickness of the reference cans) and of an 1.5 cm thick steel absorber (typical for UF_6 containers). It can be seen that the corresponding K_{abs} values may differ by up to 10 % for wide collimators.

Note: the use of calculated corrections according to the formulae given in this section should be restricted to small attenuation corrections. In case of large attenuation corrections non-negligible errors may result from uncertainties of the linear attenuation coefficients used and from uncertainties in the calculation of the detector efficiency. Therefore, it is strongly recommended to determine the attenuation correction experimentally, if the wall thickness of the samples under assay deviates significantly from that of the samples used for the calibration of the measurement system. A procedure serving for this purpose is described in Section 4.3 of this manuel.

APPENDIX B

Characteristic gamma rays from the decay of uranium isotopes

(Energies, gamma emission probabilities and half-lives from references [7], [8], [12])

Table B1 Characteristic gamma rays from the decay of ^{235}U in the energy range 120-300 keV. Emission rates of ^{231}Th are given for secular equilibrium, i.e. >1 week after separation.

Gamma energy [keV]	Emitting Isotope	Photons / s per initial g ^{235}U
124.9	^{231}Th	$4.7\ 10^{1}$
134.0	^{231}Th	$2.0\ 10^{1}$
135.7	^{231}Th	$6.5\ 10^{1}$
140.8	^{235}U	$1.9\ 10^{2}$
143.8	^{235}U	$8.7\ 10^{3}$
145.9	^{231}Th	$2.8\ 10^{1}$
150.9	^{235}U	$6.5\ 10^{1}$
163.1	^{231}Th	$1.3\ 10^{2}$
163.4	^{235}U	$4.0\ 10^{3}$
174.2	^{231}Th	$1.5\ 10^{1}$
182.1	^{235}U	$3.4\ 10^{2}$
183.5	^{231}Th	$2.8\ 10^{1}$
185.7+++	^{235}U	$4.6\ 10^{4}$
194.9	^{235}U	$5.0\ 10^{2}$
198.9	^{235}U	$3.2\ 10^{1}$
202.1	^{235}U	$8.5\ 10^{2}$
205.3	^{235}U	$4.0\ 10^{3}$
215.3	^{235}U	$2.3\ 10^{1}$
217.9	^{231}Th	$3.3\ 10^{1}$
233.5	^{235}U	$3.4\ 10^{1}$
240.9	^{235}U	$6.8\ 10^{1}$
246.8	^{235}U	$5.1\ 10^{1}$
275.3	^{235}U	$4.2\ 10^{1}$

+++ This line is used for the determination of ^{235}U enrichment

Table B2 Characteristic gamma rays from the decay of ^{238}U in the energy range 120 - 300 keV. Emission rates of ^{238}U descendants are given for secular equilibrium, i.e. >3 months after separation.

Gamma energy [keV]	Emitting Isotope	Photons / s per initial g ^{238}U
(49.5 ++	^{238}U	40)
(63 ++	^{234}Th	9160)
125.4	^{234}Pa	0.16
131.0	^{234}Pa	3.25
137.7	^{234}Pa	0.02
140.1	^{234m}Pa	0.11
140.3	^{234}Pa	0.16
143.6	^{234}Pa	0.06
152.7	^{234}Pa	1.1
159.1	^{234}Pa	0.1
170.7	^{234}Pa	0.08
174.6	^{234}Pa	0.03
184.7 +	^{234m}Pa	0.15
186.0 +	^{234}Pa	0.32
193.4	^{234m}Pa	0.06
193.6	^{234}Pa	0.10
196.4	^{234}Pa	0.01
199.9	^{234m}Pa	0.05
200.6	^{234}Pa	0.18
203.0	^{234}Pa	0.19
209.9	^{234m}Pa	0.11
226.4	^{234}Pa	0.96
227.2	^{234}Pa	0.89
243.7	^{234m}Pa	0.05
245.2	^{234}Pa	0.15
247.7	^{234m}Pa	0.08
248.9	^{234}Pa	0.46
257.9	^{234m}Pa	7.01
267.1	^{234}Pa	0.03
272	^{234}Pa	0.21
275.5	^{234m}Pa	0.02
277.9	^{234}Pa	0.11
286.1	^{234}Pa	0.02
289.6	^{234}Pa	0.02
293.6	^{234}Pa	0.06
299.0	^{234m}Pa	0.06
(1001.2 ++	^{234m}Pa	73

+ Possible interference with 185.7 keV line from ^{235}U

++ Given for additional information

Table B3 Characteristic gamma rays from the decay of ^{234}U in the energy range 120 - 300 keV. Emission rates of ^{234}U descendants are given for different time periods after separation.

Gamma energy [keV]	Emitting Isotope	Photons / s per initial g ^{234}U T=0	T=1 y	T=5 y	T=10 y
(53.3++	^{234}U	$2.8\ 10^5$)			
120.9	^{234}U	$9.4\ 10^4$			
185.8 +	^{230}Th	0	0.2	0.9	1.8
186.2 +	^{226}Ra	0	0.02	0.4	1.6
241.9	^{214}Pb	0	0.04	0.8	3.3
253.5	^{230}Th	0	0.2	1.1	2.1
295.2	^{214}Pb	0	0.1	2.1	8.2

\+ Possible interference with 185.7 keV line from ^{235}U

++ Given for additional information

Table B4 Characteristic gamma ray from the decay of ^{236}U.

Gamma energy [keV]	Emitting Isotope	Photons / s per g ^{236}U
112.8	^{236}U	$4.5\ 10^2$

Table B5 Characteristic gamma rays from the decay of ^{232}U in the energy range 120 - 300 keV. Emission rates are given per initial gram ^{232}U for different time periods after separation.

Gamma energy [keV]	Emitting Isotope	Photons / s per initial g ^{232}U T=0	T=1 y	T=10 y
(57.8 ++§	^{232}U	$1.6\ 10^{9}$	$1.6\ 10^{9}$	$1.5\ 10^{9}$)
129.1 §	^{232}U	$5.4\ 10^{8}$	$5.3\ 10^{8}$	$4.9\ 10^{8}$
141.0	^{232}U	$2.6\ 10^{4}$	$2.5\ 10^{4}$	$2.3\ 10^{4}$
191.0	^{232}U	$2.4\ 10^{5}$	$2.4\ 10^{5}$	$2.2\ 10^{5}$
209.5	^{232}U	$8.4\ 10^{4}$	$8.3\ 10^{4}$	$7.6\ 10^{4}$
270.2 §	^{232}U	$2.3\ 10^{7}$	$2.3\ 10^{7}$	$2.1\ 10^{7}$
131.6	^{228}Th	0	$3.0\ 10^{8}$	$8.9\ 10^{8}$
142.0	^{228}Th	0	$3.2\ 10^{3}$	$9.6\ 10^{3}$
144.0	^{212}Bi	0	$2.3\ 10^{7}$	$6.9\ 10^{7}$
164.0	^{212}Bi	0	$1.1\ 10^{7}$	$3.2\ 10^{7}$
166.4	^{228}Th	0	$2.3\ 10^{8}$	$6.9\ 10^{8}$
176.7	^{212}Pb	0	$1.2\ 10^{8}$	$3.6\ 10^{8}$
182.2 +	^{228}Th	0	$1.3\ 10^{4}$	$3.7\ 10^{4}$
205.9	^{228}Th	0	$4.4\ 10^{7}$	$1.3\ 10^{8}$
211.4	^{208}Tl	0	$1.4\ 10^{8}$	$4.2\ 10^{8}$
216.0	^{228}Th	0	$5.7\ 10^{8}$	$1.7\ 10^{9}$
228.5	^{228}Th	0	$4.4\ 10^{4}$	$1.3\ 10^{5}$
233.4	^{208}Tl	0	$2.5\ 10^{8}$	$7.7\ 10^{8}$
238.6 §	^{212}Pb	0	$1.0\ 10^{11}$	$3.1\ 10^{11}$
241.0	^{224}Ra	0	$9.4\ 10^{9}$	$2.8\ 10^{10}$
252.6	^{208}Tl	0	$6.5\ 10^{8}$	$2.0\ 10^{9}$
277.4	^{208}Tl	0	$5.6\ 10^{9}$	$1.7\ 10^{10}$
292.7	^{224}Ra	0	$1.4\ 10^{7}$	$4.2\ 10^{7}$
300.1	^{212}Pb	0	$7.8\ 10^{9}$	$2.4\ 10^{10}$
(588.1 ++§	^{208}Tl	0	$7.0\ 10^{10}$	$2.1\ 10^{11}$)
(2614.5 ++§	^{208}Tl	0	$8.2\ 10^{10}$	$2.5\ 10^{11}$)

\+ Possible interference with 185.7 keV line from ^{235}U

++ Given for additional information

§ These strong lines may be used to detect ^{232}U or its descendants present in a sample

Table B6 Characteristic gammma rays from the decay of ^{233}U in the energy range 120 - 300 keV. Emissions rates of ^{233}U descendants are given for different time periods after separation.

Gamma energy [keV]	Emitting Isotope	Photons / s per initial g ^{233}U T=0	T=1 y	T=10 y
120.8	^{233}U	$9.2\ 10^{3}$		
135.3	^{233}U	$7.9\ 10^{3}$		
145.4	^{233}U	$5.5\ 10^{3}$		
146.3	^{233}U	$2.2\ 10^{4}$		
164.5	^{233}U	$2.2\ 10^{4}$		
184.5 +	^{233}U	$< 5\ \ 10^{2}$		
188.0 +	^{233}U	$7.1\ 10^{3}$		
208.2	^{233}U	$8.6\ 10^{3}$		
217.1	^{233}U	$1.2\ 10^{4}$		
245.3	^{233}U	$1.4\ 10^{4}$		
248.7	^{233}U	$5.4\ 10^{3}$		
278.1	^{233}U	$4.3\ 10^{3}$		
288.0	233	$3.3\ 10^{3}$		
291.3	^{233}U	$2.0\ 10^{4}$		
(317.2 ++	^{233}U	$2.8\ 10^{4}$)		
124.5	^{229}Th	0	$1.2\ 10^{3}$	$1.2\ 10^{4}$
137.0	^{229}Th	0	$5.4\ 10^{2}$	$5.4\ 10^{3}$
148	^{229}Th	0	$3.7\ 10^{2}$	$3.7\ 10^{3}$
150.1	^{225}Ac	0	$2.2\ 10^{2}$	$2.4\ 10^{3}$
156.5	^{229}Th	0	$7.4\ 10^{2}$	$7.4\ 10^{3}$
157.3	^{225}Ac	0	$1.0\ 10^{2}$	$1.1\ 10^{3}$
186.1 +	^{225}Ac	0	$6.1\ 10^{0}$	$6.7\ 10^{1}$
188.0 +	^{225}Ac	0	$1.6\ 10^{2}$	$1.8\ 10^{3}$
193.6	^{229}Th	0	$1.5\ 10^{3}$	$1.5\ 10^{4}$
211.0	^{229}Th	0	$1.1\ 10^{3}$	$1.1\ 10^{4}$
216.2	^{225}Ac	0	$1.0\ 10^{2}$	$1.1\ 10^{3}$
218.0	^{221}Fr	0	$3.8\ 10^{3}$	$4.2\ 10^{4}$
292.3	^{213}Bi	0	$1.1\ 10^{2}$	$1.2\ 10^{3}$

\+ Possible interference with 185.7 keV line from ^{235}U

++ Given for additional information

Table B7 Characteristic gamma rays from the decay of ^{237}U in the energy range 120 - 300 keV. Emission rates are given per initial gram ^{237}U for different time periods after separation.

Gamma energy [keV]	Emitting Isotope	Photons / s per initial g ^{237}U T=0	T=1 m	T=1 y
(59.9++§	^{237}U	$1.1\ 10^{15}$	$4.8\ 10^{13}$	< 0.1)
164.6	^{237}U	$5.9\ 10^{12}$	$2.6\ 10^{11}$	-
208.0 §	^{237}U	$6.9\ 10^{14}$	$3.1\ 10^{13}$	< 0.05)
221.8	^{237}U	$6.6\ 10^{11}$	$2.9\ 10^{10}$	-
234.4	^{237}U	$6.3\ 10^{11}$	$2.8\ 10^{10}$	-
267.6	^{237}U	$2.3\ 10^{13}$	$1.0\ 10^{12}$	-
292.7	^{237}U	$8.5\ 10^{10}$	$3.7\ 10^{9}$	-
(86.5++§	^{237}Np	0		$3.3\ 10^{6}$)
131.1	^{237}Np	0		$2.5\ 10^{4}$
134.2	^{237}Np	0		$2.0\ 10^{5}$
143.3	^{237}Np	0		$1.2\ 10^{4}$
151.3	^{237}Np	0		$6.6\ 10^{4}$
155.2	^{237}Np	0		$2.6\ 10^{4}$
162.5	^{237}Np	0		$1.1\ 10^{4}$
169.1	^{237}Np	0		$2.1\ 10^{3}$
170.6	^{237}Np	0		$4.8\ 10^{3}$
175.9	^{237}Np	0		$6.1\ 10^{3}$
180.7	^{237}Np	0		$6.1\ 10^{2}$
186.8 +	^{237}Np	0		$8.6\ 10^{3}$
191.3	^{237}Np	0		$6.1\ 10^{4}$
193.0	^{237}Np	0		$1.3\ 10^{4}$
194.7	^{237}Np	0		}$5.7\ 10^{4}$
194.9	^{237}Np	0		
196.8	^{237}Np	0		$6.5\ 10^{3}$
201.7	^{237}Np	0		$1.2\ 10^{4}$
209.1	^{237}Np	0		$4.7\ 10^{3}$
212.3	^{237}Np	0		$4.3\ 10^{4}$
213.9	^{237}Np	0		$1.2\ 10^{4}$
229.8	^{237}Np	0		$3.3\ 10^{3}$
237.9	^{237}Np	0		$1.9\ 10^{4}$
271.6	^{233}Ra	0		$8.2\ 10^{4}$
(300.2++	^{233}Ra	0		$1.3\ 10^{5}$)
(312.9++§	^{233}Ra	0		$9.7\ 10^{6}$)

\+ Possible interference with 185.7 keV line from ^{235}U

++ Given for additional information

§ These strong lines may be used to detect ^{237}U or its descendents present in a sample

APPENDIX C

Physical constants used in the calculation of the 186 keV gamma counting rate

APPENDIX C

Physical constants used in the calculation

Avogadro constant	$A = 6.022\ 10^{23}$	$[mol^{-1}]$
Atomic weight of ^{235}U	$M_{235} = 235.0$	$[g \cdot mol^{-1}]$
Half-life of ^{235}U [8]	$T_{1/2} = (7.038 \pm 0.007)\ 10^{8}$	[a]
	$= (2.220 \pm 0.002)\ 10^{16}$	[s]
Emission probability of a 185.7 keV photon per decay of a ^{235}U atom [7]	$P_{186} = 0.575 \pm 0.009$	
Attenuation cross section for 185.7 keV photons in U (narrow-beam cross section minus coherent cross section [9])	$\sigma_U = (582 \pm 30)\ 10^{-24}$	$[cm^2]$

Derived values

Number of 185.7 keV photons emitted per second per ^{235}U atom	$\dot{n}_{186} = P_{186} \cdot \ln 2 / T_{1/2}$	
	$= (1.80 \pm 0.03)\ 10^{-17}$	$[s^{-1}]$
Number of 185.7 keV photons emitted per second per gram ^{234}U	$\dot{n}^{M}_{186} = \dot{n}_{186} \cdot A / M_{235}$	
	$= (4.60 \pm 0.07)\ 10^{4}$	$[s^{-1} \cdot g^{-1}]$

Number of 185.7 keV photons emitted per cm^2 surface area of an infinitely thick U metal sample into the halfspace (2π) per second per % ^{235}U isotope abundance (atom %), neglecting coherent photon scattering and assuming uniform ^{235}U isotope abundance in the sample:

$$I_{186} = \frac{\dot{n}_{186}}{4 \cdot \sigma_U} \cdot \frac{1}{100}$$

$$= (77 \pm 4)\ [cm^{-2} \cdot s^{-1} \cdot (\%\ ^{235}U)^{-1}]$$

Note: The uncertainties of the photon cross sections and of the related attenuation coefficients given in Tables C1, C2 and C3 are about $\pm$ 5 % [9].

Table C1 Photon cross sections for 185.7 keV gamma rays and related constants given for selected elements.

Element	Photon cross section 1) (barn)	Mass attenuation coefficient 2) ($cm^2 \cdot g^{-3}$)	Metal density 3) ($g \cdot cm^{-3}$)	Linear attenuation coefficient (cm^{-1})
H	0.415	0.248		
Be	1.66	0.111	1.85	0.205
B	2.07	0.116		
C	2.49	0.125		
N	2.90	0.125		
O	3.31	0.125		
F	3.74	0.119		
Mg	5.02	0.124		
Al	5.47	0.122	2.70	0.329
Si	5.91	0.127		
Cl	7.36	0.125		
Ca	9.03	0.136		
Ti	10.3	0.129		
V	11.0	0.130		
Cr	11.7	0.135		
Mn	12.5	0.137		
Fe	13.3	0.144	7.86	1.13
Co	14.3	0.147		
Ni	15.3	0.157		
Cu	16.3	0.155	8.92	1.38
Zn	17.5	0.161		
Zr	34.9	0.231		
Mo	40.1	0.252		
Cd	60.0	0.321	8.64	2.78
In	64.1	0.336		
Sn	68.6	0.348		
Sm	143.	0.572		
Eu	152.	0.601		
Gd	160.	0.613		
Dy	178.	0.661		
W	269.	0.882	19.4	17.1
Pb	389.	1.13	11.3	12.8
Bi	405.	1.17	9.80	11.4
Th	540.	1.40		
U	582.	1.47	19.0	28.0
Pu	629.	1.56		

1) Narrow-beam cross section minus coherent cross section interpolated to 185.7 keV from values given in [9]

2) Conversion factors from photon cross sections to mass attenuation coefficients taken from [9]

3) Metal densities taken from [21].

For a uniform chemical compound c the photon cross sections σ_i of the elements i in the compound, the mass attenuation coefficient μ_c, and the linear attenuation coefficient λ_c are related by the following equation:

$$\lambda_c = \mu_c \rho_c = \frac{A \cdot \sum_i n_i \cdot \sigma_i}{m_c} \cdot \rho_c$$

A	=	Avogadro constant
n_i	=	Number of atoms of element i in the compound molecule (stoichiometry)
σ_i	=	photon cross section of element i
m_c	=	molecular mass of the compound
ρ_c	=	density of the compound
μ_c	=	mass attenuation coefficient of the compound
λ_c	=	linear attenuation coefficient of the compound.

Table C2 Mass attenuation coefficients for 185.7 keV photons for some uranium compounds.

Uranium compound	Molecular mass ($g \cdot mol^{-1}$) [21]	Mass attenuation coefficient ($cm^2 \cdot g^{-1}$)
U metal	238	1.473
UO_2	270	1.313
U_3O_8	842	1.268
UF_4	314	1.145
UF_6	352	1.034
Uranyl nitrate $UO_2(NO_3)_2 \cdot 6H_2O$	502	0.767

Table C3 Linear attenuation coefficients for 185.7 keV photons for some absorber materials.

Absorber material	Density ($g \cdot cm^{-3}$)	Linear attenuation coefficient (cm^{-1})
Polyethylene $(CH_2)_n$	0.95	0.14
Aluminium	2.70	0.329
Steel	7.9	1.25
Copper	8.92	1.38
Brass (61.5 % Cu 35.5 % Zn 3.0 % Pb)	8.5	1.58
Cadmium	8.64	2.78
Lead	11.3	12.8
Tungsten	19.4	17.1

APPENDIX D

Tables of test statistics

Table D1 Confidence limits x for the modified chi-square distribution $\omega^2 = \chi^2/DOF$ at various probability levels P (DOF = degrees of freedom).

$P(\omega^2 < x)$ / $P(\omega^2 \geq x)$ / DOF	1 % / 99 %	5 % / 95 %	10 % / 90 %	50 % / 50 %	90 % / 10 %	95 % / 5 %	99 % / 1 %
1	0.0002	0.004	0.02	0.46	2.71	3.84	6.63
2	0.01	0.05	0.11	0.69	2.30	3.00	4.60
3	0.04	0.12	0.19	0.79	2.08	2.60	3.78
4	0.08	0.18	0.27	0.84	1.94	2.36	3.32
5	0.11	0.23	0.32	0.87	1.85	2.21	3.02
6	0.15	0.27	0.37	0.89	1.77	2.10	2.80
7	0.18	0.31	0.41	0.91	1.72	2.01	2.64
8	0.21	0.34	0.44	0.92	1.67	1.94	2.51
9	0.23	0.37	0.46	0.93	1.63	1.88	2.41
10	0.26	0.39	0.49	0.94	1.60	1.83	2.32
20	0.41	0.53	0.62	0.97	1.42	1.57	1.88
30	0.50	0.62	0.69	0.98	1.34	1.46	1.70

Table D2 Confidence limits x for the t-distribution at various probability levels P (DOF = degrees of freedom).

$P(t < x)$ / $P(t \geq x)$ / DOF	50 % / 50 %	90 % / 10 %	95 % / 5 %	99 % / 1 %
1	1.0	6.4	12.7	63.7
2	.82	2.9	4.3	9.9
3	.76	2.4	3.2	5.8
4	.74	2.1	2.8	4.6
5	.73	2.0	2.6	4.0
6	.72	1.9	2.5	3.7
7	.71	1.9	2.4	3.5
8	.70	1.9	2.3	3.4
9	.70	1.8	2.3	3.3
10	.70	1.8	2.2	3.2
20	.69	1.7	2.1	2.9
30	.68	1.7	2.0	2.8

APPENDIX E

ER2FIT

A BASIC program for the calibration of ^{235}U enrichment assay systems

```
10 REM ************************************************************
20 REM
30 REM           PROGRAMM  E R 2 F I T  VERS. MAY 1984
40 REM
50 REM       LINEAR LEAST SQUARES FIT WITH INDIVIDUAL ERRORS
60 REM       IN BOTH OBSERVATIONS AND GIVEN VARIANCES FOR EACH
70 REM       OBSERVATION.  FIT FUNCTION  E = A*P + C
80 REM
90 REM                     P. MATUSSEK
100 REM                    KFK / IK III
110 REM                    P. O. B.  3640
120 REM                    D-7500 KARLSRUHE
130 REM                    GERMANY
140 REM
150 REM ************************************************************
160 REM
170 REM    :::::::::::: PART 1: INPUT SECTION  ::::::::::::::
180 REM
190 REM ************************************************************
200 REM
210 DIM P(21),DP(21),E(21),DE(21),G(21),D(21),ES(21)
220 PRINT:PRINT "NUMBER OF DATA POINTS (MAX.  20) =";
230 INPUT N
240 REM ..................................................
250 REM      TO INVOKE TEST DATA, INPUT A NEGATIVE NUMBER !
260 REM ..................................................
270 IF N<0 THEN GOTO 410
280 IF N<3 THEN GOTO 540
290 IF N>20 THEN GOTO 540
300 REM ..................................................
310 FOR I = 1 TO N
320 PRINT:PRINT "INPUT DATA POINT #";I
330 PRINT "185 KEV NET-PEAK GAMMA COUNTING RATE  =";: INPUT P(I)
340 PRINT "ABSOLUTE ERROR OF GAMMA COUNTING RATE =";: INPUT DP(I)
350 PRINT "DECLARED ENRICHMENT VALUE             =";: INPUT E(I)
360 PRINT "ABSOLUTE ERROR OF ENRICHMENT VALUE    =";: INPUT DE(I)
370 NEXT I
380 PRINT
390 GOTO 630
400 REM ..............  TEST DATA ..........................
410 N=5
420 DATA  11.349,  0.033,  0.3205,  0.0001
430 DATA  25.428,  0.051,  0.7210,  0.0001
440 DATA  69.128,  0.104,  1.9658,  0.0003
450 DATA 105.061,  0.147,  2.9843,  0.0005
460 DATA 159.182,  0.207,  4.5167,  0.0007
470 REM
480 REM ..............  READ TEST DATA.....................
490 FOR I=1 TO N
500 READ P(I),DP(I),E(I),DE(I)
510 NEXT I
520 GOTO 630
530 REM ............  INPUT-ERROR EXIT ....................
540 PRINT: PRINT "INPUT ERROR !!!":PRINT
550 GOTO 220
560 REM
```

```
570 REM ************************************************************
580 REM
590 REM  :::::::::::::::: PART 2: CALCULATION ::::::::::::::::
600 REM
610 REM ************************************************************
620 REM
630 FOR I=1 TO N
640 G(I)=1.
650 D(I)=0.
660 NEXT I
670 REM ..............  ITERATION LOOP ........................
680 FOR J=1 TO 6
690 SG=0.
700 EP=0.
710 GE=0.
720 GP=0.
730 P2=0.
740 GD=0.
750 REM ..................................................
760 FOR I = 1 TO N
770 SG=SG+G(I)
780 EP=EP+G(I)*E(I)*P(I)
790 GE=GE+G(I)*E(I)
800 GP=GP+G(I)*P(I)
810 P2=P2+G(I)*P(I)*P(I)
820 GD=GD+DP(I)*DP(I)*G(I)*G(I)*D(I)*D(I)
830 NEXT I
840 REM ..............  PARAMETER ESTIMATES ....................
850 X=(SG*(P2-GD)-GP*GP)
860 A=(SG*EP-GE*GP)/X
870 DA=SG/X
880 C=(GE*(P2-GD)-GP*EP)/X
890 DC=(P2-GD)/X
900 AC=-GP/X
910 REM ...........  NEW WEIGHTS AND RESIDUALS ................
920 OM=0.
930 FOR I=1 TO N
940 G(I)=1./(DE(I)*DE(I)+A*A*DP(I)*DP(I))
950 ES(I)=A*P(I)+C
960 D(I)=ES(I)-E(I)
970 OM=OM+G(I)*D(I)*D(I)
980 NEXT I
990 OM=OM/(N-2)
1000 REM ........  ADJUSTMENT OF VARIANCES AND COVARIANCE .......
1010 D1=DA*OM
1020 D2=DC*OM
1030 D3=AC*OM
1040 REM ............  ITERATION PRINT ........................
1050 PRINT:PRINT "ITERATION NR.  ";J
1060 PRINT "SLOPE = ";:PRINT USING "#.#####^^^^";A;
1070 PRINT " +- ";:PRINT USING "#.#####^^^^";SQR(D1);
1080 PRINT "    COVARIANCE    = ";:PRINT USING "#.#####^^^^";D3
1090 PRINT "OFFSET= ";:PRINT USING "#.#####^^^^";C;
1100 PRINT " +- ";:PRINT USING "#.#####^^^^";SQR(D2);
1110 PRINT "    OMEGA SQUARE = ";:PRINT USING "#.#####^^^^";OM
1120 NEXT J
1130 REM ............  END OF ITERATION LOOP ..................
1140 REM
```

```
1150 REM ************************************************************
1160 REM
1170 REM  ::::::  PART 3 : PRINT RESIDUALS AND RESULTS ::::::
1180 REM
1190 REM ************************************************************
1200 REM
1210 PRINT:PRINT:PRINT "TABLE OF RESIDUALS"
1220 PRINT:PRINT "                                                    EXPECTED";
1230 PRINT "   CONFIDENCE"
1240 PRINT "OBS.NR   OBS.VALUE   ESTIMATE   RESIDUAL    ERROR";
1250 PRINT "    LIMITS OF FIT":PRINT
1260 FOR J=1 TO N
1270 PRINT USING "###.";J;:PRINT"     ";
1280 PRINT USING "##.####";E(J);:PRINT "     ";
1290 PRINT USING "##.#####";ES(J);:PRINT "    ";
1300 PRINT USING "##.#####";D(J);:PRINT "   +-";
1310 PRINT USING "#.#####";SQR(1/G(J));:PRINT "   +-";
1320 PRINT USING "#.#####";SQR(P(J)*P(J)*D1+2.*P(J)*D3+D2)
1330 NEXT J
1340 PRINT: PRINT "************************************************************";
1350 PRINT "***************"
1360 PRINT:PRINT "SLOPE                =  ";:PRINT USING "#.#####^^^^";A;
1370 PRINT "  +-  ";:PRINT USING "#.#####^^^^";SQR(D1)
1380 PRINT       "OFFSET               =  ";:PRINT USING "#.#####^^^^";C;
1390 PRINT "  +-  ";:PRINT USING "#.#####^^^^";SQR(D2)
1400 PRINT:PRINT "OMEGA SQUARE         =  ";:PRINT USING "##.###";OM
1410 PRINT       "DEGREES OF FREEDOM   =  ";N-2
1420 PRINT:PRINT "VARIANCE SLOPE       =  ";:PRINT USING "#.#####^^^^";D1
1430 PRINT       "VARIANCE OFFSET      =  ";:PRINT USING "#.#####^^^^";D2
1440 PRINT       "COV (SLOPE,OFFSET)   =  ";:PRINT USING "#.#####^^^^";D3
1450 PRINT
1460 END
```

DATA SET I (INPUT DATA SEE PROGRAM LISTING)

```
RUN

NUMBER OF DATA POINTS (MAX. 20) =-1

ITERATION NR.  1
SLOPE = 0.28388E-01 +- 0.11242E-01     COVARIANCE    = -.93554E-02
OFFSET= 0.94639E-04 +- 0.10295E+01     OMEGA SQUARE  = 0.18361E+01

ITERATION NR.  2
SLOPE = 0.28419E-01 +- 0.22197E-04     COVARIANCE    = -.11825E-07
OFFSET= -.17875E-02 +- 0.80084E-03     OMEGA SQUARE  = 0.64366E+00

ITERATION NR.  3
SLOPE = 0.28419E-01 +- 0.22222E-04     COVARIANCE    = -.11851E-07
OFFSET= -.17853E-02 +- 0.80171E-03     OMEGA SQUARE  = 0.64366E+00

ITERATION NR.  4
SLOPE = 0.28419E-01 +- 0.22221E-04     COVARIANCE    = -.11851E-07
OFFSET= -.17854E-02 +- 0.80171E-03     OMEGA SQUARE  = 0.64365E+00

ITERATION NR.  5
SLOPE = 0.28419E-01 +- 0.22220E-04     COVARIANCE    = -.11850E-07
OFFSET= -.17852E-02 +- 0.80168E-03     OMEGA SQUARE  = 0.64360E+00

ITERATION NR.  6
SLOPE = 0.28419E-01 +- 0.22221E-04     COVARIANCE    = -.11850E-07
OFFSET= -.17854E-02 +- 0.80170E-03     OMEGA SQUARE  = 0.64364E+00


TABLE OF RESIDUALS

                                                    EXPECTED    CONFIDENCE
OBS. NR    OBS. VALUE    ESTIMATE    RESIDUAL       ERROR     LIMITS OF FIT

  1.         0.3205      0.32074      0.00024    +-0.00094    +-0.00066
  2.         0.7210      0.72086     -0.00014    +-0.00145    +-0.00060
  3.         1.9658      1.96278     -0.00302    +-0.00297    +-0.00117
  4.         2.9843      2.98397     -0.00033    +-0.00421    +-0.00190
  5.         4.5167      4.52205      0.00535    +-0.00592    +-0.00306

*************************************************************************

SLOPE                 =   0.28419E-01   +-   0.22221E-04
OFFSET                =   -.17854E-02   +-   0.80170E-03

OMEGA SQUARE          =    0.644
DEGREES OF FREEDOM    =    3

VARIANCE SLOPE        =   0.49378E-09
VARIANCE OFFSET       =   0.64272E-06
COV (SLOPE,OFFSET)    =   -.11850E-07

OK
```

DATA SET II

```
RUN

NUMBER OF DATA POINTS (MAX. 20) = 5

INPUT DATA POINT # 1
185 KEV NET-PEAK GAMMA COUNTING RATE  = 33.33
ABSOLUTE ERROR OF GAMMA COUNTING RATE = .06
DECLARED ENRICHMENT VALUE             = .3205
ABSOLUTE ERROR OF ENRICHMENT VALUE    = .0001

INPUT DATA POINT # 2
185 KEV NET-PEAK GAMMA COUNTING RATE  = 74.91
ABSOLUTE ERROR OF GAMMA COUNTING RATE = .097
DECLARED ENRICHMENT VALUE             = .721
ABSOLUTE ERROR OF ENRICHMENT VALUE    = .0001

INPUT DATA POINT # 3
185 KEV NET-PEAK GAMMA COUNTING RATE  = 203.6
ABSOLUTE ERROR OF GAMMA COUNTING RATE = .12
DECLARED ENRICHMENT VALUE             = 1.9658
ABSOLUTE ERROR OF ENRICHMENT VALUE    = .0003

INPUT DATA POINT # 4
185 KEV NET-PEAK GAMMA COUNTING RATE  = 308.25
ABSOLUTE ERROR OF GAMMA COUNTING RATE = .22
DECLARED ENRICHMENT VALUE             = 2.9843
ABSOLUTE ERROR OF ENRICHMENT VALUE    = .0005

INPUT DATA POINT # 5
185 KEV NET-PEAK GAMMA COUNTING RATE  = 464.93
ABSOLUTE ERROR OF GAMMA COUNTING RATE = .23
DECLARED ENRICHMENT VALUE             = 4.5167
ABSOLUTE ERROR OF ENRICHMENT VALUE    = .0007


ITERATION NR.  1
SLOPE = 0.97211E-02 +- 0.15074E-01    COVARIANCE   = -.49309E-01
OFFSET= -.78673E-02 +- 0.40412E+01    OMEGA SQUARE = 0.28153E+02

ITERATION NR.  2
SLOPE = 0.97020E-02 +- 0.17120E-04    COVARIANCE   = -.27147E-07
OFFSET= -.42411E-02 +- 0.23743E-02    OMEGA SQUARE = 0.15758E+02

ITERATION NR.  3
SLOPE = 0.97019E-02 +- 0.17088E-04    COVARIANCE   = -.27044E-07
OFFSET= -.42344E-02 +- 0.23697E-02    OMEGA SQUARE = 0.15758E+02

ITERATION NR.  4
SLOPE = 0.97019E-02 +- 0.17088E-04    COVARIANCE   = -.27044E-07
OFFSET= -.42343E-02 +- 0.23697E-02    OMEGA SQUARE = 0.15758E+02

ITERATION NR.  5
SLOPE = 0.97019E-02 +- 0.17088E-04    COVARIANCE   = -.27044E-07
OFFSET= -.42340E-02 +- 0.23697E-02    OMEGA SQUARE = 0.15758E+02

ITERATION NR.  6
SLOPE = 0.97019E-02 +- 0.17088E-04    COVARIANCE   = -.27044E-07
OFFSET= -.42344E-02 +- 0.23697E-02    OMEGA SQUARE = 0.15758E+02
```

TABLE OF RESIDUALS

OBS. NR	OBS. VALUE	ESTIMATE	RESIDUAL	EXPECTED ERROR	CONFIDENCE LIMITS OF FIT
1.	0.3205	0.31913	-0.00137	+-0.00059	+-0.00203
2.	0.7210	0.72254	0.00154	+-0.00095	+-0.00179
3.	1.9658	1.97107	0.00527	+-0.00120	+-0.00259
4.	2.9843	2.98638	0.00208	+-0.00219	+-0.00409
5.	4.5167	4.50647	-0.01023	+-0.00234	+-0.00660

****

SLOPE = 0.97019E-02 +- 0.17088E-04
OFFSET = -.42344E-02 +- 0.23697E-02

OMEGA SQUARE = 15.758
DEGREES OF FREEDOM = 3

VARIANCE SLOPE = 0.29200E-09
VARIANCE OFFSET = 0.56155E-05
COV (SLOPE,OFFSET) = -.27044E-07

OK